Development of an all-optical method to measure surface diffusion at electrochemical interfaces

Dissertation

in fulfilment of the requirements for the degree of

Doctor of Natural Sciences (Dr. rer. nat.)

of the Faculty of Mathematics and Natural Sciences

at Kiel University

submitted by

Lasse Kattwinkel

Kiel, 2023

Author:	Lasse Kattwinkel
Institution:	Faculty of Mathematics and Natural Sciences, Kiel University
First examiner:	Prof. Dr. Olaf M. Magnussen
Second examiner:	Prof. Dr. Michael Bauer
Date of the oral examination:	12.04.2023
Authorized for printing:	12.04.2023
URN:	urn:nbn:de:gbv:8:3-2023-00266-9
License:	CC BY 4.0

Das kulturelle Antriebsmoment jener Lebensform, die wir modern nennen,
ist die Vorstellung, der Wunsch und das Begehren, Welt verfügbar zu machen.
Lebendigkeit, Berührung und wirkliche Erfahrung
aber entstehen aus der Begegnung mit dem Unverfügbaren.

— Hartmut Rosa, Unverfügbarkeit

ABSTRACT

In this work, a new *in situ* method for measuring the surface diffusion rates of adsorbates on electrodes in electrochemical environment was developed.
Surface diffusion processes play an important role in many reactions at electrode surfaces and are of relevance to electrocatalysis, electrodeposition, and many other areas. Such processes have therefore been extensively studied on solids under vacuum conditions with a variety of different methods. In sharp contrast, only few studies exist to measure surface diffusion in electrochemical environment due to the lack of suitable methodology. We aim on partially filling this gap by introducing the all-optical *in situ* LOD methodology, which allows to measure surface diffusion rates over a wide range and thus overcomes limitations of established methods that are mostly restricted to slow diffusion rates. The method is based on the generation of a periodic spatial modulation of adsorbates using two interfering laser pulses. The subsequent equilibration of this pattern and thus the diffusion rate of adsorbates is probed by the linear optical diffraction (LOD) signal from a second laser.
First proof-of-principle measurements were performed on sulfur diffusion on the Pt(111) electrode. For this purpose, the optical and electrochemical properties of this systems were investigated first, including studies of the optical reflectance change induced by chemisorbed sulfur (S_{ad}) and investigations of the S_{ad} oxidation mechanism. The subsequent studies of S_{ad} surface diffusion revealed potential and coverage dependent diffusion rates which were at least an order of magnitude faster than under vacuum conditions. Supported by numerical simulations, the implications of strong adsorbate-adsorbate interaction combined with different grating modulation depths to the temporal evolution of the LOD signal were demonstrated and data accuracy and pitfalls of the method were discussed. Based on these very first findings, further improvements for the developed *in situ* LOD methodology were proposed.

ZUSAMMENFASSUNG

Im Rahmen dieser Arbeit wurde eine neuartige *in situ* Methode zur Messung der Oberflächendiffusion von Adsorbaten auf Elektroden in elektrochemischer Umgebung entwickelt.
Oberflächendiffusionsprozesse spielen bei einer Vielzahl von Elektrodenreaktionen eine wichtige Rolle und sind insbesondere bei der Elektrokatalyse, bei elektrochemischen Abscheidungsprozessen und bei vielen weiteren grundlegenden Prozessen von großer Relevanz. Die Diffusion an Oberflächen im Vakuum wird bereits seit längerem untersucht, sodass für Messungen in dieser Umgebung eine Vielzahl an verschiedenen Messmethoden zur Verfügung steht. Für die Messung der Oberflächendiffusion an elektrochemischen Grenzflächen hingegen gibt es nur wenige Messmethoden und daher auch kaum systematische Untersuchungen. Wir wollen diese Lücke mit der Einführung der neu entwickelten, rein optischen *in situ* LOD Methode schließen. Im Gegensatz zu etablierten Methoden, die zumeist auf die Messung von vergleichsweise langsamen Diffusionsraten beschränkt sind, erlaubt unsere Methode die Messung von deutlich schnelleren Diffusionsraten, und deckt somit einen weiten Messbereich ab. Die Methode basiert auf der Erzeugung einer räumlich-periodischen Adsorbatbedeckung, welche mithilfe von zwei interferierenden Laserpulsen induziert wird. Die diffusionsbedingte Auflösung dieser Struktur hin zu einer räumlich-homogenen Adsorbatverteilung wird mithilfe eines zweiten Lasers überwacht. Dazu wird das lineare optischen Beugungssingal (LOD) der Adsorbatstruktur gemessen, aus dessen Verlauf sich dann die Diffusionsrate der Adsorbate bestimmen lässt.
In ersten Proof-of-Principle-Messungen wurde die Oberflächendiffusion von adsorbiertem Schwefel (S_{ad}) auf einer Pt(111) Elektrode gemessen. Zunächst wurden die optischen und elektrochemischen Eigenschaften des S_{ad}/Pt(111)-Systems, insbesondere der S_{ad} Oxidationsmechanismus und die aus der oxidativen Desorption resultierende Änderung der optischen Reflektivität, untersucht. Die Messungen der S_{ad} Oberflächendiffusion lieferten deutlich höhere Diffusionsraten als unter Vakuumbedingungen und es konnte eine starke Abhängigkeit der Diffusionsrate von der Adsorbatbedeckung und dem Elektrodenpotential gezeigt werden. Mithilfe von numerischen Simulationen wurden die Auswirkungen von starken Adsorbat-Adsorbat-Wechselwirkungen und verschiedenen Ausprägungen der erzeugten Adsorbatstruktur auf die zeitliche Entwicklung des LOD Signals demonstriert. Die gewonnenen Erkenntnisse wurden genutzt, um die Messgenauigkeit und mögliche Fallstricke der Methodik zu diskutieren und damit weitere Optimierungsmöglichkeiten aufzuzeigen.

CONTENTS

PREFACE

This cumulative thesis is structured as follows. We start with a brief introduction into electrochemical interfaces (chapter 2) and surface diffusion (chapter 3), where we also work out the need for the development of a new methodology to measure surface diffusion at electrochemical interfaces. This methodology is subsequently presented in great detail (chapters 4-5), followed by a short description of the sample preparation (chapter 6) that was used for the subsequent measurements. First proof-of-principle *in situ* LOD measurements and additional optical reflectance studies can be found in the condensed form of publications in the chapters 7-8. Finally, in chapter 9 further improvements for the developed methodology are proposed.

Publications are reprinted as published. In this case, all references are listed directly at the end of the publication. Not yet published submitted manuscripts are reprinted as submitted. References can here be found at the end of the thesis. The Supporting Information, denoted SI 1 - SI 3, are reprinted directly after the corresponding publications. Also the references used in the Supporting Information are given at the end of this thesis. Own publications are denoted [LK1–LK3].
For a better integration into this work, single pictures and smaller sections from own publications and the corresponding Supporting Information are reused in the introductory chapters. As all publications and Supplementary Information shall be reprinted completely, there may be duplicates of single figures within this work.

1 INTRODUCTION

On the road to the age of renewable energies, energy storage and conversion systems are becoming increasingly important. Hence, there is major research efforts in developing novel catalysts for hydrogen production by electrolysis, novel electrode materials for upcoming battery technology, and energy-efficient processes for the production of synthetic fuels. What all of this rather applied research has in common is the need to fundamentally understand the basic reactions and processes that happen at electrochemical interfaces. One key process here is surface diffusion, which, simply put, describes the movement of atoms on the electrode. Surface diffusion is often important in the interplay with other reaction kinetics, e.g., for the morphological evolution during electrodeposition [1], and has thus an impact on many nucleation and growth processes [2, 3]. Its relevance for electrocatalysis is discussed in many studies [4, 5], reviews [6], and since recently specifically for the CO_2 reduction reaction [7].

Surface diffusion processes have been investigated under ultrahigh vacuum (UHV) conditions since the development of field emission microscopy in the 1930s. Since then, a variety of different methods has been developed (section 3.3) to either directly observe the motion of single adsorbed atoms (adsorbates), or to monitor collective diffusion phenomena. However, although extensive data on surface diffusion has been collected under UHV conditions [8, 9], this data does not sufficiently describe surface diffusion at electrochemical interfaces. Here, the presence of the adjacent electrolyte and strong electric fields evolving at the interface can develop a tremendous influence on surface diffusion processes [10]. Consequently, *in situ* investigations of surface diffusion at such interfaces are necessary, but prove to be challenging due to the presence of the electrolyte. Many measurement methods established in UHV are not directly applicable in this environment and the few available methods, such as video-rate scanning tunneling microscopy (VSTM), are restricted to the measurement of rather slow diffusion rates. Therefore, studies on surface diffusion at electrochemical interfaces are rare, especially when it comes to diffusion on electrodes used in current energy conversion and storage devices.

Within this work, a new method to measure surface diffusion at such interfaces was developed. The method is all-optical, and as such only little influenced by the electrolyte. It is based on the generation of a periodic spatial modulation of adsorbates (gratings) using two interfering laser pulses. The subsequent equilibration of this pattern and thus the diffusion rate of adsorbates is probed by the linear optical diffraction (LOD) signal from a second laser. This principle has been extensively used for diffusion measurements in vacuum and allows to measure diffusion rates over many orders of magnitude [11–25]. It thus overcomes limitation of established methods like VSTM.

We demonstrate the feasibility of our approach by first proof-of-principle measurements, which were performed on surface diffusion of chemisorbed sulfur (S_{ad}) on the Pt(111) electrode. Platinum electrodes are widely used, e.g., for electrolysis,

which is due to the distinct catalytic properties and the high stability of the metal surface (see chapter 6). For this catalyst, any contamination with sulfur is usually avoided due to the strong binding of S_{ad} to the surface which permanently blocks adsorption and reaction sites (the so-called sulfur-poisoning) and thus effectively inhibits all kinds of surface reactions. Yet, the surface kinetics of S_{ad} have no known influence to the sulfur-poisoning process itself, so S_{ad} diffusion on Pt(111) is basically used as a model system.

As the development of the new methodology was a major part of this work, it is presented in great detail. The overall structure of this thesis is as follows: After a brief introduction into electrochemical interfaces (chapter 2) and surface diffusion phenomena and measurement methods (chapter 3), the basics for LOD diffusion measurements are discussed (chapter 4). Subsequently, the newly developed setup for *in situ* LOD measurements of surface diffusion at electrochemical interfaces is introduced (chapter 5). In chapter 6, the sample preparation is described, which was used for all subsequent measurements. The measurements, results, and a brief description of the developed methodology are presented in the condensed form of publications, which are reprinted in the chapters 7 - 8:
Section 7.1 addresses first studies on the optical and electrochemical properties of the S_{ad}/Pt(111) system. The obtained information allowed us to perform and evaluate first proof-of-principle *in situ* LOD measurements, which are presented in section 8.1. Here, potential and coverage dependent S_{ad} surface diffusion rates could for the first time be measured. In section 8.2, the temporal evolution and interpretation of LOD signals is discussed on basis of S_{ad} surface diffusion measurements and additional numerical simulations of the equilibration of adsorbate gratings. This allowed us to qualitatively describe S_{ad} surface diffusion over a wide coverage range, identify possible pitfalls in the methodology, and develop approaches required for extracting quantitative surface diffusion rates.
Finally, in chapter 9 methodological difficulties are revisited and solutions are proposed to further enhance the developed *in situ* LOD experimental setup. Also relevant systems for subsequent *in situ* LOD studies are discussed in this chapter.

Part I

THEORETICAL BACKGROUND

2 ELECTROCHEMICAL INTERFACES

In this chapter, a brief introduction into electrochemical interfaces will be given, which is the environment where all measurements were performed. A more detailed description can be found in the textbooks of Schmickler [26] an Ibach [27]. To characterize electrodes in electrochemical environment, mainly two methods were used in this work: cyclic voltammetry and optical differential reflectance. These methods will be described in the sections 2.1 and 2.2.

An electrochemical interface is usually given by the phase boundary between a solid crystal surface (electrode) and the adjacent liquid electrolyte. Assuming an electrically isolated electrode, the ions of the electrolyte will react with the electrode surface, leading to a charge transfer. In equilibrium, this leads to a characteristic electrode potential, which is given by the specific electrode/electrolyte combination. In order to characterize and control such electrode reactions, it is necessary to measure and control the electrode potential itself. For this purpose, the potential of the electrode to be investigated, called working electrode (WE), is usually measured against the fixed potential of an additional electrode, the reference electrode (RE). A reference electrode is characterized by its stable and well-known equilibrium potential, which can be well used as reference potential. To avoid any deviation from this equilibrium potential, the potential difference between WE and RE has to be measured with virtually no current flow. By convention, potentials are usually given against the standard hydrogen electrode (SHE), which is based on the H_2/H^+ redox reaction. However, for practical reasons, also other reference electrodes are used. In this work the measurements were carried out with a mercury/mercurous sulfate electrode, which is based on the Hg/Hg_2SO_4 redox reaction. To not only measure but to control the WE electrode potential, a third electrode has to be introduced, called counter electrode (CE). In this configuration, the potential drop on the working electrode and thus its potential relative to the reference electrode is controlled by driving an additional current through counter and working electrode.
To show how controlling the electrode potential can be used to manipulate electrochemical reactions, we imagine a simple redox reaction, where a metal electrode species M is oxidized to M^+:

$$M \rightleftharpoons M^+ + e^- \,. \tag{2.1}$$

Assuming M^+ dissolves into the electrolyte, the electrode will be negatively charged. Without external current flow from the electrode, the reaction reaches equilibrium when the electrode potential equals the potential of the redox-couple. The so-called standard electrode potential Φ_0 of the corresponding redox couple is then given by the potential difference between the WE and the standard hydrogen electrode (SHE). By changing the WE potential and applying a so-called overpotential $\Delta\Phi = \Phi - \Phi_0$, the equilibrium can be disturbed and the reaction can be pushed in a certain direction.

Within this work, we study the movement (surface diffusion) of adsorbates on electrodes. Adsorbates are non-substrate species, usually contained within the electrolyte, which can bind to the electrode surface. If the binding is due to more than just electrostatic interactions, it is called specific adsorption. In this case, one usually differentiates between physisorption, which can be mainly attributed to Van-der-Waals interactions, and chemisorption, where a chemical binding between adsorbate and substrate exists. The surface diffusion studies presented in this work were performed on adsorbed sulfur (S_{ad}), which is a strongly bound chemisorbing species. Similar to redox reactions, adsorption processes are in equilibrium between binding onto the surface and desorption from the surface at a certain electrode potential. This potential is dependent on the Gibbs energy of the solvated adsorbate species in solution, respectively the adsorbed species on the electrode surface. The latter can be further influenced by adsorbate-adsorbate interactions on the surface. Although for the understanding of this work the modeling of adsorption kinetics is not necessary, it should be noted that different approaches exist to describe these kinetics (e.g. Langmuir- and Frumkin-isothermes). We conclude that adsorption processes are dependent on the electrode potential and usually lead to a charge transfer, similar to the above described redox reactions. In the subsequent section we will see that potential dependent measurements of the resulting current can be used to characterize such adsorption process.

But before focusing on these methodological aspects, we want to finish this section by briefly describing the structure of electrochemical interfaces.Even independent of specific reactions and adsorption processes, a certain structure of ions and solvent molecules con be observed here. This so-called electrochemical double layer results from the formation of an electronic excess charges on the electrode and a corresponding ionic counter charge within the electrolyte. It is in particular given by adsorbed ions, the orientation of polar solvent molecules, and an imbalance between cations and anions within the electrolyte close to the electrode. The structure extends into the electrolyte by about $5-20\,\text{Å}$, depending on the electrolyte (ion-concentration) and on the electrode potential Φ [26]. As the potential gradient is spatially localized to the extension of the double layer, strong electric fields on the order of $10^9\ \text{Vm}^{-1}$ can be observed at the interface [26]. We will later see, that these fields may have a tremendous influence to surface diffusion (section 3.2). Although the exact spatial evolution of the potential gradient is difficult to determine, modelling the double layer as a simple plate capacitor often leads to a sufficient description of the potential gradient.

2.1 CYCLIC VOLTAMMETRY

After we have described the electrochemical interface structure and introduced some basic processes at electrodes in electrolyte solution, we will now briefly explain the methods that were used to characterize electrode- and in particular adsorption processes.
One of the most widely used methods is cyclic voltammetry. Here, the potential of the WE is cycled linearly between a low and a high limit, resulting in a triangular potential curve. Simultaneously, the current density j between the WE and CE is

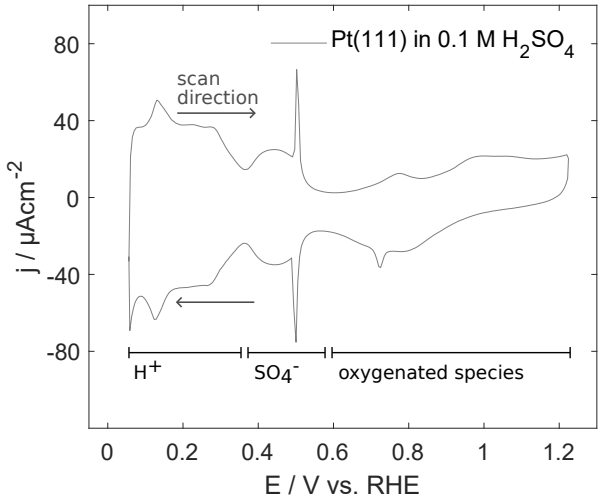

Figure 2.1: Cyclic voltammogram of Pt(111) in 0.1 M H_2SO_4 acquired with a sweep rate of 50 mVs^{-1}. The potential regions for specific adsorption of certain species are indicated.

measured. In a cyclic voltammogram (CV) the current density is plotted against potential (see figure 2.1), which allows to study charge transfer processes and their dependence on the electrode potential. By changing the sweep rate also the corresponding reaction kinetics can be determined. We will discuss this method for the CV of Pt(111) in 0.1 M H_2SO_4 as an example. In the positive going scan (increasing potential) a positive current with distinct peaks can be observed in the range between $0.05 - 0.3$ V. The positive current can be attributed to the desorption of hydrogen from the electrode, which dissolves as H^+ into the solution. The distinct peaks are due to desorption from specific (step) sites, which happens at distinct potentials. Between $0.35 - 0.5$ V a broad peak occurs which merges in another sharp peak at about 0.5 V. While the first peak can be attributed to initial SO_4^- adsorption, the second one is usually associated with a phase transition of the sulfate adlayer. At more positive potentials further peaks evolve, which are due to the adsorption of oxygenated species and surface oxide formation. For the negative going scan complementary peaks can be found. These indicate the subsequent desorption of oxygenated species, sulfate, and also the adsorption of hydrogen. It is worth mentioning, that after more than forty years of applied platinum single crystal electrochemistry, the exact interpretation of many voltammetric features is still under debate. The reason is that cyclic voltammetry is a rather unspecific method which is therefore often used in combination with other complementary methods.

2.2 OPTICAL REFLECTANCE SPECTROSCOPY

In our work, optical reflectance spectroscopy was used as a complementary method to investigate electrode processes. A detailed textbook chapter about this method including a comprehensive summary of experimental results was written by Kolb [28]. The following brief introduction into optical reflectance spectroscopy is mainly based on this publication.

In optical reflectance spectroscopy, reflectance changes of surfaces and interfaces for light in the UV-visible spectral range are measured. In this spectral range, absorption and reflectance are mainly dependent on the excitation of (bound) electrons. If a process, e.g., a chemical reaction, leads to changes in the corresponding electronic states of the system, also changes in the optical reflectance (OR) may in principle be observed. Such changes can for example be induced by changing the electrode potential, by adsorption of adsorbates, or the deposition of thin films onto the electrode. A great advantage of optical reflectance spectroscopy is that measuring OR changes can be realised *in situ* with rather simple setups. In principle only a light source (with stable frequency and intensity) and a detector to measure the reflected light intensity is needed.
In the following, we will address the impact of potential variations and, more important for our work, the impact of adsorbing species on the OR. The impact of potential variations on the OR can be studied with ideal polarizable electrodes, and thus in absence of any faradaic reactions or adsorption processes. In this case, one specifically speaks of changes in electroreflectance, which are mainly resulting from the potential drop at the interface. When changing the electrode potential, this drop leads to a different energy shift in the adsorbate surfaces states, as compared to the bulk states. Consequently, optical transitions from occupied bulk to empty surface states vary with the electrode potential. Interestingly, the resulting OR changes have not only been observed for changes in the electrode potential, but also for changes in the electrolyte concentration. This effect can be understood after recalling, that the electrolyte concentration directly influences the structure of the double layer and thus the potential gradient at the interface.
However, the potential dependent electroreflectance changes are usually rather small as compared to OR changes induced by strongly adsorbing species. Adsorbing species develop a strong OR change either if they are strongly absorbing themselves, or if they are strongly interacting with the substrate and thus changing their own, or the compounds electronic states. In this context it is worth mentioning, that molecules transparent in solution for a certain wavelength may develop a strong absorption band for the same wavelength if bound to a substrate. This effect can for example be observed for adsorbed CO on the Pt(111) surface, which has here an absorption band in the UV range that does not exist for soluted CO molecules. Strong localized bonds occur for example for the oxidation of substrate atoms, which typically leads to pronounced changes in the OR. If adsorbates are only weakly bound and no major changes in the electronic states are introduced, also the OR changes will be small. These species are therefore rather difficult to detect via reflectance spectroscopy.

As excitation spectra for solids in the optical range are often broad and rather unstructured, optical reflectance spectroscopy has no element specificity *per se*. Nevertheless, by investigating a broad optical wavelength range (which is restricted to about $1 - 6$ eV due to the electrolyte), sophisticated studies can be performed, e.g., on the spatial evolution of the potential gradient at the interface. Differential reflectance studies can also be performed at a fixed wavelength, which must not even match an absorption peak in the excitation spectrum (although the detectable OR difference is much more pronounced then). Still in this case the

signal can be used to detect adsorption processes. Also information on the coverage of adsorbates can be obtained, which was often found to be linearly dependent on the reflectance change if no, or only constant interaction between adsorbates exists. In our work, differential reflectance signals were measured for the fixed wavelength of $\lambda = 632$ nm, and were mainly used to obtain information about coverage changes of adsorbates. This was specifically important for the diffusion measurements of chemisorbed sulfur (S_{ad}), where observation of the OR signal in principle allowed to track the S_{ad} coverage *in situ* during the measurements. Apart from differential reflection measurements, optical reflectance changes play an important role also for the LOD based measurements of surface diffusion. As we will see in section 4.2, the LOD signal intensity is here directly related to the reflectance change induced by adsorbates. However, before we take a closer look at the LOD methodology, we will first discuss the basic principles of surface diffusion in the subsequent sections.

3 SURFACE DIFFUSION

Surface diffusion will be first introduced for the most basic case, which is diffusion on surfaces in vacuum environment (section 3.1). In section 3.2 the discussion will be extended to diffusion processes at the electrochemical interface. With this theoretical background provided, an overview over the available measurement methods will be given in section 3.3. This includes the most common techniques in vacuum environment (section 3.3.1) and at electrochemical interfaces (section 3.3.2). We will explicitly show the need for the development of a new measurement technique here, which will be described in the chapters 4 and 5.

3.1 DIFFUSION AT SURFACES IN VACUUM

Crystal surfaces have a certain order, which is given by the termination of the atomic bulk lattice structure. Usually, defined surfaces are obtained by cutting the bulk crystal at a specified angle with respect the crystal axes. The resulting surface lattice consists of substrate atoms arranged in ordered structures with certain translational symmetries (see figure 3.1a,b). On this lattice, adsorbed atoms, or adsorbates, are bound to specific sites. The resulting adsorbate-substrate interaction can be described by a two-dimensional periodic potential-hypersurface which has the same translational symmetry as the surface itself. In this picture, the occupied surfaces sites are given by wells within the hypersurface. However, adsorbates are not permanently bound to their sites, but may also jump to equivalent neighbouring sites. Figure 3.1c) illustrates the corresponding adsorbate-substrate interaction potential for an adsorbate movement along the axis of high symmetry. The necessary energy to overcome the potential barrier E_m between neighbouring sites is usually provided by coupling to substrate phonons. E_m is thus significantly smaller than the desorption energy E_b. In few cases, also quantum mechanical tunneling through the barrier may be relevant. If the average thermal energies $k_B T$ of adsorbates are on the order or exceeding E_m, the adsorbate movement on the surface is rather unrestricted and independent of specific sites. In most cases, however, $k_B T$ is much smaller than E_m. In these cases, the probability to overcome the energy barrier is specifically related to the energy distribution of substrate phonons. Hence, jumps to neighbouring sites can be described statistically with an average hopping frequency Γ. The hopping frequency [8, 9]

$$\Gamma = \nu \cdot exp\left(-E_m / k_B T\right) \tag{3.1}$$

is dependent on the energy barrier E_m, the temperature T and the effective attempt frequency ν. The latter can be associated with the vibrational frequency of the adsorbate in the adsorption well [8] and can for example be obtained by transition state theory. For an isotropic surface, jumps in x- and y- direction are statistically

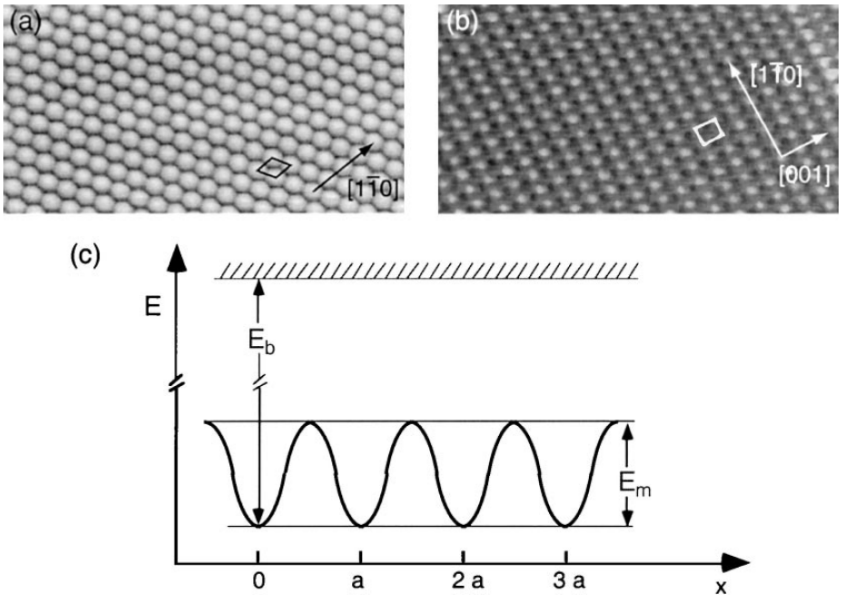

Figure 3.1: STM images resolving (a) the hexagonal atomic structure of the close-packed f.c.c.(111) surface and (b) the anisotropic f.c.c.(110) surface of Ag. The surface unit cells and high symmetry directions are marked. (c) Schematic one-dimensional potential energy surface experienced by an adsorbate along a high-symmetry surface direction (E_m: migration energy barrier; E_b: bonding energy; a: surface lattice constant). Figure and caption reprinted with permission from [8]. Copyright 2000 Elsevier Science B.V.

equally distributed and lead to a a two dimensional random walk of the adsorbate. The mean square displacement of the adsorbate can thus be described by: [8, 9]

$$< \left(\overrightarrow{r\,(t)} - \overrightarrow{r\,(t_0)}\right)^2 > \; = \; < \left(\overrightarrow{\Delta r}\right)^2 > \; = \; a^2 \Gamma t \; , \tag{3.2}$$

with a being the mean jump length between neighbouring sites and t the time elapsed. So far we considered the movement of single, isolated adsorbates, which is defined as tracer diffusion. The corresponding diffusion rate is described by the tracer diffusion coefficient D^*: [8, 9]

$$\begin{aligned} D^* &= \frac{< \left(\overrightarrow{\Delta r}\right)^2 >}{4t} && (3.3) \\ &= \frac{1}{4} a^2 \nu \cdot exp\left(-E_m / k_B T\right) && (3.4) \\ &= D_0^* \cdot exp\left(-E_m / k_B T\right) . && (3.5) \end{aligned}$$

Such a diffusion process can be described by a prefactor D_0^* and the energy barrier E_m. It is remarkable that this rather simple law could indeed be reproduced in many experiments. Especially for tracer diffusion, D_0^* was generally found to be temperature independent [8]. In these cases, equation 3.5 describes the so-called Arrhenius-behaviour. The energy barrier E_m can then be determined by temperature dependent measurements of the diffusion constant. In a graphical form, the Arrhenius-behaviour becomes evident in a linear relation between $ln\left(D^*\right)$ and T^{-1} with a slope of $-\frac{E_m}{k_B}$ (see figure 3.2).

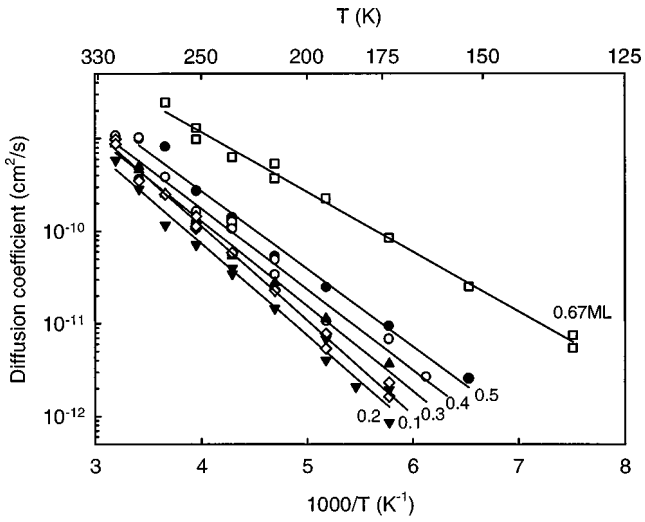

Figure 3.2: Arrhenius plots of the diffusion coefficient D for CO on Pt(111) for CO coverages from 0.1 to 0.67 ML as indicated. Figure and caption reprinted with permission from [14]. Copyright 1998 The American Physical Society.

In the above, we have investigated the movement of single, isolated adsorbates. The assumption of isolated adsorbates is certainly not always fulfilled, though. A necessary condition is that the neighbouring and nearby sites of each adsorbate are unoccupied. Let us quantify the occupation of sites by means of the local coverage $\Theta(\vec{r})$:

$$\Theta(\vec{r}) = \frac{N_{occ}(\vec{r})}{N_{tot}(\vec{r})}, \tag{3.6}$$

which is given as the relation between the occupied surface sites N_{occ} and the total number of surface sites available for adsorption N_{tot} in a certain area around $\vec{r}$. We remark that in the literature, there are two different conventions for the coverage Θ. Most commonly, the available surface sites N_{tot} are considered equal to the number of surface atoms of the substrate. Alternatively, N_{tot} is defined as the maximum number of sites that can be occupied by a specific adsorbing species, if this is packed in its most densest phase. Within this work, the first definition will be used. The maximum obtainable coverage is therefore given by a monolayer (ML) of adsorbates, meaning the number of adsorbates equals the number of substrate atoms forming the surface. Smaller coverages are given in % related to the fully covered monolayer. Measurements of tracer diffusion are usually performed at coverages on the order of 5% or lower [29, 30].
At higher coverages, adsorbate-adsorbate interactions become relevant for surface diffusion, which is not reflected in the energy barrier E_m of equation 3.5. Interestingly, however, many systems can still be described using an Arrhenius-like behaviour: [8]

$$D(\Theta) = D_0(\Theta) \cdot exp(-E_d(\Theta)/k_bT), \tag{3.7}$$

with $D(\Theta)$ called the chemical or collective diffusion coefficient, now depending on the adsorbate coverage. The corresponding energy barrier $E_d(\Theta)$ does not only

reflect the adsorbate-substrate interactions, but also the adsorbate-adsorbate interactions at a certain adsorbate coverage. It therefore equals E_m at the zero coverage limit. Figure 3.2 shows a typical Arrhenius-like behaviour for the surface diffusion of CO on Pt(111). Here, the different diffusion behaviour with alternating adsorbate coverage becomes evident.

So far, surface diffusion was described on the microscopic level, where it manifests in hopping processes of single atoms between distinct adsorption sites. However, naturally, the motion of single adsorbates is rather difficult to observe. From an experimental point of view, it might be easier to monitor collective diffusion phenomena, that occur on a macroscopic level. Correspondingly, also the developed *in situ* LOD methodology is based on the observation of such phenomena, specifically on observing the equilibration of local coverage differences.
Collective diffusion phenomena can be described by a diffusion flux density of adsorbates [8, 9]

$$\vec{j}\,(\vec{r},t) = -D\,(\Theta)\,\nabla\Theta\,(\vec{r},t)\ , \tag{3.8}$$

which, in combination with the continuity equation [8, 9]

$$\nabla\vec{j}\,(\vec{r},t) = -\frac{\delta\Theta\,(\vec{r},t)}{\delta t}\ , \tag{3.9}$$

leads to Fick's second law: [8, 9]

$$\frac{\delta\Theta\,(\vec{r},t)}{\delta t} = \nabla\cdot D\,(\Theta)\,\nabla\Theta\,(\vec{r},t)\ . \tag{3.10}$$

This equation describes macroscopic mass transport on a surface. We note that, since we have modelled the flux as macroscopic here, we ignore the microscopic surface structure. Equation 3.10 is thus only applicable if coverage variations at the atomic level are small [31]. As the coverage variations in *in situ* LOD have a periodicity of several hundreds of nanometers, equation 3.10 can be well applied to model the diffusion processes of coverage modulations that are used in the developed methodology (see section 4.3).
In section 3.3 we will introduce different methods to measure surface diffusion, before we focus on the actual LOD methodology in chapter 4. We will see, that indeed, mainly two different approaches exist for measuring surface diffusion: either by directly observing single adsorbate motion, or by observing collective diffusion phenomena, e.g., the fluctuation of local coverage variations.

3.2 DIFFUSION AT THE ELECTROCHEMICAL INTERFACE

Before describing further experimental methods, the theoretical description of surface diffusion will be completed in this section. For this purpose, the principles of diffusion at surfaces in vacuum will be extended to diffusion processes at the electrochemical interface.
In this environment, surface diffusion basically follows the same principles as on surfaces in vacuum. However, due to the presence of the electrochemical double layer (see chapter 2) the adsorbate-substrate interaction is further influenced by the

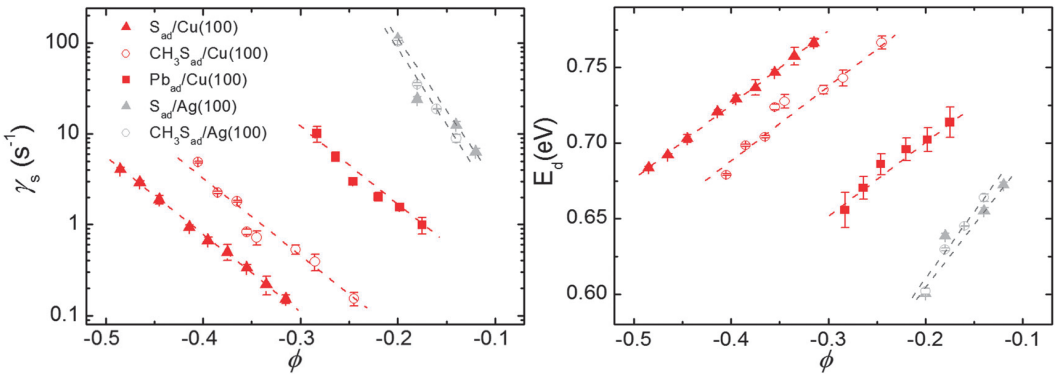

Figure 3.3: Average hopping rates γ_S between neighboring lattice sites (left) and corresponding diffusion barriers E_d (right) showing linear dependency on the electrode potential Φ for several adsorbate systems in electrochemical environment. Adapted with permission from [10]. Copyright 2013 Royal Society of Chemistry.

potential drop, respectively the strong local electric fields F_{DL} at the interface. An in-depth treatment of this interaction is rather complicated, since the exact spatial evolution of the potential gradient is difficult to determine. In view of this, it is remarkable that a linear relation between the hopping rates Γ (in figure 3.3 left, denoted γ_S) and the applied electrode potential Φ has experimentally been found for the surface diffusion of several systems. The same applies to the dependence of the diffusion barrier E_m (in figure 3.3 left, denoted E_d) on the electrode potential. In the following, we will focus on modeling this very change of the diffusion barrier E_m with the potential. Based on the experimental observations, E_m can be described with a constant term E_0 and a linear term $\alpha \cdot \Phi$ that is dependent on the potential: [10, 30, 32]

$$E_m = E_0 + \alpha \cdot \Phi \, . \tag{3.11}$$

This behavior can be explained by a simple model, that has already been used to describe the mobility of surface defects [27, 33]. Here, the potential gradient is assumed constant over the range of the electrochemical double layer. The double layer is thus, figuratively speaking, approximated by a plate capacitor. The interaction between surface species and the local electric field F_{DL} is described using the surface species' surface dipole moment μ. During adsorbate hopping to a neighboring site, the corresponding dipole moment changes by an amount $\Delta\mu$ due to the adsorbates' location- and thus the electronic structure change in the activated site [10]. In this transition state, the resulting electrostatic energy change is given by: [32]

$$\Delta W = F_{DL} \cdot \Delta\mu \tag{3.12}$$

$$= \frac{\sigma}{\epsilon_0} \cdot \Delta\mu \, . \tag{3.13}$$

Approximating the electrochemical double layer by a plate capacitor, the local electric field is given by $F_{DL} = \sigma \cdot \epsilon_0^{-1}$, and is thus only dependent on the surface

charge density σ and the dielectric constant in vacuum ϵ_0. The derivative of equation 3.13 with respect to Φ leads to:

$$\frac{\delta \Delta W}{\delta \Phi} = \frac{\Delta \mu}{\epsilon_0} \cdot \frac{\delta \sigma}{\delta \Phi} \tag{3.14}$$

$$= \frac{\Delta \mu}{\epsilon_0} \cdot C_d \, . \tag{3.15}$$

Note that equation 3.15 only holds if the differential capacitance of the electrochemical double layer C_d, which can be determined experimentally [30], and $\Delta\mu$ are constant within the studied potential range [10]. In this case, the potential dependence of the diffusion barrier E_m can be described by introducing the electrostatic energy change in the transition state as an additional term: [30]

$$E_m(\Phi) = E_0 + \left(\frac{\Delta \mu}{\epsilon_0} \cdot C_d \cdot \Phi \right) \, . \tag{3.16}$$

Similar to diffusion at surfaces in vacuum, an Arrhenius-like diffusion behaviour can also be expected at the electrochemical interface: [10]

$$D(\Phi) \sim exp\left(-E_m(\Phi)/k_b T\right) \, . \tag{3.17}$$

However, the diffusion barrier E_m can here additionally be influenced by the applied electrode potential Φ.

3.3 MEASUREMENT TECHNIQUES

With the essential theory covered, we can now discuss the techniques used to measure surface diffusion. As such measurements have been performed at surfaces in vacuum for almost a century now, we will first describe the evolution of methods in vacuum environment (section 3.3.1), followed by an overview over available methodology at electrochemical interfaces (section 3.3.2).

3.3.1 *Methods at surfaces in vacuum*

To measure surface diffusion in vacuum environment, a variety of different methods exists, and we will only briefly summarize the most common techniques in the following. The corresponding measurement ranges and typical applications of selected methods are given in table 3.1. For more details, including the comparison between single methods and a summary of measurement results of various systems, the reader is referred to the excellent reviews of R. Gomer [9] and J.V. Barth [8], on which this section is mainly based on.
Surface diffusion in vacuum environment has been observed since the development of field emission microscopy (FEM) in the 1930s. In this technique, electrons are emitted from a metal tip under the influence of a high electric field. The measured emission current is dependent on the local work function and thus the presence of adsorbates. Motion of adsorbates has been investigated using different variations of the method. In early measurements, mainly the diffusion of gas atoms (H, CO, O) on substrate metal materials (W, Mo, Re, Ta, Pt) were investigated. Today, the

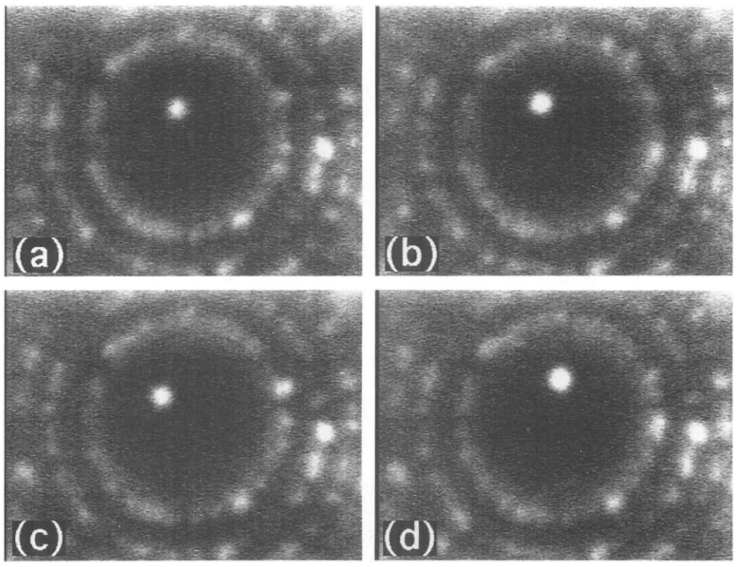

Figure 3.4: Series of field ion microscope images showing the procedure used in single-atom surface diffusion studies. The high-contrast spot is a Pt adatom on a Rh(100) plane. The images are recorded with the tip at 77 K. Adatom motion is induced by warming the tip to 345 K for 30 s between each photograph. Figure and caption reprinted with permission from [34]. Copyright 1994 Elsevier Science B.V.

technique is rather outdated due to the limited resolution of ≈ 30 Å and limitations in the substrate materials which have to withstand the high electric fields.

With field ion microscopy (FIM), developed in the 1950s, the observation of single adsorbates became possible (see figure 3.4). Using a similar setup as in FEM, the method is based on the ionisation of an imaging gas (Ar, Ne) at a metal tip in presence of a high electric field. The ionized gas atoms are accelerated along the lines of force onto a fluorescence screen. Due to the curvature of the tip, a magnification of the sample surface can be observed, with the contrast mainly resulting from differences in the local ionisation probability. To measure surface diffusion, an image of the sample surface is first acquired at low temperature for increased resolution. The sample is then heated to stimulate surface diffusion. After subsequent cooling another image is acquired and the motion of single adsorbates can be determined by changes in the particle distribution between both images. With FIM, mainly the diffusion of single metal adsorbates on metal surfaces was investigated. Less strongly bound adsorbates easily desorb in presence of the high imaging fields and are therefore more difficult to measure.

Scanning tunneling microscopy (STM), developed in the 1980s and awarded shortly after with a nobel prize, similarly to FIM allows imaging a limited area of the sample surface with atomic resolution. In contrast to FIM, the method is however far more flexible and especially not restricted to measurements in vacuum under highest electric fields and using sharp sample tips. For STM measurements, the flat (conductive) sample is scanned with an atomically sharp tip held at a distance where the tunneling current between sample and tip can be measured. Using this principle, a representation of the sample surface can be generated. The motion of single adsorbates can thus be tracked by analysing subsequently acquired STM

images. Although video-rate STM (VSTM) allows image acquisition on the order of 100 Hz, the probed spot size is restricted to something like 200 Å, which strongly limits the possible detectable diffusion rate. The method was therefore predominantly used to measure tracer diffusion of adsorbate-substrate systems with diffusion rates on the order or slower than 10^{-16} cm^2s^{-1}.
As a complementary method, quasielastic helium atom scattering (QHAS) can be used to probe a surface in reciprocal space. The presence of mobile adsorbates here leads to minor energy exchanges between adsorbates and the scattered helium atoms. The corresponding broadening in the energy distribution of the detected helium beam can be used to determine the hopping rate of adsorbates. The broadening must be within the detection range, which limits the method to diffusion rates faster than 10^{-6} cm^2s^{-1}. Hence, diffusion of rather weakly bound adsorbate like CO, H and Xe on metal surfaces have been studied so far.

The previously described methods are directly tracking single adsorbates (FIM, STM), or use collective adsorbate motion on homogenous adlayers at low coverages (QHAS) to measure adsorbate hopping rates. In a different approach, a local adsorbate coverage variation is firstly created and the subsequent equilibration of the coverage is then monitored using either electrons or optical methods. Such a process can be described using Fick's first (equation 3.8) or second law (equation 3.10). Correspondingly, these methods, usually denoted as profile evolution techniques, can in principle be used to determine the collective diffusion coefficient $D(\Theta)$ also in relation to the coverage Θ.
First approaches were developed using laser-induced thermal desorption (LITD), where an adsorbate covered sample is depleted from adsorbates in a small defined area using a focused laser pulse at the time $t_0 = 0$. Due to diffusion, the area is subsequently refilled with adsorbates. The time dependency of this process can be monitored by repeated desorption of all adsorbates within the same area with a second laser pulse at the time $t_1 > t_0$. In this way, the amount of adsorbates which have moved into the probed area can be measured by mass spectrometry. In principle, these information are sufficient to determine the diffusion coefficient. Hence, the method has been employed for a wide range of adsorbates (H, O, CO, noble gases, other physisorbates and larger molecules) on single crystal surfaces. The resolution of the method may, however, be influenced by coverage dependent adsorbate-adsorbate interactions and laser induced substrate imperfections.
In a variation of this method, the refilling of the previously depleted area (by LITD) is continuously monitored by photoemission electron microscopy (PEEM). PEEM uses the work function changes between adsorbate covered and uncovered areas to spatially resolve the adsorbate coverage evolution. In addition, PEEM images provide information about the surface morphology, which allows to study the influence of defects to surface diffusion.
The described refilling process can also be observed optically. Specifically this can be done by monitoring the optical reflectance changes ΔR within the depleted area, as the optical reflectance R directly depends on the coverage of adsorbates (see section 2.2). However, an even more sophisticated optical method was developed in the early 1990s, where instead of a hole, a one dimensional adsorbate grating structure is created by LITD using two interfering laser pulses. The equi-

libration of this structure is then monitored by the optical diffraction signal of a second laser from the grating. This can be done using either the linear optical diffraction signal (LOD) or diffraction of the second-harmonic-generated signal (SHD). In both cases, the diffusion coefficient can be determined from the signal decay. The method will be described in detail in chapter 4, as the major part of this work addresses the adaptation of LOD for diffusion measurements at electrochemical interfaces.

Table 3.1 shows that a variety of methods is available that allow diffusion measurements for most systems in vacuum environment. Smallest diffusion barriers of $E_m \leq 9.6$ meV could be observed for the diffusion of Xe on Pt(111) using QHAS [35]. Large diffusion barriers were investigated using STM, i.e., for diffusion of O on Al(111) $E_m = 1000$ meV [36] and for diffusion of S on Pt(111) $E_m = 570 \pm 50$ meV [37]. For the latter, hopping rates Γ in the range between $2 \cdot 10^{-3}$ s^{-1} at 200 °K and $5 \cdot 10^{-5}$ s^{-1} at 185 °K were measured.

Method	Remarks	Studied adsorbates	Length scale	Range of D $(\mathrm{cm^2 s^{-1}})$
STM	Tracer diffusion, direct observation, study of interactions	N, O, S, CO, O_2, C_{60}, organic molecules	10 Å	$10^{-19} - 10^{-16}$
QHAS	Tracer diffusion, frustrated translation	CO, S, H, Xe	10 Å	$> 5 \cdot 10^{-6}$
FEM	Refractory metal tips	H, N, O, CO		
Fluctuation	Collective diffusion		100 Å	$10^{-14} - 10^{-9}$
Shadowing	Collective diffusion, averages over planes		100 - 1000 Å	$10^{-12} - 10^{-10}$
LOD/SHD	Collective diffusion, coadsorbate systems	H, CO, NH_3	1 μm	$10^{-15} - 10^{-7}$
PEEM	Collective diffusion, study of defects	CO, O	$0.1 - 1000$ μm	$10^{-9} - 10^{-5}$
LITD	Collective diffusion, 'macroscopic' coadsorbate systems	H, CO, O, organic molecules	$100 - 1000$ μm	$10^{-8} - 10^{-5}$

Table 3.1: Principal methods for surface diffusion studies on non-metallic adsorbates on metals in vacuum. Table and caption reprinted with permission from [8]. Copyright 2000 Elsevier Science B.V.

3.3.2 *Methods at electrochemical interfaces*

In comparison to the extensive surface diffusion data that has been acquired in vacuum environment, surface diffusion has been only little studied at electrochemical interfaces so far. The main reason for this lack of studies is the lack of suitable experimental methodology. Experimental methods that use electrons or ions to probe the motion of individual adsorbates (FIM, QHAS) or the evolution of adsorbate coverage variation (FEM, PEEM) are not applicable here, due to the presence of the electrolyte. Also using traditional LITD, where the refilling of the previously depleted area is probed by mass spectrometry, is not possible for the same reason. From the here mentioned conventional methods used in vacuum, only all-optical methods and scanning probe microscopy can be used in presence of electrolyte solution.
Hence, most available surface diffusion studies are based on electrochemical STM or video-rate STM measurements where single adsorbate motion is either directly observed [10, 30], or by monitoring fluctuation of atomic steps [31, 38, 39] or adatom island shapes [33, 39]. As already discussed, such studies are restricted to systems with rather slow diffusion rates and therefore often limited to model systems. Lastly, few additional studies based on nuclear magnetic resonance spectroscopy (NMR) should be mentioned [40].
It becomes apparent that, to our knowledge, all-optical methods have not yet been applied in electrochemical environment. In fact, however, methods such as LOD would be particularly interesting here because of their high dynamic measurement range. To close this gap, within this work the all-optical LOD technique was adapted to measure surface diffusion also at electrode surfaces in electrochemical environment. In the upcoming chapter, we will provide a detailed overview over the LOD methodology (chapter 4), that will culminate in a brief discussion over the methodological key differences between LOD applied in vacuum environment or at electrochemical interfaces (section 4.4). This will finally lead us to a detailed description of the developed experimental setup for *in situ* LOD measurement in electrochemical environment (chapter 5).

4 MEASUREMENT OF SURFACE DIFFUSION USING LINEAR OPTICAL DIFFRACTION

Using the linear optical diffraction signal (LOD) from an adsorbate grating, collective surface diffusion phenomena can be effectively observed. The basic measurement principle of this method is depicted in figure 4.1. First, a spatial coverage modulation of adsorbates (grating) is created by two interfering laser pulses that induce localized thermal desorption of adsorbates. The diffusion-induced decay of the created grating is then monitored by the optical diffraction signal of a second laser. From the subsequent decrease of the diffraction signal, the diffusion rate of adsorbates can be determined. This way, diffusion rates can be measured over several orders of magnitude ($10^{-7} - 10^{-16}$ cm^2s^{-1}) [20], at variable adsorbate coverages Θ, and even anisotropy of surface diffusion can be investigated. Before going into further experimental details of the LOD methodology, let us first have a look at the historical evolution this technique. Therefore, we will summarize the most prominent LOD studies of the last thirty years (in vacuum environment) in order to highlight the versatility of the already existing methodology.
For surface diffusion measurements of adsorbates in vacuum, the method was to a large extent developed and improved by Zhu *et al.* [11, 18–20] and later Xiao *et al.* [21–24] in the early 1990s. In early works, CO diffusion on Ni [11, 22, 24] was investigated. The determined diffusion rates, activation energies and pre-exponential factors revealed a strongly anisotropic diffusion behaviour here. Furthermore, coverage dependent diffusion rates and repulsive CO-CO interactions could be observed for CO coverages $\Theta \geq 0.7$. On the same substrate, temperature dependent diffusion measurements of hydrogen and deuterium [12, 25] indicate the presence two different diffusion processes for both species, namely quantum mechanical under-barrier tunnelling at temperatures below 160 °K and classical over-barrier hopping at temperatures above 160 °K. A similar behaviour could be observed for the diffusion of hydrogen and deuterium on Pt(111) [13]. Here, Zeng *et. al* could even demonstrate a strong influence of the sample step density on the under-barrier tunneling rate. For the classical over-barrier hopping, repulsive H-H interaction were found in coverage dependent studies [41]. Interestingly, minor sample miscut (enhanced step density) here lead to slightly enhanced diffusion rates perpendicular to the steps as compared to the flat surface. The effects of stepped surfaces were also investigated for surface diffusion of CO on Pt(111) [14–16]. In these studies, Ma *et al.* found a dramatic decrease of diffusion rates perpendicular to the steps but a strong enhancement of the diffusion rates along the steps as compared to the flat surface. The coverage dependence of diffusion rates was found relatively weak, but a slight repulsive CO-CO interaction could still be observed. The presence of different diffusion channels, as diffusion along or perpendicular to steps and diffusion by quantum tunneling or over-barrier hopping, could also be observed for CO diffusion on a phosphorus-contaminated Pt(111) surface [17]. Here, the rather slow diffusion over the clean terraces as compared

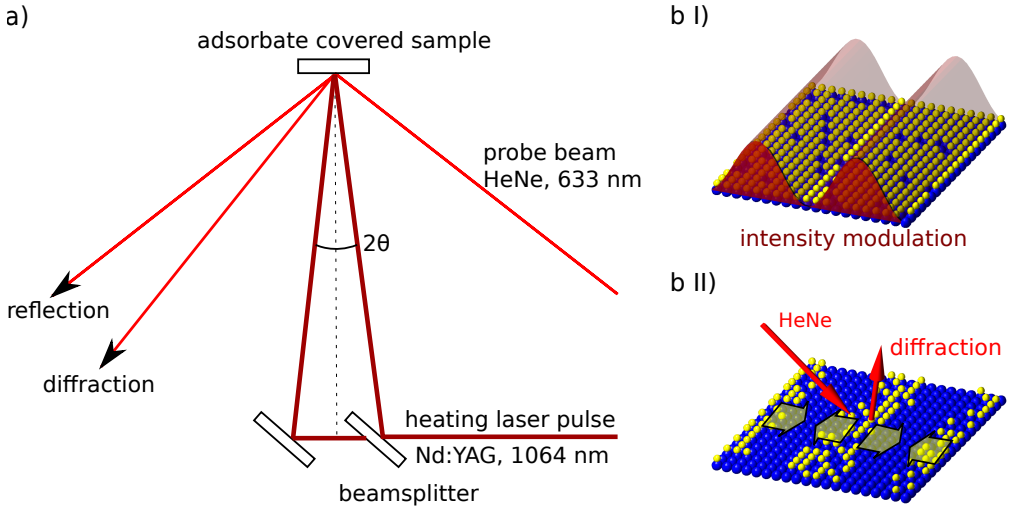

Figure 4.1: Basic setup (a) and measurement principle (b) for the creation (b I) of an adsorbate grating and detection of its diffusion-related decay (b II), which is used to determine the surface diffusion rate of adsorbates.

to faster diffusion over the contaminated surface regions could even be measured simultaneously.
After this brief overview of the most important LOD studies, the measurement method will now be described in detail step by step. In section 4.1, the laser induced creation of adsorbate coverage modulations (gratings) will be discussed. Section 4.2 deals with the detection of such gratings using optical diffraction. In section 4.3 the diffusion-related decay of such gratings and the corresponding decrease of the detected diffraction signal intensity is described using a simple model. In most cases, this model is sufficient to determine the diffusion rate of adsorbates from the evolution of the diffraction signal. Unless noted otherwise, we explicitly describe the method as it was developed for measurements in vacuum. However, all basic principles are valid also for measurements at solid-liquid interfaces. In section 4.4 the main differences between measurements in vacuum and at solid liquid interfaces will be discussed.

4.1 GRATING CREATION

For creating adsorbate gratings, the sample is first covered with an appropriate amount of adsorbates. At surfaces in vacuum, this is usually done by adsorption from the gas phase. Using two interfering laser pulses, an intensity (see section 4.1.1) and thus a temperature modulation (see section 4.1.2) is then created on the sample surface. The temperature modulation leads to localized thermal desorption of adsorbates (see section 4.1.2), creating the adsorbate grating structure.

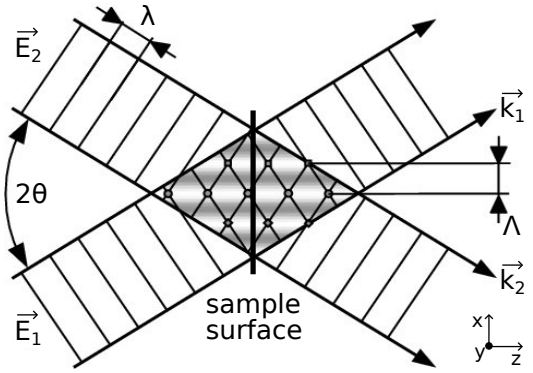

Figure 4.2: Interference grating created by the interference of two incident light waves. Adapted with permission from [42]. Copyright Springer 2006.

4.1.1 *Intensity modulation*

In the following, the interference of the two laser pulses will be briefly described. The section is based on a textbook chapter of Günther [42], where light induced dynamic gratings are described in greater detail.
The electric fields $\vec{E_j}$ of both laser pulses (j=1,2) can be described by plane wave functions (ignoring the temporal intensity evolution), which are given by:

$$\vec{E_j}(\vec{r},t) = \vec{A_j} \cdot exp\left[i\left(\vec{k_j}\cdot\vec{r} - \omega t + \varphi_j\right)\right] \quad . \tag{4.1}$$

While the angular frequency ω is the same for both waves, the phases φ_j and amplitudes $\vec{A_j} = A_j \cdot \vec{p_j}$, including polarization information $\vec{p_j}$, may differ. Also the wave vectors $\vec{k_j}$, which depend on the propagation direction, are different. For simplicity, we assume s-polarized light and symmetric incident angles $\pm\,\theta$ for both waves, as depicted in figure 4.2. In this case, the wave vectors $\vec{k_j}$ and amplitudes $\vec{A_j}$ are given by:

$$\vec{k_1} = \begin{pmatrix} -sin(\theta)\cdot\frac{2\pi}{\lambda} \\ 0 \\ cos(\theta)\cdot\frac{2\pi}{\lambda} \end{pmatrix}, \; \vec{k_2} = \begin{pmatrix} sin(\theta)\cdot\frac{2\pi}{\lambda} \\ 0 \\ cos(\theta)\cdot\frac{2\pi}{\lambda} \end{pmatrix}, \; \vec{A_j} = \begin{pmatrix} 0 \\ A_j \\ 0 \end{pmatrix}. \tag{4.2}$$

Superposition of both waves leads to a spatial intensity modulation on the sample surface:

$$\begin{aligned} I(\vec{r},t) &\propto |\vec{E_1}(\vec{r},t) + \vec{E_2}(\vec{r},t)|^2 \\ &\propto \vec{A_1}^2 + \vec{A_2}^2 + 2\vec{A_1}\cdot\vec{A_2}\cdot cos\left(\left(\vec{k_2}-\vec{k_1}\right)\cdot\vec{r} + (\varphi_2-\varphi_1)\right) \\ &\propto A_1^2 + A_2^2 + 2A_1A_2\cdot cos\left(\frac{4\pi sin(\theta)}{\lambda}\cdot x + (\varphi_2-\varphi_1)\right), \end{aligned} \tag{4.3}$$

with the periodicity Λ:

$$\Lambda \;=\; \lambda/\left(2sin(\theta)\right). \tag{4.4}$$

Assuming incident laser pulses with equal amplitudes $A_1 = A_2$, the usage of s-polarized light leads to a fully modulated intensity on the sample surface. For

single laser pulses with a length on the order of nanoseconds, the phase difference $\Delta\varphi = \varphi_2 - \varphi_1$ can be assumed constant for the length of the pulse, and has thus no influence on the spatial or temporal evolution of the grating. However, if a sequence of single pulses (pulse train) is used, any movement of the optical setup and possible density fluctuations within the propagation medium (e.g., an electrolyte), may lead to deviations in $\Delta\varphi$ between subsequent pulses. Such deviations would manifest in positional fluctuations between the corresponding interference patterns. The same effect would also be expected for drifts in the beam point position between subsequent pulses. Unfortunately, we could indeed observe such effects in the performed *in situ* LOD measurements (see section 8.1 and [43]). We will later see, that this may complicate the grating creation process, if the use of multiple pulses is necessary here (see section 4.4).
For LOD measurements, it would be useful to create gratings with variable average adsorbate coverage and different modulation depths. Specifically, the creation of adsorbate gratings with shallow modulation depth is important in order to obtain accurate measurements results (see section 8.2). In vacuum environment, such gratings were obtained by introducing an addition intensity offset, instead of using the fully modulated intensity. Such an offset can be obtained by turning the polarization of one beam by the angle ξ using a half wave plate. Neglecting any phase differences $\Delta\varphi$ and assuming equal amplitudes $A = A_1 = A_2$, the spatial intensity modulation on the sample surface is then given by: [20]

$$I^{mix}\left(\vec{r}\right) = 2A^2 + 2A^2 \cdot cos\left(\xi\right) \cdot cos\left(\frac{4\pi sin\left(\theta\right)}{\lambda} \cdot x\right) \quad , \tag{4.5}$$

with an intensity offset of $2A^2\left(1 - cos\left(\xi\right)\right)$. Even greater flexibility in controlling the intensity offset can be obtained by additionally adjusting the intensity of one beam [20].

4.1.2 *Energy transfer and thermal desorption*

The energy transfer and temperature evolution on the sample surface can be described by a simple laser heating model [44]. The resulting thermal desorption kinetics will be described at the end of this section.
For the heating model, one assumes that the fraction of energy which is not reflected from the sample surface is instantaneously converted into heat. The heat flux $q\left(x,t\right)$ onto the sample surface $\left(x = 0\right)$ is then given by:

$$q\left(x = 0, t\right) = \left(1 - R\right) \cdot I\left(t\right) \ . \tag{4.6}$$

Assuming the sample surface being the interface between two different media (j=1,2), e.g., a vacuum-solid, or a liquid-solid interface, further heat fluxes will develop into both media depending on their thermal conductivities κ_j and thermal diffusivities α_j. In this case, evaluation of the heat equation

$$\frac{\delta^2 \Delta T}{\delta x^2} = \frac{1}{\alpha_j}\frac{\delta \Delta T}{\delta T} \tag{4.7}$$

has the following solution for the temperature change at the interface (x=0): [44]

$$\Delta T\left(t\right) = \left[\frac{\kappa_1}{\sqrt{\alpha_1}} + \frac{\kappa_2}{\sqrt{\alpha_2}}\right]^{-1} \int_0^t \frac{\left(1 - R\right) I\left(t - t'\right)}{\sqrt{\pi t}} dt' \ . \tag{4.8}$$

For a uniform laser pulse with the pulse length t_0, this expression can be simplified to: [44]

$$\Delta T(t) = \frac{2(1-R)I}{\sqrt{\pi}} \left[\frac{\kappa_1}{\sqrt{\alpha_1}} + \frac{\kappa_2}{\sqrt{\alpha_2}} \right]^{-1} \left(\sqrt{t} - \sqrt{t - t_0} \right) . \tag{4.9}$$

The expression is valid for $t > t_0$. It will now be used to estimate the laser induced temperature changes for different interfaces and laser parameters as applied in LOD measurements. A uniform s-polarized laser pulse (wavelength $\lambda = 532$ nm, pulse energy $E = 300$ mJ, pulse width $t_0 = 5$ ns, beam diameter $d = 9.5$ mm, incident angle $\theta = 17.9°$, normalized intensity $I = 75$ MWcm^{-2}) incident at the vacuum-platinum interface ($\kappa_2 = 0.69$ Wcm^{-1}K^{-1} [45], $\alpha_2 = 0.24$ cm^{2}s^{-1} [45], $\kappa_1 = 0$, refractive index $n_2 = 0.48 - 4.87i$ [46], reflectance $R = 0.93$ according to fresnels' law) would result in a maximum temperature change of $\Delta T_m = 2 \cdot 297$ °K $= 594$ °K at the surface (considering the factor 2 for constructive interference). For the water-platinum interface ($\kappa_1 = 5.9 \cdot 10^{-3}$ Wcm^{-1}K^{-1} [47], $\alpha_1 = 1.43 \cdot 10^{-3}$ cm^{2}s^{-1} [47], refractive index $n_1 = 1.33 - 1.50 \cdot 10^{-9}i$ [48], reflectance $R = 0.91$ according to fresnels' law), a maximum temperature change of $\Delta T_m = 2 \cdot 344$ °K $= 688$ °K can be expected. The calculated temperature changes are similar, as in both cases most heat dissipates through the platinum crystal and the presence of water mainly influences the reflectance R. The values were calculated for the newly developed experimental setup with maximum pulse energies possible. Pulse energies of around $E = 50$ mJ, which were finally used for the measurements, result in smaller temperature changes of only $\Delta T_m = 115$ °K. We conclude that by using nanosecond laserpulses with energies of up to a hundred mJ, temperature changes can be obtained which are sufficient to induce thermal desorption of adsorbates without damaging the substrate itself. However, we already denote here that the pulse energies must be strictly limited to avoid damaging the sample surface. Exceeding certain pulse energies, grating structures can be even created within the substrate [43].
For $t >> t_0$, the temperature evolution at the interface can be approximated by: [44]

$$\Delta T(t) \approx \Delta T_m \sqrt{\frac{t_0}{t}} . \tag{4.10}$$

Accordingly, after the time $t = 0.5$ μs (pulse length $t_0 = 5$ ns), ΔT has subsided to $10\% \cdot \Delta T_m$ and after $t = 50$ μs, ΔT is already at $1\% \cdot \Delta T_m$. Consequently, laser induced temperature changes and thus the thermal desorption process occurs within the time range of nano- to microseconds.

The thermal desorption kinetics are directly dependent on the temperature evolution and can be described using the Polanyi-Wigner equation: [49]

$$\frac{d\Theta}{dt} = -\nu(\Theta)\,\Theta^n \cdot exp\left[-E_{des}(\theta)/k_B T(t)\right] , \tag{4.11}$$

with the pre-exponential factor $\nu(\Theta)$, the desorption energy $E_{des}(\Theta)$ and the kinetic desorption order $0 \leq n \leq 2$ strongly depending on the described system. As an example, in the case of thermal desorption of CO from Ni(110), the process follows first-order desorption kinetics ($n = 1$) with ν and E_{des} rather constant over a wide

coverage range.[49] It is thus obvious that an enhanced desorption rate can be expected in areas of increased temperature, which finally leads to the formation of an adsorbate grating structure.

4.2 GRATING DETECTION

Depending on the laser parameters used for grating creation (section 4.1.1) and the thermal desorption kinetics of the system (section 4.1.2), variously shaped grating structures can be created. In this section, we will first model such arbitrary grating structures and then explain how these structures can be detected by optical diffraction methods.
The local coverage $\Theta(x,t)$ of any arbitrary, yet periodically shaped gratings can be described using a Fourier series: [19][21]

$$\Theta(x,t) = \Theta_0 + \sum_{n=1}^{\infty} \Theta_n(t)\, cos\left(2n\pi x/\Lambda\right), \tag{4.12}$$

with Θ_0 being the average coverage, Λ the periodicity of the grating, and $\Theta_n(t)$ the coverage modulation of the n-th harmonic of the grating.
In principle, two methods exist to monitor such a grating: a) using the linear optical diffraction signal (LOD), or b) using the second-harmonic generated (SHG) diffraction signal from the grating. The latter was used for first proof-of-principle diffusion measurements [11, 22], as it is intrinsically surface sensitive and has thus a very low diffuse scattering background. However it also suffers from very low diffraction intensities which have the order of typically $I_{out}(2\omega)/I_{in}(\omega) \approx 10^{-15}$ and are thus in the range of single photon counting [20]. The LOD signal strength is about 10^8 times higher [20] and therefore much easier to detect. Hence, this method was predominantly used for surface diffusion measurements [12–15, 17, 24, 25, 50]. However, also the diffuse scattering background is higher for LOD. Depending on the roughness of the substrate and the coverage modulation of the grating, diffuse scattering might have the same order of magnitude or be even greater than the LOD signal itself. Consequently, depending on the measurement, additional methods might be necessary to suppress the diffuse scattering background, which will be discussed at the end of this section.
The n-th order LOD signal strength [19]

$$\frac{I_{out,n}}{I_{in}} \geq \frac{1}{2}\left(\frac{\Delta R}{R}\right)^2 \left[\frac{\Theta_n}{2\left(1-\Theta_0\right)}\right]^2 \tag{4.13}$$

is directly dependent on the modulation amplitude of the n-th harmonic of the grating Θ_n^2 and on the differential reflectance $(\Delta R/R)^2$. The differential reflectance is defined as the reflectance change ΔR between the fully adsorbate covered and uncovered surface, normalized to the reflectance of the uncovered surface $R(\Theta = 0)$. Note that equation 4.13 is only valid if the reflectance R is linearly proportional to the coverage of adsorbates Θ. However, such dependency was already found for several systems, like sulfate adsorption on Pt(111) in vacuum environment [51, 52] or bromide adsorption on Au(111) in electrochemical environment [53]. In general, $\Delta R/R$ not only depends on the adsorbate-substrate system, but also on the probe wavelength (see section 2.2). Typical values are on the order of few ‰, e.g.,

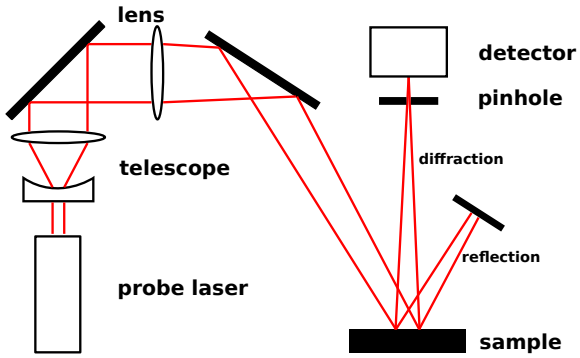

Figure 4.3: The diffuse scattering background can be reduced by focusing the diffracted beam into a pinhole in front of the detector, which drastically reduces the detected solid angle.

$3 \cdot 10^{-3}$ for hydrogen on W(110) at $\lambda = 632$ nm [54]. Using this value, typical first order (n=1) LOD signal strengths of $I_{out}/I_{in} = 4 \cdot 10^{-6}$ can be obtained for a fully modulated hydrogen grating on W(110) ($\Theta_0 = 0.5,\ \Theta_1 = 0.5$) [19]. In case of lower modulation depths, the signal strength decreases with Θ_n^2. Consequently, a grating with a shallow modulation depth of $\Theta_1 = 0.05$ has a diffraction signal strength of only 1% as compared to a fully modulated grating.
For laser induced adsorbate gratings, the higher harmonic modulation amplitudes Θ_n with $n > 1$ are typically much smaller than $\Theta_{n=1}$. Following equation 4.13, this leads to much weaker LOD signals of higher order ($n > 1$) as compared to the first order ($n = 1$) LOD signal. As an example, for a model grating of Rhodamine 6G on fused silica [19] the second order LOD signal was found 2 orders of magnitude smaller and the third order LOD signal even 4 orders of magnitude smaller than the first order diffraction signal. Measurement of higher diffraction orders could in principle provide all information necessary to recover the complete local coverage evolution $\Theta(x,t)$. These information would be valuable especially for evaluating coverage dependent diffusion rates [55] (see section 8.2). However, such measurements have not been realized so far, because of the extremely low LOD signal strengths for the diffraction orders $n > 2$. Furthermore, the LOD signal strengths can be expected much smaller than the diffuse scattering background itself (depending on the sample substrate), which makes their detection extremely challenging. Consequently, detection of only the first order linear diffraction signal has become standard procedure to observe the diffusion related decay of adsorbate gratings. Consequently, unless indicated otherwise, the term LOD will in the following be used to describe the *first order* linear optical diffraction. The same applies for the expressions "modulation amplitude" or "modulation depth" of the grating, which will in the following be used to denote the first harmonic modulation amplitude $\Theta_{n=1}$ of the grating. For a more intuitive description, also the term $\Delta\Theta = 2\Theta_{n=1}$ is used to describe the modulation depth.

For samples with high diffuse scattering background, which mainly results from the residual surface roughness [19], additional methods might be necessary to increase the signal to background ratio. In most existing methods, this is achieved by using the intrinsic difference between the diffracted signal, which is directed,

and the scattered signal, which is undirected. Consequently, diffuse scattering can be effectively reduced by minimizing the detected solid angle. The most simple approach is to increase the distance between the sample and detector, or to place a pinhole with small aperture in front of the detector [19]. However, the aperture of the pinhole is limited by the spatial dimensions of the diffracted beam. This limitation can be largely overcome by focusing the diffracted beam into the pinhole, as shown in figure 4.3. This way, Zhu *et al.* could reduce the pinhole aperture from 3 mm to 240 μm, respectively reduce the detected solid angle from $3 \cdot 10^{-6}$ sr to $1.2 \cdot 10^{-7}$ sr and thus demonstrate suppression of the diffuse scattering by a factor 60 [19].
In a more sophisticated approach, the detected background noise is reduced by a polarization modulation method. This method makes use of the strong dependence of the LOD signal strength on the probe beam polarization. In stark contrast, the diffuse scattering signal is, for the most part, independent of polarization. By periodically rotating the polarization of the probe beam between s- and p-polarization using a photoelastic modulator (PEM, typical frequency $f_{PEM} = 50$ KHz), also the detected LOD signal intensity I_{PEM} will be modulated. Assuming a polarization independent diffuse scattering signal $I_{scatter}$, the detected signal can be described by:

$$I_{PEM} = I_{scatter} + I_S \cdot sin\left(2\pi f_{PEM} t\right)^2 + I_P \cdot cos\left(2\pi f_{PEM} t\right)^2 \ , \tag{4.14}$$

with I_S and I_P being the LOD signal intensities for pure s-polarization, respectively p-polarization. According to equation 4.13 (and presuming a linear relation between the reflectance R and the coverage of adsorbates Θ), the LOD intensities are related to the corresponding differential reflectances by:

$$I_S / I_P = \left(\Delta R/R\right)_S^2 / \left(\Delta R/R\right)_P^2 \ . \tag{4.15}$$

Using this relation, equation 4.14 can be reformulated to:

$$I_{PEM} = I_{scatter} + I_S \left[sin\left(2\pi f_{PEM} t\right)^2 + \frac{\left(\Delta R/R\right)_P^2}{\left(\Delta R/R\right)_S^2} cos\left(2\pi f_{PEM} t\right)^2 \right] \ . \tag{4.16}$$

The detected signal I_{PEM} is thus composed of a constant component, and a component modulated with the frequency of $2f_{PEM}$. The amplitude of the modulated component

$$I\left(2f_{PEM}\right) = \frac{1}{2}\left(1 - \frac{\left(\Delta R/R\right)_P^2}{\left(\Delta R/R\right)_S^2}\right) I_S \tag{4.17}$$

can be effectively detected using a Lock-In scheme. While $I\left(2f_{PEM}\right)$ is directly proportional to I_S, the diffuse scattering signal is effectively suppressed here. Using this scheme, Xiao *et al.* could reduce the diffuse scattering background by more than 4 orders of magnitude, as compared to the detection with a pinhole of 3 mm aperture [23]. Consequently, the scheme was used in many LOD measurements to suppress the diffuse scattering background [14, 15, 17, 41].

4.3 SURFACE DIFFUSION MEASUREMENT

By continuously monitoring the first order LOD signal of the grating, the adsorbate grating evolution and thus the diffusion rate of adsorbates can be determined. In the following, this process will be described by a simple model, where a constant (or negligible) adsorbate-adsorbate interaction is assumed. The more complex behaviour for the case of coverage dependent adsorbate-adsorbate interactions will be discussed in section 8.2.
Surface diffusion results in a gradual equilibration of the adsorbate distribution, i.e., a decay of the adsorbate grating. This process can be described by the one-dimensional diffusion equation:

$$\frac{\delta\Theta}{\delta t} = \frac{\delta}{\delta x}\left(D\left(\Theta\left(x,t\right)\right)\frac{\delta\Theta}{\delta x}\right) , \tag{4.18}$$

with the diffusion coefficient $D\left(\Theta\right)$ generally being dependent on the coverage $\Theta\left(x,t\right)$. If the modulation amplitude of the adsorbate grating is small, D can be approximated by a constant value. In this case, the time evolution of an arbitrary grating can be calculated analytically by combining equation 4.12 and 4.18, resulting in: [21, 24]

$$\Theta_n\left(t\right) = \Theta_n\left(t=0\right)\cdot exp\left(\frac{-4\pi^2 n^2 D}{\Lambda^2}t\right) , \tag{4.19}$$

with $\Theta_n\left(t=0\right)$ being the initial coverage modulation of the n-th harmonic. The diffraction signal $I_n\left(t\right)$ is proportional to $\Theta_n^2\left(t\right)$ (see equation 4.13), if the reflectance R is linearly dependent on the coverage of adsorbates Θ. This relation is explicitly valid for gratings with small modulation depth, where $I_n\left(t\right)$ can be described by: [21, 24]

$$I_n\left(t\right) = I_n\left(t=0\right)\cdot exp\left(\frac{-8\pi^2 n^2 D}{\Lambda^2}t\right) . \tag{4.20}$$

The time evolution of the first order (n=1) diffraction signal, which is measured in linear optical diffraction, is therefore given by:

$$I_1\left(t\right) = I_1\left(t=0\right)\cdot exp\left(\frac{-8\pi^2 D}{\Lambda^2}t\right) . \tag{4.21}$$

Thus, the diffusion constant D can be determined from the exponential decay of the intensity over an arbitrary time interval from $t_1 \geq 0$ to $t_2 > t_1$.

4.4 ADAPTION TO SOLID-LIQUID INTERFACES

After we have looked at the key aspects for the LOD methodology in vacuum environment, we will now work out the differences between LOD measurements in vacuum and in electrochemical environment. The main difference is given by the grating creation process. While under vacuum conditions, the grating is directly created by thermal desorption of adsorbates, with no readsorption occurring, this principle cannot be used at the electrochemical interface due to the presence of

the electrolyte. Here, adsorbates may directly readsorb onto the surface, making grating creation extremely inefficient.
To overcome this restriction, two approaches exist for an efficient grating creation at the solid-liquid interface. Assuming the desorbed adsorbates perform a random walk within the electrolyte prior to readsorption, a grating can be created by redistribution of adsorbates on the sample surface. For a longer mean path length of adsorbates within the electrolyte, a spatially more homogeneous readsorption pattern can be expected. If the grating constant is on the order of or smaller than the mean path length of adsorbates, readsorption is spatially more uniform than the preceding desorption, resulting in the desired redistribution of adsorbates. Consequently, the efficiency of the redistribution process increases with a decreasing grating constant, which should therefore be chosen as small as possible. Still, the use of multiple pulses and full intensity modulation depth may be necessary for an effective redistribution of adsorbates.
A more effective approach exists for species which can be oxidized to products that desorb permanently and dissolve into the electrolyte. Usually, the onset potential for such an oxidation process is depending on the temperature. Typical examples for this behavior are the oxidation of sulfur to SO_4^{2-} [56, 57] or the oxidation of CO to CO_2 [58, 59]. In this case, the electrode potential can be set to the onset of the oxidation potential at the same time that the temperature modulation is induced by the laser. An increased adsorbate oxidation rate can then be observed in the areas of higher temperature which leads to the creation of an adsorbate grating. Due to the complete desorption of oxidized species, this process is expected to be more efficient than the redistribution of adsorbates and should therefore be favoured. Nevertheless, also for this approach the usage of multiple pulses and a full intensity modulation depth may be necessary.
Unfortunately, the electrolyte not only influences the grating creation process itself. It also absorbs electromagnetic radiation within the optical, and much stronger within the near infrared spectrum. At a wavelength of $\lambda = 1064$ nm, which was most commonly used for the grating creation process in vacuum, water has an absorption coefficient of $\alpha_{1064} = 0.6\ \mathrm{cm}^{-1}$ [48]. For a wavelength of $\lambda = 532$ nm, absorption is fundamentally weaker with $\alpha_{532} = 3.5 \cdot 10^{-4}\ \mathrm{cm}^{-1}$ [48]. To reduce absorption, a grating at the solid-liquid interface may either be created using a wavelength of $\lambda = 1064$ nm in combination with a thin film electrochemical cell. Or a wavelength in the optical spectrum like $\lambda = 532$ nm can be used, which means less restrictions for the electrochemical cell design. Moreover, the latter has the inherent advantage that smaller grating constants are created (see equation 4.4). Consequently, for the grating creation process in the newly developed *in situ* LOD setup, a wavelength of $\lambda = 532$ nm was used. The grating detection in vacuum environment is usually performed with HeNe lasers ($\lambda = 632$ nm), which have the advantage of low intensity fluctuations and long coherence lengths. As water has an absorption coefficient of only $\alpha_{632} = 2.9\ \mathrm{cm}^{-1}$ [48] at this wavelength, the HeNe laser is well suited also for the grating detection at solid-liquid interfaces.

Part II

EXPERIMENTAL

5 EXPERIMENTAL SETUP

We will now focus on the developed experimental setup for *in situ* LOD measurements in electrochemical environment. The development of the new methodology started during my master thesis [43] and was continued within this work. Therefore, the basic principles from LOD measurements under vacuum conditions were adapted for measurements at the solid-liquid interface. The key differences of both environments and their implications for the experimental setup were already discussed in section 4.4. In the following sections, the newly developed *in situ* LOD setup will be introduced, including the optical setup (section 5.1), the developed electrochemical cell (section 5.2) and special considerations for the cell handling (section 5.3).

5.1 OPTICAL SETUP

The optical setup is shown in figure 5.1. The optical beam path for the grating creation process is highlighted in green and the probe laser path in red. We will first describe the optical setup as a whole and then focus on single aspects, like geometrical considerations for the grating creation and detection processes (section 5.1.1), the properties of the used Nd:YAG laser (section 5.1.2), and further considerations for the detection of adsorbate gratings (section 5.1.3).
The grating is created using a seeded, frequency doubled, 10 Hz, s-polarized Nd:YAG laser with a beam diameter of 9.5 mm (a, Continuum Surelite EX, see table 5.1). In order to use the pure second harmonic with a wavelength of $\lambda = 532$ nm, residuals of the fundamental wavelength are blocked directly at the laser output (b). At $\lambda = 532$ nm, the pulse energies are about 320 mJ and the pulse length is about $3 - 5$ ns. As the laser pulses continuously, the specific number of pulses necessary for grating creation (up to single pulses) can be selected using a shutter (c, NM Laser Products LSTXYW8-2). The laser pulses are then attenuated using a combination of a half wave plate (d) and two polarization depended beam splitter cubes (e,h). Pulse energies between 1% and 100% of the initial power can be realized this way. For stronger attenuation, additional neutral density filters (g) can be used. However, for typical working energies between $30 - 60$ mJ, these are not necessary. The timing of the pulses is monitored by a silicon detector (j, Thorlabs DET36A/M) using the diffuse scattering of the blocked beam (i). For grating creation, the beam is then split up at a $50 : 50$ ratio (k) and brought to interference on the sample within the electrochemical cell (F). This way a full intensity modulation is obtained on the sample surface in order to increase the efficiency of the grating creation process.
The grating is monitored using a 5 mW polarized HeNe laser with a beam diameter of 0.8 mm (A, Thorlabs HNL050L-EC). For safety reasons, also this beam can be blocked by a shutter (B, Thorlabs DET36A/M). In order to compensate the expected laser power deviations (0.2% between 30 Hz $-$ 10 MHz, respectively $\pm$2.5% over

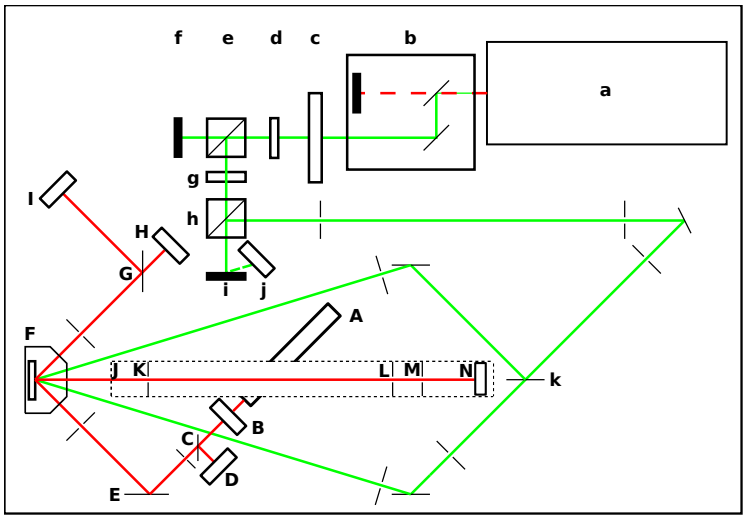

a) Nd:YAG laser
b) infrared separation
c) shutter
d) half wave plate
e) beamsplitter (pol. dependent)
f) beam dump
g) nd filter
h) beamsplitter (pol. dependent)
i) beam dump
j) Si detector (pulse acquisition)
k) beamsplitter (50:50)

A) HeNe laser
B) shutter
C) beamsplitter (10:90)
D) Si detector (HeNe monitor)
E) periscope
F) cell / sample
G) beamsplitter (90:10)
H) position sensitive detector
I) Si detector (reflection)
J) optical bench (covered)
K) iris
L) variable horizontal slit
M) variable vertical slit
N) PMT detector

(a)

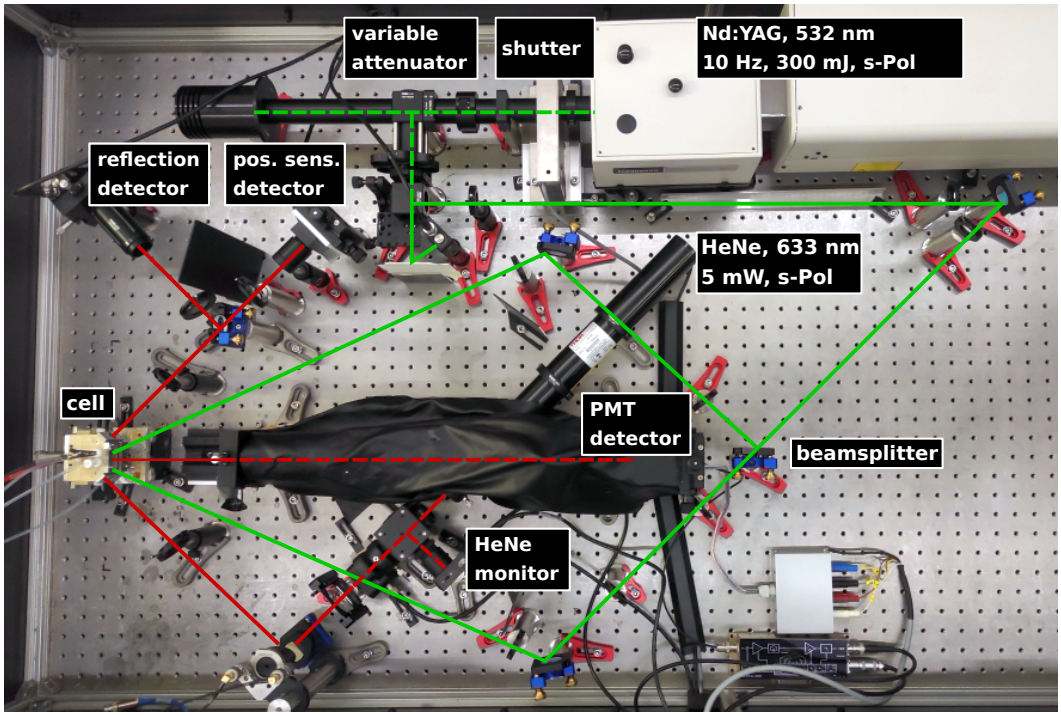

(b)

Figure 5.1: Scheme (a) and image (b) of the optical setup. Reprinted with permission from [LK2]. Copyright XXXX The Authors.

8 hours according to the datasheet), the laser power is additionally monitored by a combination of a beamsplitter (C) and a silicon detector (D). The sample is then probed by the HeNe beam under an incident angle of 46.9°, so that the diffraction signal can be detected perpendicular to the sample surface (see section 8.1, Supporting Information SI 2.1). The detection of this signal is realized using a combination of a pinhole (K) and two variable slits (L,M) in front of a photomultiplier-tube detector (N, Hamamatsu H11901-01). All of these components are freely movable on an optical bench (J). The reflected beam is monitored using a silicon detector (I, Thorlabs DET36A/M), and its position, which is used for cell alignment (see section 5.3), is tracked with a position sensitive detector (H, Thorlabs PDP90A).

5.1.1 *Geometrical considerations*

The chosen beam path mainly results from considerations made for the grating creation process at the solid-liquid interface (see section 4.4). In order to create a grating with small periodicity, the Nd:YAG beam with $\lambda = 532$ nm is interfered on the sample under an angle of $\theta = 17.9°$ (as compared to $\theta = 1.5°$, which is typically used in vacuum environment [22]). Following equation 4.4, a coverage modulation with a periodicity of $\Lambda = 650$ nm is created this way (as compared to $\Lambda = 20$ μm, typically used in vacuum [22]). A more detailed description is provided in section 8.1, Supporting Information SI 2.1. The diffraction signal of the grating is detected perpendicular to the sample by using an incident angle of 46.9° for the HeNe probe beam. Oblique incidence and perpendicular detection was chosen for the probe beam, as this geometry allows a simple cell design where the probe beam passes all windows perpendicularly (see section 5.2).

Surelite EX		
laser system	Nd:YAG (seeded, flash lamp-pumped)	
beam profile	flattop	
beam diameter	9.5 mm	
repetition rate	10 Hz	
wavelengths	1064 nm	532 nm (SHG)
pulse energies	625 mJ	300 mJ
energy stability (shot to shot for 99.9% of pulses)	±2.5%	±3.5%
energy stability (RMS)	±0.8%	±1.2%
polarization	horizontal	vertical
pulsewidth	$4-6$ ns	$3-5$ ns
linewidth	0.005 cm^{-1}	
coherence length	2 m	
beampoint stability	50 μrad	

Table 5.1: Nd:YAG laser specifications according to the datasheet. The coherence length was derived from the linewidth.

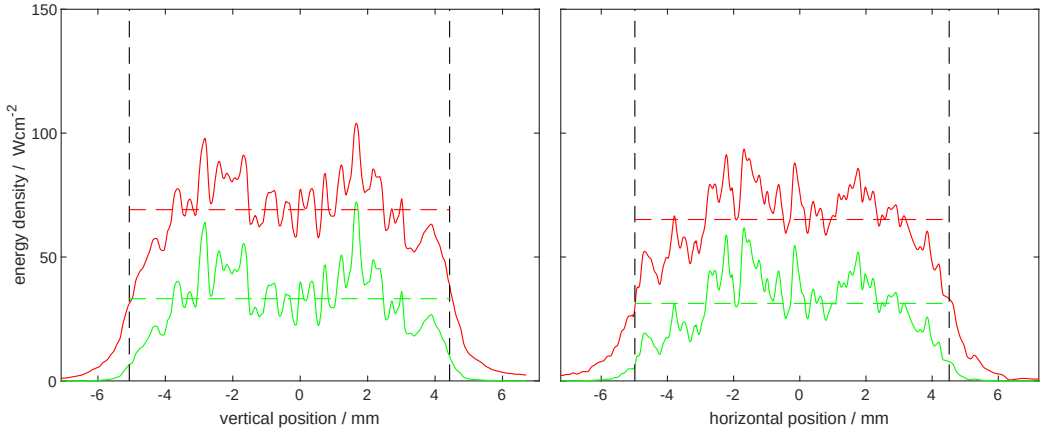

Figure 5.2: Spatial energy density of the Nd:YAG laser beam measured over the vertical (left) and horizontal axis (right). The data for the fundamental wavelength (1064 nm, red) was acquired during commissioning. The data for the first harmonic (532 nm, green) was estimated by squaring the spatial energy density of the fundamental wavelength [60] and normalizing the results to the average energy density (see table 5.1).

5.1.2 *Nd:YAG laser*

To create adsorbate gratings which are spatially homogeneous over a wide area, a Nd:YAG laser with a uniform flattop beam profile was chosen. The specifications of the used Surelite EX are summarized in table 5.1. Unlike depicted in the datasheet, measurements of the beam profile showed significant fluctuations in the spatial energy density (see figure 5.2). As a result, the created gratings cannot be expected to be homogeneous over the whole illuminated area. The implications for the measurement procedure are summarized in section 5.3.2.
In order to use multiple pulses for the grating creation process, positional fluctuations of the interference patterns between individual pulses should be as small as possible. Measurements during my master thesis [43] and first experimental results (section 8.1) showed that the creation of adsorbate gratings with multiple pulses is possible. However, the detected LOD intensity and the number of pulses used for grating creation was not completely reproducible. In [43] this relation was investigated for a grating created within a silicon substrate at the air. Here, an increasing LOD signal intensity could be observed for about the first 10 pulses. In the time range of 100 pulses, the LOD intensity showed strong fluctuations, but no continuous increase. From these measurements we concluded that the interference patterns between individual pulses must be fluctuating. This can either be induced by instabilities of the optical setup, or by deviations of the Nd:YAG beam point position (see section 4.1.1). Presumably, this effect is also influenced by deviations in the pulse energy between single pulses which is rated with $\pm 2.5\%$.

5.1.3 *Grating detection*

We will now discuss the specific requirements for the optical setup and especially for the detector to measure LOD signals from adsorbate gratings. The diffraction

intensities from such gratings are expected to be on the order of 10^{-6} of the incident probe beam or lower (see section 4.2). As the intensity strongly depends on the optical properties of the adsorbate-substrate system and on the coverage of adsorbates, detection must be possible over a wide intensity range. The measurement was realized using a photomultiplier-tube with variable gain (Hamamatsu H11901-01), which has a maximum radiant sensitivity of about $0.8 \cdot 10^5$ AW^{-1} at $\lambda = 632$ nm and a dark current of typically 1 nA. Diffraction intensities of up to 10^{-10} mW can be detected with a signal to noise ration of $SNR = 10$. Assuming the diffraction signal to be 10^{-6} of the 5 mW incident probe beam for a grating with full modulation depth ($\Delta\Theta = 1$), then the signal strength for a grating with a shallow modulation depth ($\Delta\Theta = 0.01$) would be $5 \cdot 10^{-10}$ mW (see equation 4.13). Consequently, even gratings with shallow modulation depth and gratings with a coverage of only few % ML should be detectable using the described setup.
However, to realize such measurements, the diffuse scattering from the sample must not obscure the actual diffraction signal. In order to enhance the ratio between the (directed) diffraction signal and the (undirected) diffuse scattering signal, we used a simple system of pinholes and slits with typical apertures of around 1 mm in front of the detector. If necessary, the diffuse scattering signal can be easily further reduced, e.g., by focusing the diffracted beam to the slits in front of the detector. In this case, the apertures of the slits can be further reduced to about 0.2 mm. Additionally, a polarization-modulation scheme can be used to detect the LOD signal. Both methods were already described in section 4.2 and can in principle be applied in the developed setup. For the proof-of-principle measurements of sulfur diffusion on Pt(111) further reduction of the diffuse scattering was however not necessary, as the flat platinum sample surface exhibited only weak diffuse scattering as compared to the diffraction signal strength.

5.2 ELECTROCHEMICAL CELL

To realize LOD measurements in electrochemical environment, a new cell was designed from scratch (see figure 5.3). The cell was specifically developed to meet the following requirements: First of all, the positional stability of the cell during LOD measurements must be assured in order to precisely perform optical measurements. In addition, an easy and reproducible alignment of the cell must be possible. For the optical measurements, several windows are necessary. At the same time, the cell volume should be kept as small as possible, to allow exchanging the electrolyte. Furthermore, most electrochemical measurements require the highest possible level of purity, so that an easy and effective cleaning of the cell must be possible.
The optical cell design (see figure 5.3c) is mainly based on the optical beam paths, described in the previous section. For the desired grating constant of $\Lambda = 650$ nm, the Nd:YAG beams must interfer on the sample under an incident angle of about 17.9°. For perpendicular detection of the diffraction signal, the HeNe beam must have an incident angle of 46.9°. The incident probe laser beam (as well as the diffraction and reflection signal) should pass all windows perpendicularly to simplify the cell alignment and allow performing also polarization dependent measurements. Therefore a cell design with 3 windows, a big front window and two smaller side windows was chosen. For the side windows, standardized parts (fused silica C7980

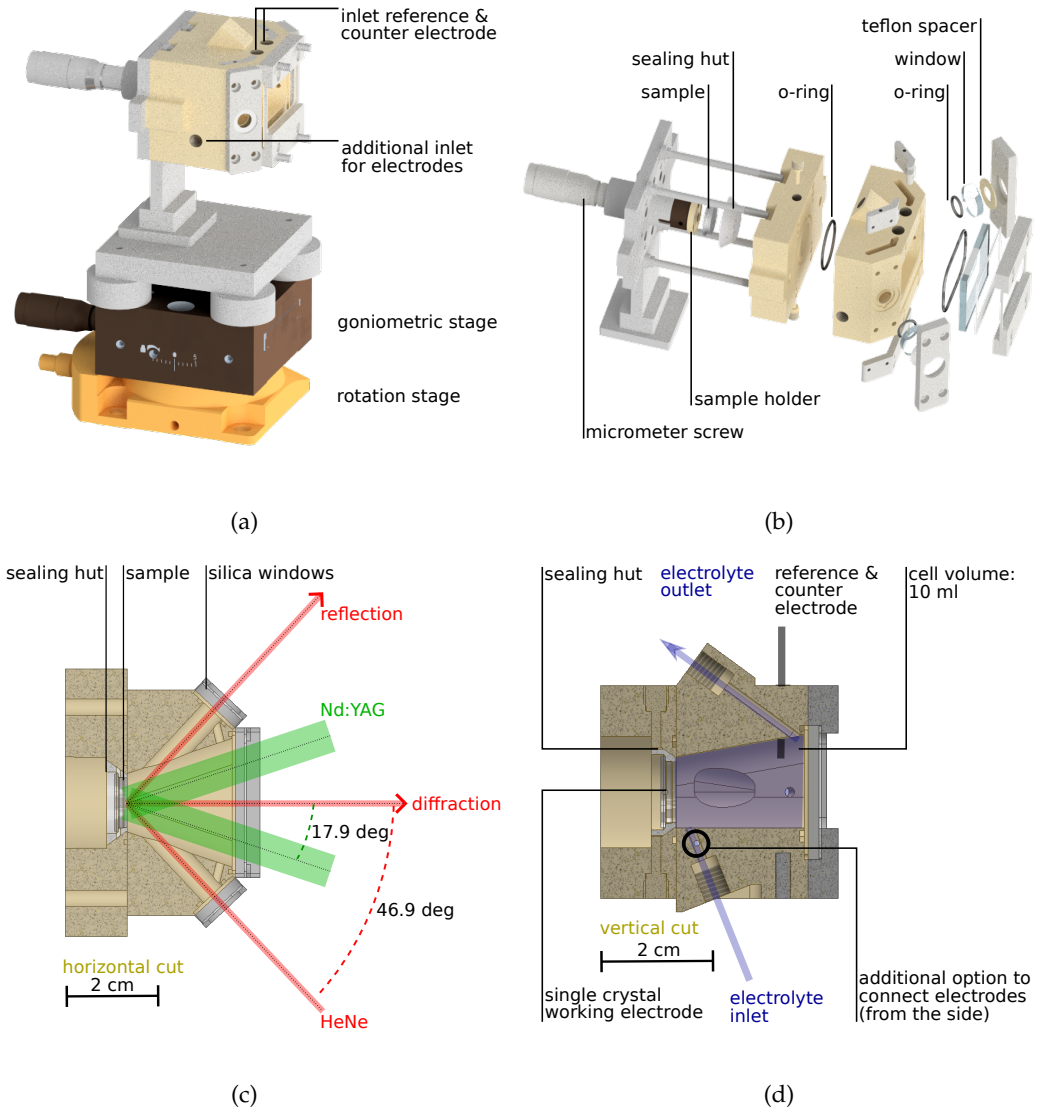

Figure 5.3: Newly developed electrochemical cell. The cell can be easily integrated into the optical setup by mounting it on designated stages (a). It is specifically designed for optical (LOD) measurements (c), electrochemical measurements (d), and can be easily disassembled into its single parts (b). Figures (a,c,d) adapted with permission from [LK2]. Copyright XXXX The Authors.

windows, Ø12.7 x 3.175 mm) could be used. The front window was custom made (fused silica C7980 window, 34 x 26 x 3 mm). The used windows are not AR coated, so they can be easily cleaned using highly concentrated caro acid. Although the transmission for a wavelength of $\lambda = 632$ nm is already about 93% for these windows, they still have the disadvantage of unwanted back reflections. However, such back reflection could not even be completely avoided using AR coated windows, with the coating only on the outer side (see section 5.3.1). To avoid leakage and ensure a reproducible window orientation also after reassembling the cell, the windows are directly pressed against the cell with additional o-rings (material: FFPM)

sealing the connection.
To assure clean electrochemical measurements, all parts that may come into contact with the electrolyte are either made of PEEK (polyether ether ketone), teflon, or fused silica. On the one hand, these materials do not interact with the electrolyte which could otherwise influence the electrochemical measurements. On the other hand, the materials can be easily cleaned to highest purity using caro acid. For cleaning purposes, the cell can be easily disassembled into its single parts (see figure 5.3b), and reproducibly reassembled after cleaning. A detailed procedure for cleaning and storage is provided in the appendix, section A.1. In assembled state, the cell has a volume of about 10 ml (see figure 5.3d). It can be filled, or electrolyte can be exchanged using the designated electrolyte inlet (from below) and electrolyte outlet (to the top). Both can be connected using standardized screw connectors made of teflon (bola tube end fittings, 1/4-28 UNF). For the electrochemical measurements, a 3 electrode configuration is used. Therefore, reference and counter electrodes can be mounted from the top side of the cell, using the same standardized screw connectors. As both electrodes are located in the main chamber of the cell close to the electrolyte outlet, possible bubble formation does not have direct influence to the measurement. Bubbles accumulate at the electrolyte outlet, where they can be easily removed by exchanging small quantities of electrolyte. Alternatively, both electrodes can also be mounted from the side of the cell. They are then connected to the channel where electrolyte is flowing into the cell. Due to repeated problems with potential control, which can most probably be attributed to bubble formation, this configuration was however not used. The single crystal working electrode is located on the back side of the cell. It is covered with a conical shaped teflon hut and pressed into the designated, also conical shaped, opening of the cell. Therefore, the crystal is placed on a sample holder which can be moved using a micrometer screw (see figure 5.3b). A similar design was already used for other electrochemical cells [61]. The design has the major advantage that the crystal position within the cell is completely reproducible and fixed. Furthermore, only the crystal surface is exposed to the electrolyte. The crystal itself is connected from below, using a wire that is fed through the sample holder out of the cell. A detailed procedure for the sample transfer into the cell is provided in the appendix, section A.1.
To ensure easy alignment and high stability of the cell within the optical setup, the cell is placed on a fixed position on top of two stages (see figure 5.3a). The ensemble is designed so that the pivot point of both, the rotation and the goniometric stage, is located in the center of the sample surface. This way, the sample can be rotated or tilted without changing its position on the horizontal plane. The stages are controlled using micrometer screws, which can be easily replaced by motorized actuators, if necessary.

5.3 CELL AND LASER ALIGNMENT

After we have described the optical setup and the electrochemical cell separately in the previous sections, we will now describe the alignment of the cell within the optical setup. Furthermore, we will shed light on unwanted effects that may

inhibit precise *in situ* LOD measurements. This includes interference effects from back-scattering (section 5.3.1) and considerations on the probe beam position for spatially inhomogeneous adsorbate gratings (section 5.3.2).
In order to detect the LOD signal, the alignment of the lasers, cell and detector (slits) must be precisely coordinated. With small misalignment, the diffracted beam is blocked at the detector slits and LOD measurements become impossible. Adjusting the slits during the measurement is difficult due to the low diffraction intensities and the high, spatially non uniform diffuse scattering background. Consequently, a procedure was developed to align the cell at the beginning of every measurement by using the beam point position of the reflected HeNe beam.
For this to work, initially, the alignment of the lasers, cell and detector slits must be coordinated. Therefore, the Nd:YAG beams are firstly aligned to hit the single crystal sample in the center. The cell may be slightly tilted so that back reflections from the cell windows can be blocked. The HeNe probe beam is then oriented as described in the sections 5.3.1-5.3.2. Using this configuration, a weak surface grating is created on the Pt(111) single crystal sample using pulse energies of about 150 mJ. While the grating in the platinum substrate can be easily removed by later annealing, it offers much higher diffraction intensities than adsorbate gratings. Consequently, the created grating can be used to align the slits in front of the PMT detector for maximum intensity. As a reference for the configuration set, the position sensitive detector is finally adjusted so that the reflected HeNe beam is exactly centered on this detector.
For subsequent measurements, the Nd:YAG, HeNe, and detector slit alignment must not be changed anymore. At the beginning of each measurement it is sufficient to slightly adjust the cell position, so that the reflected HeNe beam is again centered on the position sensitive detector. With this alignment, also the LOD signal will be detected.

5.3.1 *Interference effects*

During the first experiments, the diffraction signal was superimposed by strong oscillations that had an amplitude of up to 30% of the actual LOD signal. Retrospectively, these oscillations could be assigned to interference effects. Specifically, the back reflections from the cell windows (see figure 5.4a) interfered with the incident beam, if the cell alignment was "too accurate". The interference effects could be avoided by tilting the incident beam slightly downward out of the horizontal plane.
The oscillations could be linked to interference effects by having a closer look at the time evolution of the oscillations (see figure 5.4b). These typically started with an initial frequency of around 50 mHz. During the measurement this frequency was continuously decreasing until reaching a value of around 0.2 mHz after about an hour. Changing the electrolyte lead to repetition of this behaviour. Such behaviour can only be explained by interference of the back reflected beam with the incident beam, if the optical path length of the back reflected beam is continuously changing. This can however be expected if the temperature of the electrolyte is increasing slightly during the measurement. The corresponding change in its refractive index is then directly leading to a change in the optical path length. With time, the tem-

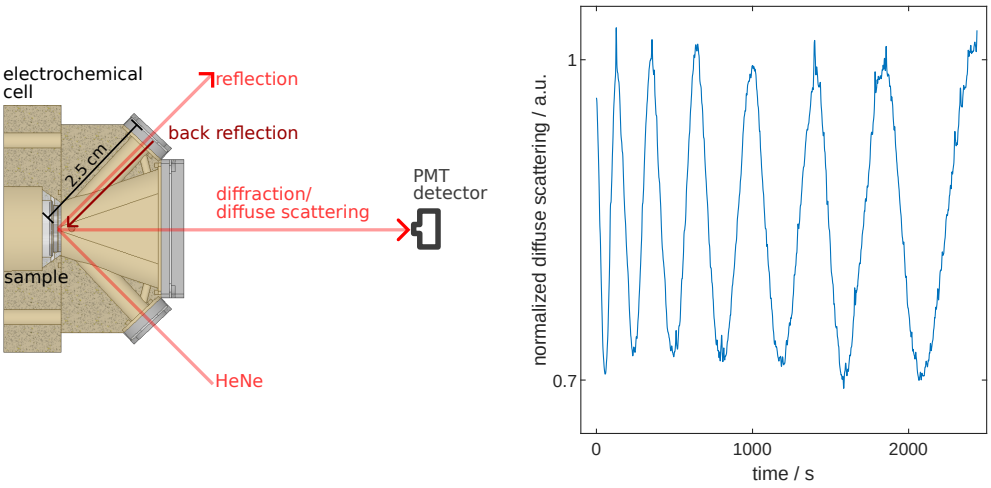

(a) (b)

Figure 5.4: Back-reflections from the cell windows (a), can interfere with the incident beam which creates strong oscillations on the LOD signal. The same can be observed (b) for the diffuse scattering signal (diffraction signal prior to surface grating creation) of a freshly prepared Pt(111) sample in 0.1 M H_2SO_4.

perature is coming closer to equilibrium, the effect slows down, and the oscillation period increases. In order to estimate this effect, one can assume an additional path length of about $d = 5$ cm for the back reflected beam, compared to the incident beam. The change in refractive index $\Delta n/n$, that is needed to increase the optical path length by a full wavelength λ, is then given by:

$$\frac{\Delta n}{n} = \frac{\lambda}{d} = 1.3E-5\,. \tag{5.1}$$

This value corresponds to a temperature change of about 0.2 °C, assuming the electrolyte to be water with temperature of 20 °C [62]. Hence, one oscillation period can be correlated to a temperature change of the electrolyte of about 0.2 °C.
The first approach to reduce these interference effects included the usage of AR coated windows. However, to avoid contamination, no coating could be used on the electrolyte-side. Still, the usage of these single-sided AR coated windows could reduce the oscillation amplitude to about 5% of the actual signal. For the complete elimination of interference effects, spatial overlap of the incident beam and the back reflected beam on the sample surface had to be avoided. This could finally be achieved by tilting the incident beam slightly downward by about 1.5° out of the horizontal plane.

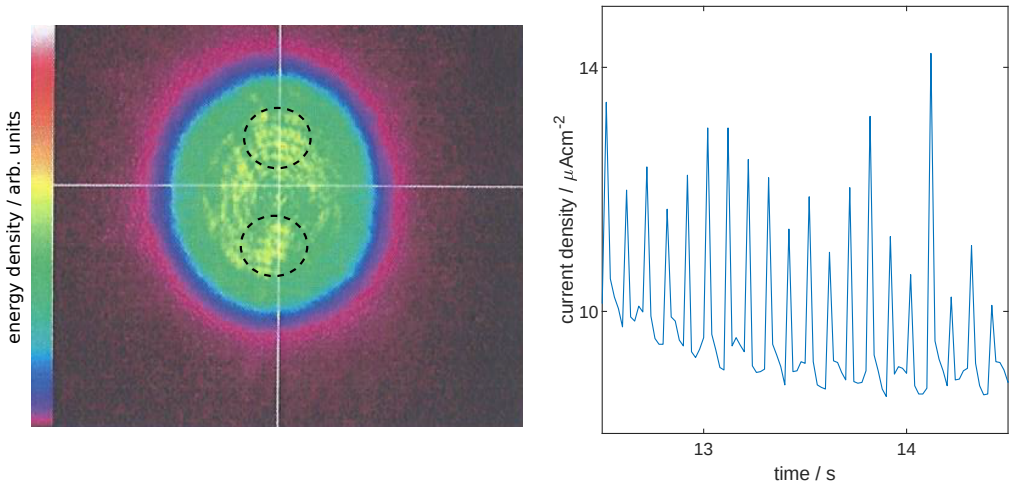

(a) (b)

Figure 5.5: a) Spatial energy density of the Nd:YAG laser beam (linear color scale). The profile was acquired for the fundamental frequency of the laser ($\lambda = 1064$ nm) during commissioning. Areas of highest intensity are outlined with circles.
b) Oxidative desorption of adsorbates during the grating creation process manifests in small current spikes that occur simultaneously with Nd:YAG laser penetration. The spikes' amplitude is a good indicator for the efficiency of the grating creation process.

5.3.2 *HeNe beam point position*

For the developed setup, also the specific area probed via LOD is relevant. Due to fluctuations in the spatial energy density of the Nd:YAG laser (see figure 5.5a), the grating creation process on the sample can be expected to be non uniform. In areas of high energy density (marked with circles), the created adsorbate grating will be most pronounced, while in other areas the energy density might not even be sufficient to create a grating at all. The sample was therefore not probed in the center, but slightly below, where LOD signals developed the highest intensities. In the following, we will see that this procedure allows to correlate the optical with the electrochemical data acquired during the grating creation process.
While the laser beam is probing only a small area, the electrochemical data results from processes averaged over the whole sample surface. As an example, for the creation of sulfur adsorbate gratings (see section 8.1), the oxidative desorption of sulfur leads to a charge transfer (see section 7.1). The charge transfer is visible in small current spikes, that occur simultaneously with the laser penetration (see figure 5.5b). By integrating these current spikes over time, the corresponding sulfur oxidation charge and thus the amount of oxidatively desorbed surface sulfur can in principle be determined. However, due to the non uniform spatial grating evolution over the sample, we cannot define specific areas on the sample, where sulfur oxidation occurs. Consequently, it is not possible to quantitatively interpret the current spikes, e.g., in order to determine the local coverage modulation amplitude. Still, the amplitude of these spikes is a good indicator for the efficiency of the

grating creation process via oxidative desorption.
In summary, the current spikes are indicating grating creation only *somewhere* on the sample, not necessarily *all over* the sample. If we want to use these information to find parameters (laser power, electrode potential) for an effective grating creation via oxidative desorption, an area must be probed optically where the created gratings are most pronounced. This was found to be slightly below the center of the sample. By optically probing this area, the electrochemical features can be correlated to the measured LOD signals.

6 SAMPLE PREPARATION

First proof-of-principle LOD measurements were performed for sulfur diffusion on platinum single crystal electrodes. Platinum electrodes are highly relevant especially in energy conversion and storage systems, which largely depend on the electrocatalytic properties of the metal. Although there has been extensive research on platinum electrodes over the last forty years [63, 64], basic questions like platinum surface oxidation and the corresponding changes in surface morphology [65–67] are still under discussion. While these corrosion processes play a major role especially in terms of long term stability of the electrodes, the catalytic properties can strongly depend also on the mobility of reactants on the surface itself [8]. Hence, surface diffusion has already been investigated for various species at platinum electrodes in vacuum [9, 15, 16, 68, 69], but there are almost no studies on surface diffusion at electrochemical interfaces, due to the lack of experimental measurement methods.
In order to investigate surface diffusion at platinum electrodes, atomically flat surfaces have to be prepared. This was firstly achieved by Clavilier *et al.* [70] by annealing the single crystal in a hydrogen flame. Although this method is most commonly used still today, alternative methods were developed in the previous years, e.g., the inductive annealing. Hereby, rapidly alternating magnetic fields induce electric currents within the sample that lead to resistance heating. This is usually achieved by placing the sample in the center of an inductional coil that is driven by high frequent alternating currents. To prevent oxidation, the sample can be contained within a protective gas atmosphere during this process. However, depending on the setup, in principle any gas atmosphere can be used during annealing. Also the temporal evolution of annealing temperature can be freely chosen and easily reproduced. In contrast to flame annealing, the process raises fewer safety issues and was therefore often used at synchrotron beam facilities by the Magnussen group, where the method is established for several years already.
The setup, which was used for the annealing procedure, was completely redeveloped during this work. It will be introduced in section 6.1, followed by the detailed preparation procedure and sample characterization of the Pt(111) single crystal samples (section 6.2).

6.1 INDUCTIONAL OVEN SETUP

The redeveloped inductional oven setup, which was designed in collaboration with Timo Fuchs, is shown in figure 6.1. The main improvements concern a) an easy sample transfer and b) the possibility of coating the samples with electrolyte or performing electrochemical characterization directly after annealing within the gas atmosphere.
The sample is placed onto a custom made silica sample holder, attached to a piston (made of PEEK) which can be moved up and downwards. The ensemble is

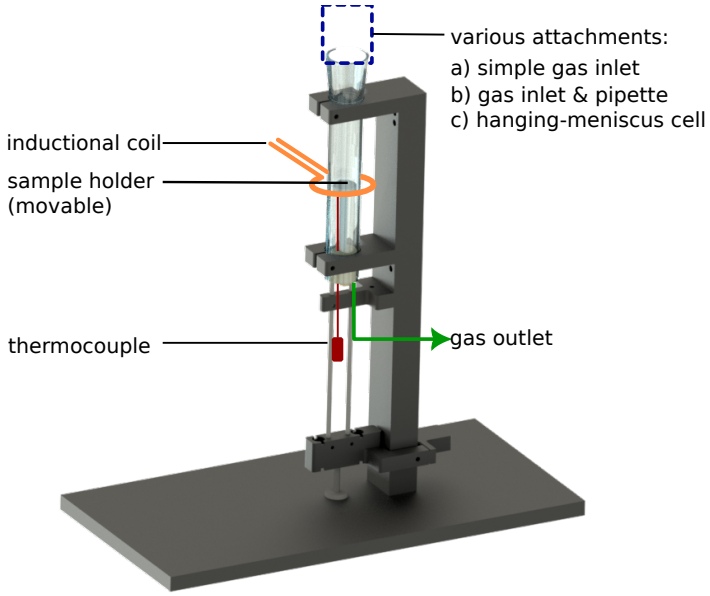

Figure 6.1: Developed inductional oven setup for crystal annealing.

placed within a silica tube, which is on the bottom side sealed by o-rings (made of FFPM) embedded in the piston. Additional bores are provided for the gas outlet and for attaching a thermocouple (Type S, Pt-Rh) to the sample in order to determine its temperature during annealing. The top side of the tube consists of a ground glass joint, where different kinds of fittings can be connected to. In principle this can be 1) a simple gas inlet, 2) a pipette in combination with a gas inlet or 3) an electrochemical hanging-meniscus cell in combination with a gas inlet. For the measurements presented in this work, the pipette-fitting was used. All parts can be easily reassembled and cleaned with concentrated caro acid, so that a high level of purity is assured. In order to allow a smooth movement of the piston within the glass tube, the o-rings should additionally be wrapped with teflon tape.

6.2 PLATINUM SINGLE CRYSTAL ELECTRODE PREPARATION

For the sample preparation itself, the Pt(111) single crystal was extensively rinsed with ultrapure water (18 MΩcm) and placed into the inductional oven, which was then flushed with either 100% argon or 100% hydrogen. The sample was annealed for about 15 minutes at a peak temperature of about $900 - 1000$ °C, which was controlled using the thermocouple. After slowly cooling down the sample to room temperature (within 10 minutes), it was coated using the prefilled pipette, still under protective gas atmosphere. For experiments with the clean Pt(111) crystal, coating was performed with 0.1 M H_2SO_4 electrolyte solution in order to protect the sample surface during transfer into the electrochemical cell. For experiments with the sulfur covered surface, sulfur was deposited by exposing the surface to 10 mM Na_2S solution. As a fully covered monolayer of adsorbed sulfur can be expected after 5 min of deposition time [71, 72], the sample was then rinsed with ultrapure water under ambient atmosphere to remove all residues of Na_2S solution. Subsequently, the sample was transferred into the electrochemical cell which

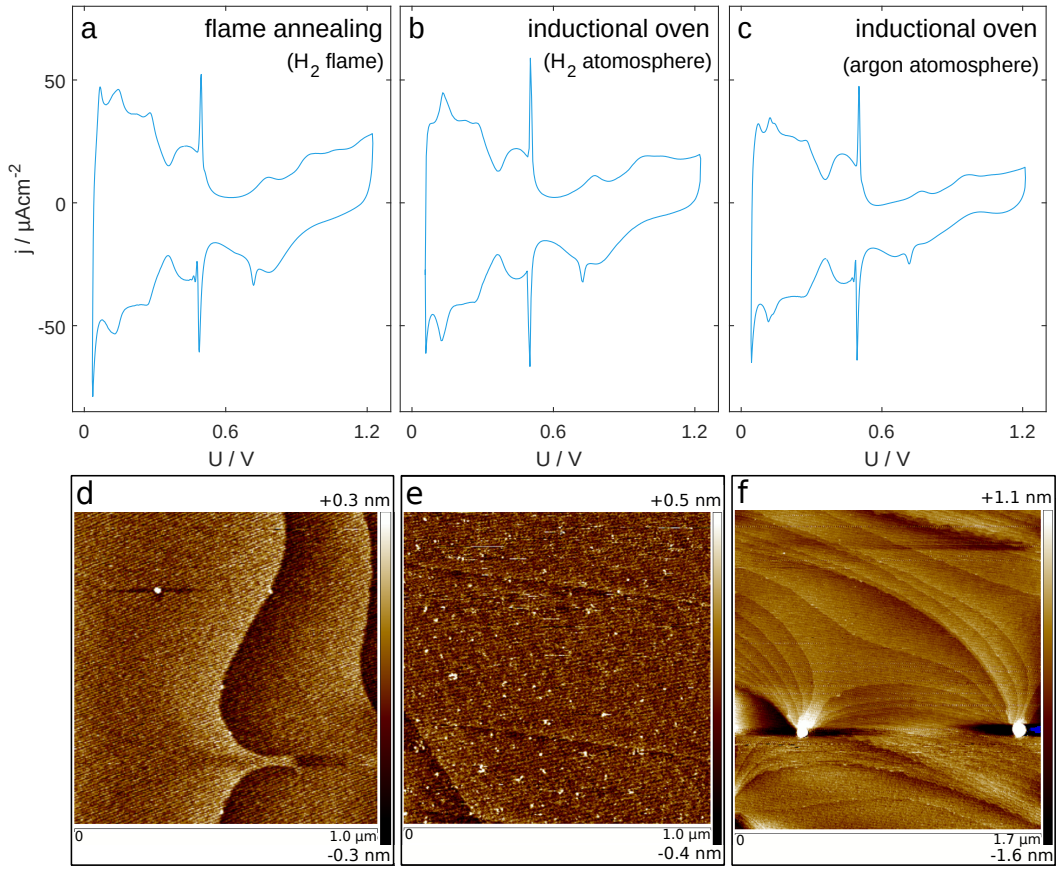

Figure 6.2: CVs in 0.1 M H_2SO_4 (a-c) and AFM images (d-f) for a freshly prepared Pt(111) crystal using different preparation procedures. Annealing in a hydrogen flame for 10 minutes and subsequent cooling under argon flow (a,d) leads to similar CVs (scan-rate: 50 mVs^{-1}) as compared to annealing with an inductional oven for 10 minutes either in 100% H_2 atmosphere (b,e) or in 100% argon atmosphere (c,f). The AFM images show atomically flat surfaces for all procedures, but reveal the presence of larger particles after annealing with the inductional oven in pure argon atmosphere (f). Figures (b,e) are adapted with permission from [LK2]. Copyright XXXX The Authors.

was firstly filled with deaerated H_2SO_4 electrolyte solution and secondly flushed with another 150 ml of electrolyte while keeping the sample under potential control.

The Pt(111) single crystal sample was initially prepared by annealing in pure argon atmosphere using the inductional oven setup. At that time, this was the standard procedure for annealing Pt(111) single crystals in our group [65]. Electrochemical characterization (see figure 6.2c) showed the typical features that indicate an atomically flat surface, which could also be confirmed by AFM images (see figure 6.2f). However, the AFM images also revealed the presence of particles with a diameter of about 15 nm. Characterization with XPS could not determine the nature of these particles, probably due to their relatively low coverage. Furthermore, the particles could not be removed using caro or hydrofluoric acid. In order to investigate, whether the particles' origin could be connected to the annealing procedure itself, sample preparation by flame annealing with H_2 was attempted

as complementary method for comparison. In fact, AFM images showed an almost particle free platinum surface after flame annealing (see figure 6.2d). Even previously detected particles were removed from the surface. Interestingly, the particles seem to have negligible influence on the CVs, which are comparable for both methods (see figure 6.2a,b). In trying to reproduce the obtained results, also inductive annealing was attempted in hydrogen atmosphere. The results are similar to annealing the surface in a hydrogen flame. AFM images (see figure 6.2e) show an atomically flat, particle free surface and characterization by cyclovoltammetry (see figure 6.2c) shows comparable CVs as for surfaces prepared by the other methods. Moreover, a reproducible surface quality could be obtained in various subsequent preparations, according to the corresponding CVs. In stark contrast, the surface quality for samples prepared by flame annealing was much more dependent on the individual preparation. Consequently, the single crystal samples were subsequently prepared by inductive annealing in pure hydrogen atmosphere.

Part III

SCIENTIFIC CONTRIBUTIONS

7

OPTICAL REFLECTANCE STUDIES

Prior to the diffusion measurements of chemisorbed sulfur on the Pt(111) surface in 0.1 M H_2SO_4, the optical and electrochemical properties of this system were investigated first. More specifically, the electrochemical oxidation of sulfur on Pt(111) was studied by simultaneous cyclovoltammetry and optical reflectance measurements, which allowed us to gain further insight into the intermediate steps of the oxidation process. To completely remove chemisorbed sulfur from the electrode, multiple oxidation cycles are necessary. In the corresponding cyclic voltammogram, two cathodic current peaks could be assigned to intermediates of the sulfur oxidation process.
Furthermore, the influence of various adsorbed species to the optical reflectance of the Pt(111) electrode was studied. These investigations are essential for the interpretation of LOD signals in the subsequent surface diffusion studies. Detailed studies on the reflectance change induced by chemisorbed sulfur allowed us to determine the relation between sulfur coverage and reflectance change $\Delta R/R$. The obtained relation was in turn used in the subsequent *in situ* LOD studies to determine the sulfur coverage.

This chapter is based on an article published in Electrochimica Acta [LK1], available under `https://doi.org/10.1016/j.electacta.2022.141297` and reprinted with permission from Lasse Kattwinkel and Olaf M. Magnussen.

L. Kattwinkel and O. M. Magnussen, “Optical reflectance studies on the oxidation of chemisorbed sulfur at the pt(111) electrode,” Electrochimica Acta 434, 141297 (2022)

Electrochimica Acta 434 (2022) 141297

Contents lists available at ScienceDirect

Electrochimica Acta

journal homepage: www.journals.elsevier.com/electrochimica-acta

Optical reflectance studies on the oxidation of chemisorbed sulfur at the Pt(111) electrode

Lasse Kattwinkel, Olaf M. Magnussen *

Institut für Experimentelle und Angewandte Physik, Christian-Albrechts-Universität zu Kiel, Leibnizstraße 19, Kiel, 24118, Germany

ARTICLE INFO

Keywords:
Sulfur oxidation
Pt(111) electrode
Interface structure
Optical reflectance

ABSTRACT

The oxidation of chemisorbed sulfur on Pt(111) was studied in 0.1 M H_2SO_4 using combined electrochemical and *in situ* optical reflectance. The adsorbed sulfur adlayer, prepared by immersion of the Pt electrode in Na_2S solution, was successively removed by potential cycling between 0.05 and 1.22 V vs. RHE. Correlation of the electrochemical data with the parallel measured changes in optical reflectance provides insight into the intermediate steps of the sulfur oxidation process. In addition to features related to sulfur oxidation and Pt oxide formation and reduction, two transient cathodic current peaks at rather negative potentials (0.19 and 0.41 V) are observed the first cycles, which can be assigned to intermediates of the sulfur oxidation process. The sulfur coverage oxidized in each cycle is initially large but then decreases rapidly, becoming negligibly small after about 10 cycles. Furthermore, a nonlinear change of the reflectance with decreasing sulfur coverage is observed, which suggests changes in the nature of the S-Pt bond with coverage.

1. Introduction

Sulfur poisoning has a dramatic influence on the efficiency of PEM fuel cells or platinum based catalysts, due to the strong site blocking capabilities of sulfur species. A common way for regenerating poisoned interfaces includes cycling to high potentials, which effectively removes adsorbed surface sulfur by oxidative desorption [1–3]. Although the sulfur oxidation process on Pt-containing electrodes [1–5] and, especially, on polycrystalline platinum [5–14] has been extensively researched, this process is not yet completely understood. One reason is the complex dependency of the oxidation process on parameters such as the sulfur coverage [15], the actual sulfurous species that is adsorbed [5,14], the presence of oxygen [15,16], the temperature [12], the sample surface [5], and the potential limits [12] used during cycling. The adsorbed species and its coverage typically depend on the electrolyte and the deposition procedure. For example, in SO_2 containing electrolyte various adsorbate species exist (S^0, SO_2, and (bi)sulfate), whose coverage strongly depends on the electrode potential [17,18], whereas adsorption from Na_2S predominantly results in an atomic sulfur adsorbate [9,19]. However, Sung et al. [16] suggested an initial desorption/oxidation of S_2 molecules at high coverages of about 1 ML, similar as observed for Pt under vacuum conditions [20–22] and in theoretical studies [23]. We may therefore expect the nature of the sulfur adsorbate to be highly dependent on the sulfur coverage, also at the electrochemical interface.

In this work, we focus on the oxidation of chemisorbed sulfur (from Na_2S solution) on the Pt(111) single crystal surface in acid media. For this model system, only few studies exist [5,15,16]. The overall oxidation reaction for sulfur oxidation on Pt is given by:

$$Pt - S_{ads} + 4H_2O \rightarrow Pt + SO_4^{2-} + 8H^+ + 6e^- \quad (1)$$

As expected for a charge transfer reaction involving $6e^-$, this occurs in a multi-step process. Furthermore, Sung et al. showed in studies of sulfur oxidation on Pt(111) that multiple oxidation cycles to potentials of at least 1.2 V/RHE are necessary to completely oxidize the surface sulfur [15]. They explained this behavior assuming adsorbed oxygenated species are reactive towards chemisorbed sulfur only in a certain electrode potential window and have finite oxidation kinetics. They postulated the formation of a compact oxide cage around the partly oxidized sulfur which may stabilize the structure, inhibiting further oxidation. Other groups proposed the formation of strongly bound intermediates that are formed in the oxidation process beside surface oxide [5,13,24]. While early studies [8] proposed this species to be S–O, later studies considered coexistence of several sulfur oxides. For example, sulfates or sulfites were found to be coadsorbed with S–O using X-ray photoelectron spectroscopy (XPS) on partly oxidized polycrystalline platinum that had been coated with sulfur [5]. On the same surface Bucur et al. [13] proposed SO_3 to be the main intermediate species. In a mixture of sulfuric/acetic acid Chen et al. [14] found

* Corresponding author.
E-mail addresses: kattwinkel@physik.uni-kiel.de (L. Kattwinkel), magnussen@physik.uni-kiel.de (O.M. Magnussen).

https://doi.org/10.1016/j.electacta.2022.141297
Received 1 August 2022; Received in revised form 16 September 2022; Accepted 2 October 2022
Available online 5 October 2022

different intermediate species, such as SO, SO_2 and SO_3, after sulfur oxidation on single crystal surfaces. Here, a big influence of the surface on the oxidation process was observed.

Apart from the oxidation process itself, the reduction of the formed intermediates in the negative-going scan of the potential cycle is not fully understood yet. There is consensus that the intermediates are strongly bound to the surface and their reduction manifest in cathodic current peaks [5,12,14,15,24]. However, these "reduction waves", which take place between 0.60 and 0.06 V [24], could not yet be assigned to any specific reaction.

A general problem in these studies is to determine accurately the coverage of adsorbed sulfur. Typically, this is done by coulometry of the sulfur oxidation peak [15,16] or by considering the hydrogen adsorption region [5]. The first method proved to work well, however, the individual steps of sulfur oxidation are not yet completely understood and the charge integration therefore is not trivial. The latter method is based on sulfur blocking surface sites in the hydrogen adsorption region. Hydrogen coverage in this region is found to directly dependent on the sulfur coverage [6,25] but the number of sites blocked by sulfur are still under debate [12,16,25,26].

In this work, we investigate the sulfur oxidation process by a combination of electrochemical measurements and *in situ* optical reflectance (OR) studies. Optical reflectance techniques are well established in electrochemistry [27] and have been employed e.g. for *in situ* investigations of bisulfate adsorption [28] and CO oxidation [29] on platinum single crystals. To our knowledge however these techniques have not yet been used for investigating the sulfur oxidation process on platinum single crystal electrodes. Only one study on polycrystalline platinum has been reported, which indicated a strong influence of adsorbed sulfur on the optical reflectance [10].

In the following, we will present data on the optical reflectance changes occurring during the oxidation of chemisorbed sulfur on Pt(111). We will discuss the relation of these changes to the electrochemical data, which will allow us to propose some specific intermediate reactions happening during the oxidation process. Second, we will show that the reflectance change is directly related to the change in sulfur coverage and thus provides a way to determine this independently of the electrochemical response.

2. Experimental

All experiments were carried out in 0.1 M H_2SO_4, made of ultrapure water (18 MΩcm) and 96% H_2SO_4 (Merck, Suprapur) using a hat shaped Pt(111) single crystal (MaTeck) with a diameter of 12 mm and a $Hg/HgSO_4$ reference electrode (SI Analytics, ScienceLine Hg/Hg_2SO_{4-}, K_2SO_4 0,6 mol/l), a platinum wire as counter electrode, and an IVIUM CompactStat potentiostat. A home-build electrochemical cell made of PEEK with fused silica windows and a volume of 10 ml was used, that allowed us to perform parallel optical reflectance and electrochemical measurements *in situ*. The reflectance signal was acquired using a 5 mW p-polarized He-Ne laser (Thorlabs HNL050L-EC) at an incident angle of 45 degrees in combination with a photodiode detector (Thorlabs DET36A/M). To compensate intensity fluctuations of the laser beam, its incident intensity was additionally monitored using a second, identical photodiode detector, located directly at the laser output. The OR experiment is part of a more extensive setup, which will be described in details elsewhere.

Prior to each measurement the sample was flushed with ultrapure water, annealed using an induction oven, and then cooled down to room temperature. For studies of sulfur covered samples, the sample was subsequently covered with a droplet of 10 mM Na_2S solution, prepared from ultrapure water (18 MΩcm) and sodium sulfide (Alfa Aesar, anhydrous granular). The whole process was performed in pure hydrogen atmosphere to prevent oxygen exposure, as the latter may influence the sulfur deposition process [15,16]. After 5 min of deposition time, after which a fully covered monolayer of sulfur is expected [7,9], the crystal was rinsed with ultrapure water to remove all residues of the Na_2S solution, and transferred into the electrochemical cell. The cell was then filled up with deaerated H_2SO_4 electrolyte solution and flushed with another 150 ml of electrolyte while keeping the sample under potential control.

In the *in situ* OR measurements, the sulfur was removed from the surface by potential cycles between 0.05 and 1.22 V vs. RHE, starting from 0.37 V in negative direction. The scan rate was 50 mV/s. At least 14 consecutive cycles were acquired, which was sufficient to remove the adsorbed sulfur almost completely (see below). For all measurements, the reflectance signal is normalized to the maximum measured reflectance R_{max} and given as normalized differential reflectance $\Delta R/R = \frac{R_{max}-R}{R_{max}}$. The $\Delta R/R$ curves were recorded simultaneously to the CVs and were slightly smoothed by a moving average filter. For easier comparison with the literature, all potentials are given with respect to the reversible hydrogen electrode (RHE) in the following.

3. Results and discussion

3.1. Sulfur-free electrolyte

The interpretation of the results on sulfur-covered Pt(111) requires a detailed understanding of how the optical reflectance is influenced by other adsorbing species, such as hydrogen, sulfate, hydroxyl, and Pt surface oxide, as well as by the surface roughness. We therefore first describe briefly the results obtained for clean, sulfur-free Pt(111) electrodes in $HClO_4$ and H_2SO_4 solution. These observations are in good agreement with previous OR measurements of these systems [30,31].

The cyclic voltammogram (CV) and differential reflectance $\Delta R/R$ in 0.1 M $HClO_4$ is shown in Fig. 1a. For freshly prepared flat Pt(111) surfaces (blue line), $\Delta R/R$ is decreasing monotonically in the anodic scan. Closer observation reveals several linear segments that can be assigned to the voltammetric features. More specific, the slope changes drastically at the "butterfly" peak at 0.80 V, associated with OH adsorption [32–34], and the peak at 1.05 V, where Pt surface oxidation commences with the onset of place exchange between adsorbed oxygen and Pt surface atoms [35]. The adsorption of hydrogen leads to a 0.07% increase of $\Delta R/R$ at 0.05 V with respect to that in the double layer region at 0.35 V (Table 1). In contrast, OH adsorption causes a decrease of $\Delta R/R$ by 0.34% at 0.85 V. An even stronger decrease of 0.65% is found for surface oxide formation (1.25 V). Apart from some hysteresis in the surface oxidation region, which results from the shift between Pt oxidation and oxide reduction, these changes in $\Delta R/R$ are highly reversible.

For freshly prepared Pt(111) in 0.1 M H_2SO_4 (Fig. 1b, blue line) the increase in $\Delta R/R$ between 0.35 and 0.05 V due to H adsorption is identical to that in 0.1 M $HClO_4$. Adsorption of sulfate in the "butterfly" peak region up to ≈ 0.55 V results in a similar, albeit smaller decrease (0.12%) as found for OH adsorption in $HClO_4$. At even more positive potentials $\Delta R/R$ first slightly increases and then decreases above 0.95 V. These small changes may be caused by the adsorption of oxygenated species, we could also observe at the roughened surface (see below). Although the sulfate adlayer inhibits OH co-adsorption on the surface in this potential region [36,37] and also Pt–O formation is shifted to higher potentials [38], adsorption of oxygenated species at step edges is feasible and could account for these weak features.

Potential cycles to upper limits ≤1.22 V did not induce major surface roughening in 0.1 M H_2SO_4 solution, as indicated by the CV and the OR data (Fig. 1b, blue line). To determine a possible influence of surface roughening on the reflectance signal, the influence of potential cycling to higher potentials in the oxidation regime was investigated. The latter results in roughening [39,40], as can be easily identified by the increase of the hydrogen adsorption peak at 0.13 V [41]. After 15 cycles to 1.25 V (Fig. 1a, black line), only minor changes in the potential-dependent reflectance signal are found in the range between H adsorption and the "butterfly" peak. At more positive potentials in

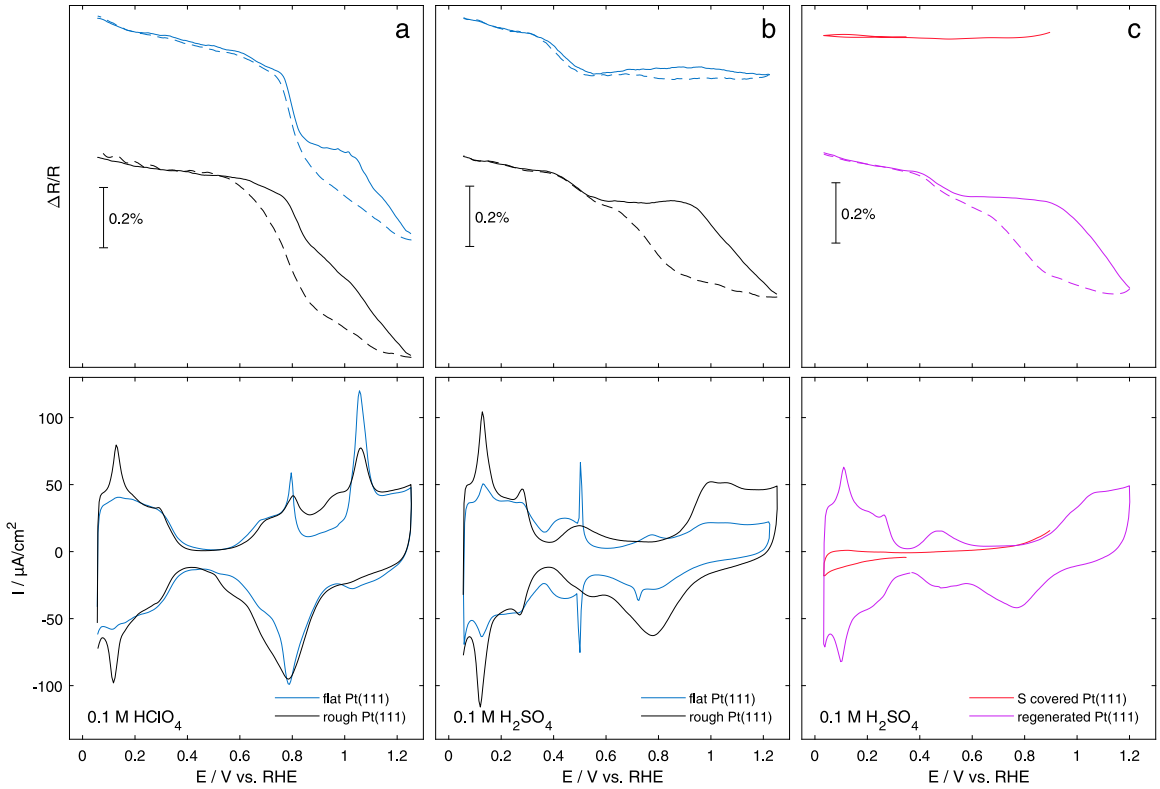

Fig. 1. Single cycles of the CV (bottom) and differential reflectance $\Delta R/R$ (top) of a freshly prepared flat (blue) and a roughened (black) Pt(111) crystal in (a) 0.1 M $HClO_4$ and (b) 0.1 M H_2SO_4. Surface roughening was achieved by 15 cycles to 1.25 V in $HClO_4$. For $\Delta R/R$, the potential sweeps in positive and negative direction are indicated by solid and dashed lines, respectively. (c) CV (bottom) and $\Delta R/R$ (top) of a fully sulfur-covered surface (red) and the corresponding surface (purple) after sulfur stripping removal by 14 cycles to 1.22 V. Note that the 2 reflectance curves shown in each panel are offset with respect to each other by an arbitrary amount.

Table 1
Reflectance change $\Delta R/R$ on the flat Pt(111) surface in 0.1 M $HClO_4$ and 0.1 M H_2SO_4 at characteristic potentials, corresponding to different adsorbed species. $\Delta R/R$ is given with respect to the double layer region (0.35 V) and was determined from the values in the anodic scan, averaged over at least 10 cycles.

$HClO_4$			H_2SO_4		
Potential		$\Delta R/R$	Potential		$\Delta R/R$
0.05 V	(H)	+0.07%	0.05 V	(H)	+0.07%
0.85 V	(OH)	−0.34%	0.55 V	(SO_4)	−0.12%
1.25 V	(Pt–O)	−0.65%	1.22 V		−0.12%

perchloric acid, the pronounced decreases in the positive-going sweep around 0.80 V and 1.05 V are stretched over a wider potential range and the recovery of $\Delta R/R$ in the cathodic sweep is slightly delayed. Both observations are consistent with the broadening of the corresponding peaks in the CV. In sulfuric acid, the main influence of surface roughening is a much stronger decrease in $\Delta R/R$ at potentials $E > 0.9$ V (Fig. 1b, black line). This can be explained by Pt oxidation/reduction, which is indicated by the presence of corresponding features in the CV. In this regime, the associated change in $\Delta R/R$ is similar as in $HClO_4$ solution, whereas the behavior in the potential range below 0.9 V is very similar to that on the flat Pt(111) surface. In both electrolytes, surface roughening by potential cycling leads to no major shift of $\Delta R/R$ at potentials below the "butterfly" peak, indicating that the reflectance signal is not affected by the nanoscale morphology *per se*. This is in accordance with previous work which show that the OR is predominantly influenced by the electronic surface structure, which in turn is influenced by chemisorbing adsorbates [27].

3.2. Sulfur oxidation

To examine the sulfur oxidation process, a crystal with a saturation coverage of adsorbed sulfur was prepared, as described in the experimental section, and then studied by combined CV and *in situ* OR. As long as the potential is kept negative of 0.8 V, the electrochemical current is negligible and $\Delta R/R$ is approximately constant (Fig. 1c, red line). This indicates that the sulfur adlayer remains at high coverages from potentials up to 0.8 V down to the negative potential limit (0.05 V) and blocks all available surface sites. The surface sulfur was then successively removed by repeated cycling between potentials of 0.05 and 1.22 V, starting from 0.37 V in negative direction. After 14 cycles (Fig. 1c, purple line), the resulting CV and OR curve is nearly identical to that found on clean but rough Pt(111) in 0.1 M H_2SO_4 (Fig. 1b, black line), verifying the complete stripping of sulfur from the Pt surface. The latter is also shown by an in-depth analysis (see 3.3), which verifies that the amount of residual surface sulfur is negligible at this stage. Furthermore, the sulfur oxidation process also seems to lead to a significant roughening of the Pt surface. In total, the reflectance increases in the transition from a sulfur-saturated to a sulfur-free surface by a value between 0.7 and 1.2%, depending on the detailed preparation. This variation can be attributed to differences in the initial coverage (see 3.3).

For a more detailed description of this process, the full CVs and OR data recorded during these potential cycles are shown in Fig. 2. After sweeping the potential to values > 0.8 V in the first cycle, sulfur oxidation starts, manifesting itself by an increasing anodic current [5]. This current is accompanied by a strong increase of $\Delta R/R$ up to a plateau at $\approx$ 1.15 V. In the subsequent negative-going scan, $\Delta R/R$ continues to increase between 1.15 and 0.4 V and then drops again. The increase indicates the presence of a continuous reduction or desorption

process within the negative-going scan. This is in accordance with observations of Bucur et al. who found for the oxidation of sulfur on platinum in 0.1 M NaOH a weight loss for the negative-going scan, which they attributed to the desorption of an intermediate, namely SO_3 [13]. In the following scan in positive direction, the value reached at the potential limit of 0.05 V is approximately maintained up to 0.9 V, where sulfur oxidation starts again. It is noteworthy that the overall increase in $\Delta R/R$ after the first cycle is already 20%–30% of that required for the complete stripping of the sulfur adlayer, although the corresponding CV is almost featureless apart from a cathodic peak at $\approx$ 0.19 V. The first observation suggests that a large fraction of the sulfur is already removed in the first cycle, the second that also incomplete sulfur adlayers can strongly block surface sites, especially in the hydrogen adsorption region.

The overall behavior observed during the first cycle is also found in the following cycles, leading to a gradual increase of $\Delta R/R$ from cycle to cycle, i.e. a successively lower sulfur coverage. However, the increase in $\Delta R/R$ per cycle becomes continuously smaller with increasing cycle number. Furthermore, distinct new peaks start to evolve in the CV during cycling. These peaks are accompanied by corresponding features in the OR. We will analyze these phenomena in greater details below. The main shift in $\Delta R/R$ and the most pronounced changes in the potential-dependence of the OR curves are found in the first 5 to 7 cycles. After this, the OR curves are rather stable and resemble strongly those recorded on sulfur-free Pt(111) electrodes after potential cycling. Again, these observations are in good agreement with the corresponding CVs, which are qualitatively similar from this point on and only exhibit smaller potential shifts and increases in height of the current peaks with cycle number. According to these observations, the main sulfur oxidation occurs in the first few cycles.

In the following, we will have a closer look at the intermediate steps of the sulfur oxidation process. For this purpose, the voltammetric data is compared with the derivative of the reflectance signal $1/R(\delta R/\delta E) = \delta(\Delta R/R)/\delta E$. Both signals are related, if reflection change is dependent on the coverage change of a certain species. For several systems, e.g. sulfate adsorption on Pt(111) [28,42], the oxidation of polycrystalline platinum [42,43], and bromide adsorption on Au(111) [44], even a linear relation between both properties has been found. In this case the $1/R(\delta R/\delta E)$ signal is directly sensitive to surface processes and can be easily compared with electrochemical measurements [42,45,46]. Assuming a similar behavior also for the species involved in the sulfur oxidation process, we will use the combination of electrochemical data and $1/R(\delta R/\delta E)$ signal to identify intermediate steps and species involved in the sulfur oxidation process.

Selected CVs and the corresponding derivatives of the reflectance signals for sulfur oxidation are shown in Fig. 3. For better visibility, the first five cycles and selected cycles (5, 7, 9, 12, 14) of the later stages of the process are displayed separately. Furthermore, the last oxidation cycle, corresponding to the rough, sulfur-free surface, is added in black for comparison. The displayed electrochemical and $1/R(\delta R/\delta E)$ data are an average of 4 individual measurements. The resulting curves were low-pass filtered, leading in some broadening of the characteristic features.

We will first discuss the anodic processes within the first cycles (left panel). While the first positive-going potential sweep only exhibits a smoothly rising current without any distinct peaks, two current peaks (A1 at 1.0 V and A2 at 1.19 V) start developing in the following cycles. The first anodic peak A1 is increasing until the third cycle, after which it deceases again. The second anodic peak A2 increases until the fifth cycle. To both peaks, matching features in the reflectance derivative are found. In peak A1, a positive reflectance change is observed, that is decreasing after the second cycle. Peak A2 is accompanied by a negative reflectance change, which is increasing continuously. Considering the different sign in $1/R(\delta R/\delta E)$, the peaks have to be associated to different processes.

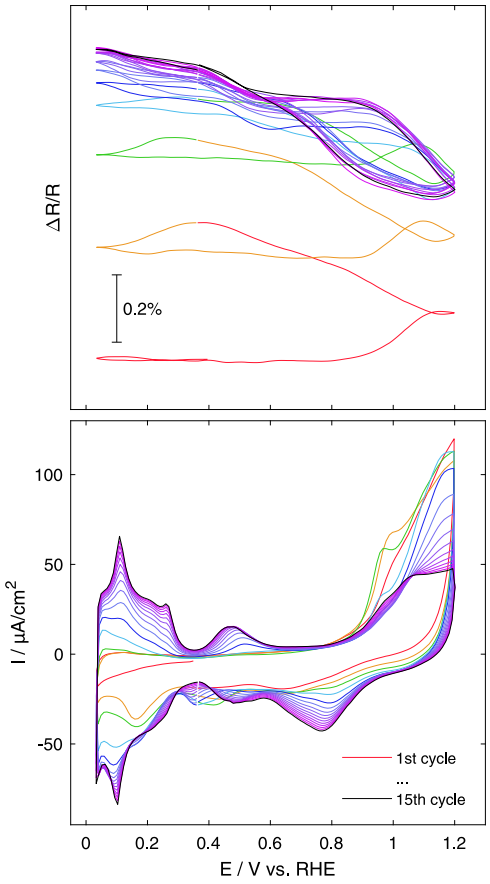

Fig. 2. CV (bottom) and differential reflectance $\Delta R/R$ data (top) acquired during oxidative desorption of a previously sulfur covered Pt(111) crystal by potential cycling (scan rate 50 mV/s) in 0.1 M H_2SO_4.

We attribute the first peak (A1) to sulfur oxidation, as it is accompanied by a positive reflectance change. This assignment is based on the pronounced overall increase in $\Delta R/R$ upon oxidative removal of sulfur. The combined CV and $1/R(\delta R/\delta E)$ data shows that with increasing number of cycles peak A1 (i) initially increases and then decreases and (ii) continuously shifts towards negative potentials. This behavior can be explained by considering the mechanism of the sulfur oxidation reaction, which is assumed to require adsorbed oxygen species as reactants [14]. Initially, sulfur is blocking most of the surface sites and the reaction is limited by the availability of such oxygen species (denoted O_{ad} in the following). After the first cycle, the sulfur coverage is significantly reduced, facilitating O_{ad} adsorption, and the sulfur oxidation rate reaches its maximum. Further cycling leads to a continuous decrease of the sulfur coverage, resulting in a decrease in the oxidation rate. The shift in peak potential with cycle number reflects the increasing number of surface sites that are available for O_{ad} adsorption.

The second peak (A2), which is accompanied by a negative reflectance change, can be assigned to Pt surface oxide formation. This is consistent with the decrease in reflectance observed in this potential range for oxide formation on the sulfur-free Pt surface. Although Pt oxide formation on flat sulfur-free Pt(111) in H_2SO_4 is negligible for potentials $<$ 1.2 V, the presence of Pt–O was reported in previous studies of the sulfur-covered surface [19]. Also Sung et al. suggested the presence of strongly bound co-adsorbed oxygen on this surface and assumed it to form stable structures with adsorbed sulfur at high potentials [15]. The absence of peak A2 and a corresponding decrease of $\Delta R/R$ in the first positive-going sweep, suggests that initially all adsorbed oxygen species are consumed in the sulfur oxidation reaction.

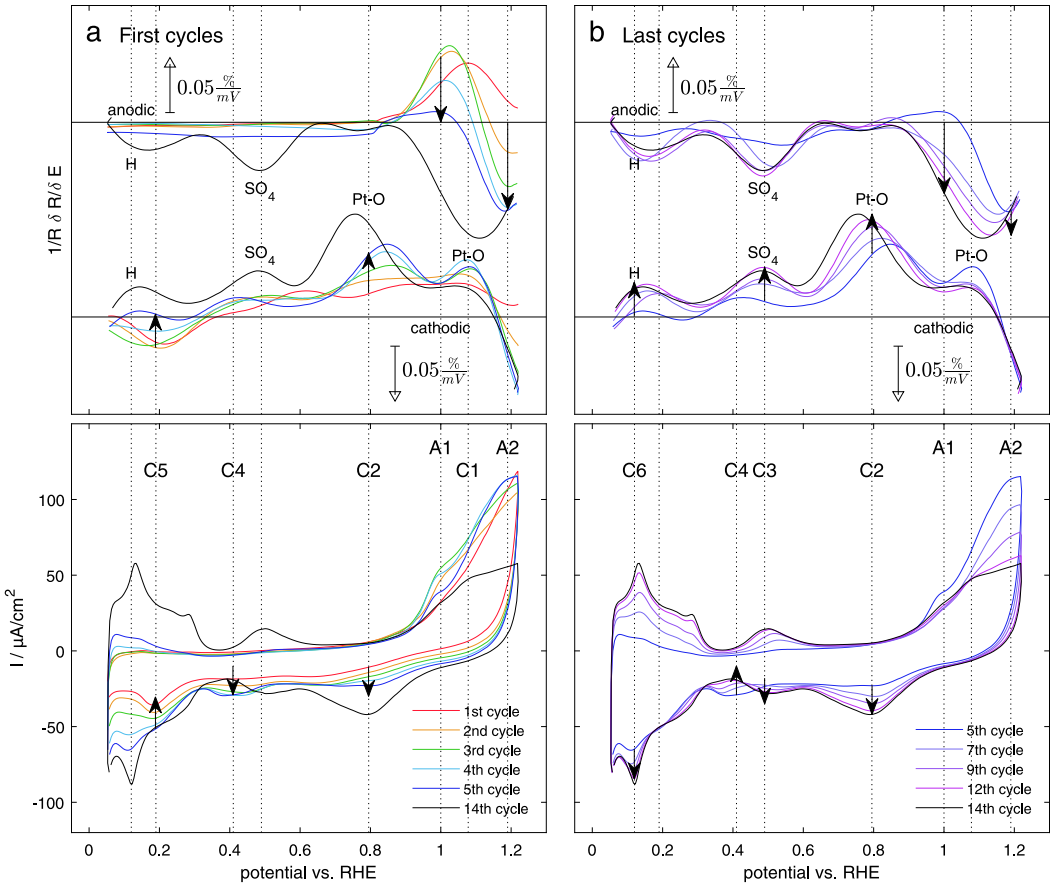

Fig. 3. CV (bottom) and $1/R(\delta R/\delta E)$ data (top) recorded during the sulfur oxidation process of an initially sulfur covered Pt(111) surface in 0.1 M H_2SO_4. The electrochemical current and $1/R(\delta R/\delta E)$ data correspond to an average of four independent measurements. Shown are the first five cycles (left panels) and selected cycles of the latter stages of the oxidation process (right panels), together with the 14th cycle, which represents the sulfur-free surface (black line). The evolution of the anodic peaks A1–A2 and the cathodic peaks C1–C6 is indicated by arrows.

In the subsequent cycles, current peak A2 starts to evolve and the decrease in reflectance becomes increasingly pronounced. In the first five cycles, this change can be attributed to the decrease in sulfur coverage and the resulting increase in the number of Pt surface sites that are available for oxygen co-adsorption. In the later cycles, the increasing roughness of the Pt surface facilitates an increasing formation of Pt surface oxide. This hypothesis is supported by the slight shift and broadening of the A2 peak from the 5th cycle on, leading after 15 cycles to the characteristic $\Delta R/R$ curve of the roughened but sulfur-free surface.

It is also reasonable to assume, that sulfur oxidation is not limited to the A1 peak, but does also occur at higher potentials. This assumption is backed by the observation, that surface sulfur cannot be completely removed by cycling to potential limits of 1.1 V, while a completely regenerated surface is obtained when cycling to 1.2 V [12]. Furthermore Contractor et al. could resolve two distinct sulfur oxidation peaks (at 0.97 V and 1.10 V) at elevated temperatures of 80 °C, while at room temperature only a broad oxidation wave appeared [8]. Considering this behavior, sulfur oxidation is clearly visible in the increased current for potentials above 1.1 V. This current is decreasing between the first and second cycle. It then increases until it reaches its maximum with the fourth cycle, after which it decreases monotonically again. This behavior cannot be explained by Pt–O formation alone, where an increase in current would be expected with increasing cycle number, as more surfaces sites are becoming available. Interestingly, the reflectance signal in this potential range stays almost constant during the first positive-going scan. Thus, this sulfur oxidation process has either weak influence on the OR signal, or a possible positive reflectance change is compensated by the negative reflectance change obtained from coadsorbing oxygen.

In the negative-going sweeps, we find in the first 5 cycles a broad reduction wave over the whole potential range, with distinct peaks evolving at 0.8 V (C2), 0.41 V (C4), and 0.19 V (C5). Peak C2 is continuously increasing, also for cycles > 5. Peak C4 increases until the 5th cycle after which it decreases again, and peak C5 is only present within the first 5 cycles. In the later cycles, two additional peaks evolve at 0.49 V (C3) and 0.13 V (C6). These features were already reported in previous studies of sulfur oxidation on platinum [5,12,14–16,24], but not all of the observed features could be unambiguously assigned to distinct cathodic processes.

Peak C2 can be clearly attributed to reduction of a Pt surface oxide, as shown by comparison with oxide reduction on the sulfur-free surface. The peak current and the reflectance change both increase with every cycle — a consequence of the increasing oxygen adsorption during the anodic cycle, described above. Nevertheless, even after 15 cycles only a fraction of the surface is covered by the Pt surface oxide based on the charge associated with peak C2. In addition, we find around 1.08 V a weaker feature (C1) in $1/R(\delta R/\delta E)$, which evolves in parallel to peak C2 but then decreases with increasing magnitude of peak C2. This feature is observed also on the sulfur-free surface. We attribute it to the desorption of an oxygen species that is more weakly bound to the Pt substrate than the oxygen in the Pt oxide, most probably to O_{ad} on the flat Pt(111) surface surrounding the Pt oxide islands.

In addition, we find in the first cycles characteristic features that are not observed on the sulfur-free surface. Specifically, we observe in the first 3 cycles a pronounced reduction peak in the hydrogen adsorption

region (C5), which was already reported in previous voltammetric studies of sulfur or S_2 covered Pt(111) [24]. This peak is clearly not caused by hydrogen adsorption/sulfate desorption. First, no anodic peaks due to hydrogen desorption are found in the subsequent positive-going scan, which is in good agreement with the strong suppression of hydrogen adsorption by adsorbed sulfur reported previously [12,16,25,26]. Second, peak C5 is associated with a pronounced decrease in $\Delta R/R$, whereas hydrogen adsorption/sulfate desorption leads to an increase in $\Delta R/R$ (see Fig. 1). Also the reduction of "heavily reducable" surface or subsurface platinum oxides, as proposed by Loučka [47], seems unlikely, as the reduction of platinum oxides leads to an increase in $\Delta R/R$ on the sulfur free surface (see Fig. 1). Consequently, this process has to be assigned to the reduction, hydrogenation, or adsorption of an intermediate, as already proposed in the previous electrochemical study [24]. Most likely seems the reduction of an SO_x species back to sulfur. For example, studies of SO_2 reduction observed a similar current peak at 0.22 V [24].

Also peak C4, which reaches its maximum after the 5th cycle and then decreases again, is not observed on the sulfur-free surface. Interestingly, this peak is associated only with a weak feature in $1/R\,(\delta R/\delta E)$ that suggests a slight increase in $\Delta R/R$. Sung et al. assumed this peak to be associated with reduction of an intermediate or with the reduction of platinum oxides on the surface [16]. However, the latter process should be accompanied by a significant increase in the OR signal, which is not seen in the data. Furthermore, peak C4 is only found at intermediate sulfur coverages, indicating that it involves a sulfur species. A sulfur-stabilized Pt oxide may be a possibility, but this may differ only in name from an SO_x species bound to a Pt adatom. In latter stages of the process ($\geq$5th cycle), when the surface is sufficiently freed from adsorbed sulfur, two further cathodic peaks, C3 and C6, start to develop that can clearly be attributed to sulfate desorption and hydrogen adsorption, respectively. Both peaks are mirrored by corresponding anodic peaks. C3 and C6 and the associated changes in $\Delta R/R$ are found at the same potentials as sulfate and hydrogen adsorption/desorption on sulfur-free Pt(111).

3.3. Sulfur coverage — reflection relation

As shown above, OR measurements provide a more direct measure of the coverage of adsorbed sulfur, which may be exploited in future studies. We therefore examined the relation between sulfur coverage and reflectance change during the sulfur oxidation process more quantitatively, based on six measurements of the type shown in Fig. 2. For every oxidation cycle the sulfur coverage change was determined by coulometry. Here, the current was integrated over a whole cycle, starting from 0.75 V in positive direction. In addition, we applied a correction for oxygen reduction, as small amounts of residual O_2 could not be fully avoided in the experimental setup employed for the OR experiments. The sulfur coverage change per cycle was calculated assuming a 6 electron process (see equation Eq. (1)), corresponding to a charge transfer of $6\times240.8\ \frac{\mu C}{cm^2}$ per Pt surface site (for further details see Supplementary Information SI.1). The total coverage change as a function of the number of cycles is shown in Fig. 4 (bottom) for six independent measurements. Most sulfur is oxidized within the first cycle. In the following cycles the oxidation yield, i.e., the change in coverage per cycle, gets successively smaller. After the 12th cycle we see only minor coverage changes. The latter have to be attributed to inherent uncertainties of the method, specifically the correction for residual O_2 reduction (included in the estimated errors in Fig. 4a). The remaining sulfur coverage after the 14th cycle was therefore not only estimated by coulometry of the complete cycle (see Supplementary Information SI.1), but also by analyzing the hydrogen oxidative charges (see Supplementary Information SI.2). Both methods reveal similar residual coverages of 1%–4% (coulometrical data) respectively 0–2.5% (hydrogen oxidative charge), depending on the single measurement. This is consistent with former measurements where no residual sulfur was found after cycling 20 times to 1.2 V on Pt(111) [15,16]. It is also noticeably that the total coverage change, and therefore also the initial sulfur coverage, varies for the individual measurements. We attribute this effect to minor deviations in the sample preparation.

The corresponding reflectance difference per cycle was determined using the average of the reflectance signal between 0.05 and 0.15 V of consecutive positive-going scans. The total reflectance change per cycles completed is shown in Fig. 4a (top). Analogous to the sulfur coverage change, the reflectance change is greatest for the first cycle and successively decreases for the following cycles. Already after the 10th cycle, the reflectance change is rather negligible for most measurements. This suggests that sulfur is largely desorbed, which is in accordance with the coulometric results within the experimental errors of the latter.

In Fig. 4b the reflectance change is plotted as a function of sulfur coverage change. Both properties show an almost linear relationship over a wide coverage range. However, for the last $\approx$ 30% of coverage change $\Delta R/R$ increases in all experiments clearly slower with coverage. This deviation from a linear behavior can be explained by a weakening influence of surface sulfur to the OR signal at small coverages. Plotting the reflectance change as function of total sulfur coverage (see Fig. 4c), this behavior becomes even more apparent, although the uncertainties (grayed area), mainly caused by the systematic errors in the coulometric measurements, are quite high. A perfect linear relation would be only expected, if just one type of sulfur species existed on the surface and its effects on the electronic structure and thus optical properties of the Pt surface would be strictly additive. Both conditions are not given in the studied system. First, as discussed above, reaction intermediates may form during sulfur oxidation, which could contribute to the OR signal. Second and more important, the nature of the Pt–S bond may change as a function of sulfur coverage. Evidence for that was found in valence band photoemission studies of sulfur on Pt(111) under UHV conditions, which show a strong coverage dependence, suggesting a change of the Pt–S bond [21,22]. Considering the surface phase behavior of adsorbed sulfur on Pt(111), the deviation from a linear behavior in the reflectance occurs roughly at a coverage, where a crossover from an ordered close-packed (2 × 2)-S adlayer to a gas-like adlayer of mobile sulfur adsorbates occurs. This is consistent with STM and LEED measurements that show a variety of ordered structures down to the coverage of 0.25 ML [15,16,19,48], while for smaller coverages the formation of 2 × 2 islands [15,48] surrounded by mobile sulfur atoms [48] was suggested. The latter species are expected to carry a higher partial charge and thus may effect the OR differently than the high-coverage ordered sulfur adlayers.

4. Conclusions

We studied the electrochemical oxidation of sulfur on Pt(111) in H_2SO_4 by simultaneous cyclovoltammetry and optical reflectance measurements. Correlation of the electrochemical and OR data sheds light on the origin of the various anodic and cathodic current peaks that are observed during this complex process. Specifically, it allowed to separate the parallel oxidation/reduction of the Pt surface from other processes and provided evidence that the additional cathodic peaks found near the hydrogen adsorption regime are caused by intermediates of the sulfur oxidation reaction. Our data indicate further that Pt oxidation is initially suppressed, most like because of consumption of adsorbed oxygen in the sulfur oxidation process, but becomes possible at lower sulfur surface coverages. In addition, we find that the amount of sulfur that is oxidized per cycle decreases gradually, in accordance with previous results. Because the optical reflectance data are only weakly dependent on the Pt morphology in the potential range of the oxide-free surface, they allow an easier determination of the number of cycles required for complete removal of the sulfur adsorbate than coulometric measurements. Furthermore, analyzing the relation

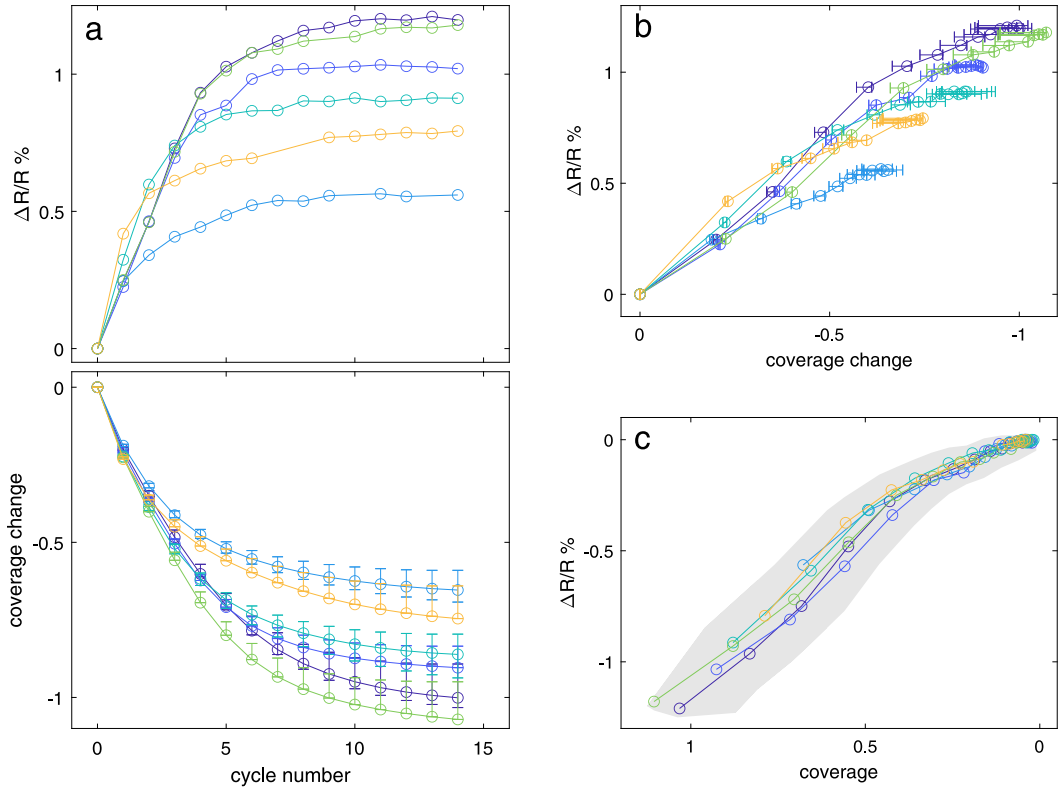

Fig. 4. The left panels (a) show the reflectance change $\Delta R/R$ (top) and sulfur coverage change from coulometry (bottom) as function of oxidation cycles completed. In (b), $\Delta R/R$ is displayed as function of sulfur coverage change. Six independent measurements with an initially sulfur covered Pt(111) surface are shown. $\Delta R/R$ and the coverage change are given with respect to the initially sulfur covered surfaces. In (c), $\Delta R/R$ is displayed as function of sulfur coverage in respect to the sulfur free surface. The coverage is obtained by summing up the coverage changes per oxidation cycle. The corresponding uncertainties from coulometry are shaded in gray. The detailed analysis is described in the Supplementary Information SI.1.

between sulfur coverage and optical reflectance change revealed deviations from a linear relationship at small sulfur coverages, which can be explained by a different influence of isolated sulfur adsorbates on the electronic structure of the Pt(111) surface as compared to close-packed ordered sulfur adlayers. From an experimental point of view, our study shows that valuable additional information on surface processes can be obtained by combining electrochemical studies with *in situ* optical reflectance measurements.

CRediT authorship contribution statement

Lasse Kattwinkel: Conceptualization, Methodology, Software, Validation, Formal analysis, Investigation, Data curation, Visualization, Writing – original draft. **Olaf M. Magnussen:** Conceptualization, Writing – review & editing, Supervision, Funding acquisition.

Declaration of competing interest

The authors declare that they have no known competing financial interests or personal relationships that could have appeared to influence the work reported in this paper.

Data availability

Data will be made available on request.

Acknowledgment

We gratefully acknowledge support by the Struktur- und Exzellenzbudget des Lands Schleswig-Holstein.

Appendix A. Supplementary data

Supplementary material related to this article can be found online at https://doi.org/10.1016/j.electacta.2022.141297.

SI.1. Determining sulfur coverage by coulometry

SI.2. Determining residual sulfur by analysing the hydrogen oxidative charge

References

[1] Y. Nagahara, S. Sugawara, K. Shinohara, The impact of air contaminants on PEMFC performance and durability, J. Power Sources 182 (2) (2008) 422–428, http://dx.doi.org/10.1016/j.jpowsour.2007.12.091.

[2] V.A. Sethuraman, J.W. Weidner, Analysis of sulfur poisoning on a PEM fuel cell electrode, Electrochim. Acta 55 (20) (2010) 5683–5694, http://dx.doi.org/10.1016/j.electacta.2010.05.004.

[3] P. Jayaraj, P. Karthika, N. Rajalakshmi, K. Dhathathreyan, Mitigation studies of sulfur contaminated electrodes for PEMFC, Int. J. Hydrogen Energy 39 (23) (2014) 12045–12051, http://dx.doi.org/10.1016/j.ijhydene.2014.06.011.

[4] D.E. Ramaker, D. Gatewood, A. Korovina, Y. Garsany, K.E. Swider-Lyons, Resolving sulfur oxidation and removal from Pt and Pt3Co electrocatalysts using in situ X-ray absorption spectroscopy, J. Phys. Chem. C 114 (27) (2010) 11886–11897, http://dx.doi.org/10.1021/jp101977g.

[5] C.-H. Chen, A. Halford, M. Walker, C. Brennan, S.C. Lai, D.J. Fermin, P.R. Unwin, P. Rodriguez, Electrochemical characterization and regeneration of sulfur poisoned Pt catalysts in aqueous media, J. Electroanal. Soc. 816 (2018) 138–148, http://dx.doi.org/10.1016/j.jelechem.2018.03.015.

[6] T. Loučka, Adsorption and oxidation of sulphur and of sulphur dioxide at the platinum electrode, J. Electroanal. Chem. Interfacial Electrochem. 31 (2) (1971) 319–332, http://dx.doi.org/10.1016/s0022-0728(71)80162-6.

[7] T. Loučka, The adsorption of sulphur and of simple organic substances on platinum electrodes, J. Electroanal. Chem. Interfacial Electrochem. 36 (2) (1972) 369–381, http://dx.doi.org/10.1016/s0022-0728(72)80259-6.

[8] A. Contractor, H. Lal, Two forms of chemisorbed sulfur on platinum and related studies, J. Electroanal. Chem. Interfacial Electrochem. 96 (2) (1979) 175–181, http://dx.doi.org/10.1016/s0022-0728(79)80374-5.

[9] E. Lamy-Pitara, L. Bencharif, J. Barbier, Adsorption du soufre sur le platine, Electrochim. Acta 30 (7) (1985) 971–979, http://dx.doi.org/10.1016/0013-4686(85)80158-4.
[10] E. Lamy-Pitara, Y. Tainon, B. Beden, J. Barbier, Nature and effects of sulphur adsorbed on platinum in acid medium. An investigation using UV-visible reflectance spectroscopy, J. Electroanal. Chem. Interfacial Electrochem. 279 (1–2) (1990) 291–303, http://dx.doi.org/10.1016/0022-0728(90)85184-7.
[11] C. Quijada, A. Rodes, J. Vázquez, J. Pérez, A. Aldaz, Electrochemical behaviour of aqueous sulphur dioxide at polycrystalline Pt electrodes in acidic medium. A voltammetric and in-situ FT-IR study Part II. Promoted oxidation of sulphur dioxide. Reduction of sulphur dioxide, J. Electroanal. Soc. 398 (1–2) (1995) 105–115, http://dx.doi.org/10.1016/0022-0728(95)04244-6.
[12] A. Zolfaghari, G. Jerkiewicz, W. Chrzanowski, A. Wieckowski, Energetics of the underpotential deposition of hydrogen on platinum electrodes: II. Presence of coadsorbed sulfur, J. Electrochem. Soc. 146 (11) (1999) 4158–4165, http://dx.doi.org/10.1149/1.1392607.
[13] R. Bucur, State of the pre-adsorbed sulfur on a rough platinum electrode in voltammetric conditions: Microgravimetric measurements with electrochemical quartz crystal microbalance, Electrochim. Acta 87 (2013) 186–193, http://dx.doi.org/10.1016/j.electacta.2012.09.006.
[14] C.-H. Chen, C. Brennan, S.C.S. Lai, D.J. Fermin, P.R. Unwin, P. Rodriguez, Adsorption and electrochemical oxidation of small sulfur–containing anions on Pt electrodes in organic media, ChemElectroChem 5 (16) (2018) 2228–2234, http://dx.doi.org/10.1002/celc.201800478.
[15] Y.-E. Sung, W. Chrzanowski, A. Wieckowski, A. Zolfaghari, S. Blais, G. Jerkiewicz, Coverage evolution of sulfur on Pt(111) electrodes: From compressed overlayers to well-defined islands, Electrochim. Acta 44 (6) (1998) 1019–1030, http://dx.doi.org/10.1016/S0013-4686(98)00206-0.
[16] Y.-E. Sung, W. Chrzanowski, A. Zolfaghari, G. Jerkiewicz, A. Wieckowski, Structure of chemisorbed sulfur on a Pt(111) electrode, J. Am. Chem. Soc. 119 (1) (1997) 194–200, http://dx.doi.org/10.1021/ja962637h.
[17] T. Wilke, X. Gao, C.G. Takoudis, M.J. Weaver, Surface-enhanced Raman spectroscopy at transition metal-gas interfaces: adsorption and reactions of sulfur dioxide on platinum-, rhodium-, and ruthenium-coated gold, J. Catalysis 130 (1) (1991) 62–75, http://dx.doi.org/10.1016/0021-9517(91)90092-i.
[18] O.A. Baturina, B.D. Gould, A. Korovina, Y. Garsany, R. Stroman, P.A. Northrup, Products of SO2 adsorption on fuel cell electrocatalysts by combination of sulfur K-edge XANES and electrochemistry, Langmuir 27 (24) (2011) 14930–14939, http://dx.doi.org/10.1021/la2033466.
[19] N. Batina, J.W. McCargar, G.N. Salaita, F. Lu, L. Laguren-Davidson, C.H. Lin, A.T. Hubbard, Structure and composition of platinum(111) and platinum(100) surfaces as a function of electrode potential in aqueous sulfide solutions, Langmuir 5 (1) (1989) 123–128, http://dx.doi.org/10.1021/la00085a022.
[20] J.A. Rodriguez, J. Hrbek, M. Kuhn, T. Jirsak, S. Chaturvedi, A. Maiti, Interaction of sulfur with Pt(111) and Sn/Pt(111): Effects of coverage and metal–metal bonding on reactivity toward sulfur, J. Chem. Phys. 113 (24) (2000) 11284–11292, http://dx.doi.org/10.1063/1.1327249.
[21] J.A. Rodriguez, M. Kuhn, J. Hrbek, The bonding of sulfur to a Pt(111) surface: photoemission and molecular orbital studies, Chem. Phys. Lett. 251 (1–2) (1996) 13–19, http://dx.doi.org/10.1016/0009-2614(96)00066-8.
[22] Z. Yang, R. Wu, J.A. Rodriguez, First-principles study of the adsorption of sulfur on Pt(111): S core-level shifts and the nature of the Pt-S bond, Phys. Rev. B 65 (15) (2001) 155409, http://dx.doi.org/10.1103/physrevb.65.155409.
[23] C.R.B. Rodríguez, J.A. Santana, Adsorption and diffusion of sulfur on the (111), (100), (110), and (211) surfaces of FCC metals: Density functional theory calculations, J. Chem. Phys. 149 (20) (2018) 204701, http://dx.doi.org/10.1063/1.5063464.
[24] C. Quijada, J.L. Vázquez, J.M. Pérez, A. Aldaz, Voltammetric behaviour of irreversibly adsorbed SO2 on a Pt(111) electrode in sulphuric acid medium, J. Electroanal. Soc. 372 (1–2) (1994) 243–250, http://dx.doi.org/10.1016/0022-0728(93)03261-m.
[25] T. Loučka, Adsorption and oxidation of organic compounds on a platinum electrode partly covered by adsorbed sulphur, J. Electroanal. Chem. Interfacial Electrochem. 36 (2) (1972) 355–367, http://dx.doi.org/10.1016/s0022-0728(72)80258-4.
[26] E. Protopopoff, P. Marcus, Effects of chemisorbed sulphur on the hydrogen adsorption and evolution on metal single crystal surfaces, J. Chim. Phys. Phys.-Chim. Biol. 88 (1991) 1423–1452, http://dx.doi.org/10.1051/jcp/1991881423.
[27] D. Kolb, R.J. Gale, Spectroelectrochemistry Theory and Practice - UV-Visible Reflectance Spectroscopy, Plenum Press, 1988, http://dx.doi.org/10.1007/978-1-4613-0985-7.
[28] I. Fromondi, D. Scherson, (Bi)sulfate adsorption on quasiperfect Pt(111) facets from acidic aqueous electrolytes as monitored by optical techniques, J. Phys. Chem. C 111 (28) (2007) 10154–10157, http://dx.doi.org/10.1021/jp073330f.
[29] I. Fromondi, D.A. Scherson, Oxidation of adsorbed CO on Pt(111) in CO-saturated perchloric acid aqueous solutions: Simultaneous in situ time-resolved reflectance spectroscopy and second harmonic generation studies, J. Phys. Chem. B 110 (42) (2006) 20749–20751, http://dx.doi.org/10.1021/jp0653095.
[30] F. Molina, R. Parsons, Electroreflectance of well-defined Pt surfaces, J. Chim. Phys. Phys.-Chim. Biol. 88 (1991) 1339–1352, http://dx.doi.org/10.1051/jcp/1991881339.
[31] I. Fromondi, H. Zhu, D.A. Scherson, In situ spectroscopy at the quasi-perfect Pt(111) single-crystal facet|aqueous electrolyte interface, J. Phys. Chem. C 116 (37) (2012) 19613–19624, http://dx.doi.org/10.1021/jp3024414.
[32] A. Berná, V. Climent, J.M. Feliu, New understanding of the nature of OH adsorption on Pt(111) electrodes, Electrochem. Commun. 9 (12) (2007) 2789–2794, http://dx.doi.org/10.1016/j.elecom.2007.09.018.
[33] A.M. Gómez-Marín, J.M. Feliu, Oxide growth dynamics at Pt(111) in absence of specific adsorption: A mechanistic study, Electrochim. Acta 104 (2013) 367–377, http://dx.doi.org/10.1016/j.electacta.2012.10.075.
[34] T. Kondo, T. Masuda, N. Aoki, K. Uosaki, Potential-dependent structures and potential-induced structure changes at Pt(111) single-crystal electrode/sulfuric and perchloric acid interfaces in the potential region between hydrogen underpotential deposition and surface oxide formation by in situ surface X-ray scattering, J. Phys. Chem. C 120 (29) (2016) 16118–16131, http://dx.doi.org/10.1021/acs.jpcc.5b12766.
[35] J. Drnec, D.A. Harrington, O.M. Magnussen, Electrooxidation of Pt(111) in acid solution, Curr. Opin. Electrochem. 4 (1) (2017) 69–75, http://dx.doi.org/10.1016/j.coelec.2017.09.021.
[36] N. Garcia-Araez, V. Climent, P. Rodriguez, J.M. Feliu, Thermodynamic analysis of (bi)sulphate adsorption on a Pt(111) electrode as a function of pH, Electrochim. Acta 53 (23) (2008) 6793–6806, http://dx.doi.org/10.1016/j.electacta.2007.12.086.
[37] N. Garcia-Araez, V. Climent, P. Rodriguez, J.M. Feliu, Elucidation of the chemical nature of adsorbed species for Pt(111) in H2SO4 solutions by thermodynamic analysis, Langmuir 26 (14) (2010) 12408–12417, http://dx.doi.org/10.1021/la101112b.
[38] J. Clavilier, R. Faure, G. Guinet, R. Durand, Preparation of monocrystalline Pt microelectrodes and electrochemical study of the plane surfaces cut in the direction of the {111} and {110} planes, J. Electroanal. Chem. Interfacial Electrochem. 107 (1) (1979) 205–209, http://dx.doi.org/10.1016/s0022-0728(79)80022-4.
[39] K. Itaya, S. Sugawara, K. Sashikata, N. Furuya, I n s i t u scanning tunneling microscopy of platinum (111) surface with the observation of monatomic steps, J. Vac. Sci. Technol. A 8 (1) (1990) 515–519, http://dx.doi.org/10.1116/1.576378.
[40] K. Sashikata, N. Furuya, K. Itaya, In situ electrochemical scanning tunneling microscopy of single-crystal surfaces of Pt(111), Rh(111), and Pd(111) in aqueous sulfuric acid solution, J. Vac. Sci. Technol. B 9 (2) (1991) 457, http://dx.doi.org/10.1116/1.585589.
[41] A. Björling, J.M. Feliu, Electrochemical surface reordering of Pt(111): A quantification of the place-exchange process, J. Electroanal. Soc. 662 (1) (2011) 17–24, http://dx.doi.org/10.1016/j.jelechem.2011.01.045.
[42] I. Fromondi, In Situ Optical Techniques as Applied to the Study of Surface Dynamics (Ph.D. thesis), 2007, http://rave.ohiolink.edu/etdc/view?acc_num=case1179874444.
[43] I. Fromondi, P. Shi, A. Mineshige, D.A. Scherson, In situ, time-resolved normal incidence reflectance spectroscopy of polycrystalline platinum microelectrodes in aqueous electrolytes, J. Phys. Chem. B 109 (1) (2005) 36–39, http://dx.doi.org/10.1021/jp044732f.
[44] Y. Mo, E. Hwang, D.A. Scherson, Simultaneous normalized optical reflectivity and microgravimetric measurements at electrode/electrolyte interfaces: The adsorption of bromide on gold in aqueous media, Anal. Chem. 67 (14) (1995) 2415–2418, http://dx.doi.org/10.1021/ac00110a015.
[45] I. Fromondi, A.L. Cudero, J. Feliu, D.A. Scherson, In situ UV-visible reflectance spectroscopy on single crystal Pt(111) microfacets, Electrochem. Solid-State Lett. 8 (1) (2005) E9, http://dx.doi.org/10.1149/1.1830396.
[46] F. Huerta, E. Morallón, C. Quijada, J. Vázquez, L. Berlouis, Potential modulated reflectance study of the electrooxidation of simple amino acids on Pt(111) in acidic media, J. Electroanal. Soc. 489 (1–2) (2000) 92–95, http://dx.doi.org/10.1016/s0022-0728(00)00202-3.
[47] T. Loučka, The formation and reduction of an oxide layer on a platinum electrode partially covered with adsorbed sulphur, J. Electroanal. Chem. Interfacial Electrochem. 44 (2) (1973) 221–227, http://dx.doi.org/10.1016/s0022-0728(73)80248-7.
[48] H. Yoon, N. Materer, M. Salmeron, M.V. Hove, G. Somorjai, Coverage-dependent structures of sulfur on Pt(111) studied by low-energy electron diffraction (LEED) and scanning tunneling microscopy (STM), Surf. Sci. 376 (1–3) (1997) 254–266, http://dx.doi.org/10.1016/s0039-6028(96)01405-7.

Optical reflectance studies on the oxidation of chemisorbed sulfur at the Pt(111) electrode

Supporting Information

Lasse Kattwinkel and Olaf M. Magnussen

Contents

SI 1.1 DETERMINING SULFUR COVERAGE BY COULOMETRY

To determine the sulfur coverage change, the current for every oxidation cycle was integrated over the time of a whole cycle, starting from 0.75 V in positive direction. In figure SI 1.1a), this procedure is shown for selected cycles of an example measurement with 30 oxidation cycles, where the areas representing the resulting charge densities are highlighted in color. This approach was applied to cover also possible intermediate reactions of the sulfur oxidation process. The resulting charges per cycle for the same measurement are shown in figure SI 1.1b). The charge is positive for the first cycle, decreasing with every cycle, and turning negative after 4 cycles. For the later cycles, the charge slowly goes into saturation, until it stays constant after about 20 cycles. We attribute this behaviour to the superposition of a) oxygen reduction reaction (ORR) and b) sulfur oxidation. Though we used deaerated H_2SO_4 as electrolyte, oxygen was still present as one can see from the "hanging CVs" in figure 2 (main publication). ORR results in a negative charge, which should be mostly diffusion limited, and is therefore expected almost constant for all cycles. Sulfur oxidation, on the other hand, results in a positive charge that will ultimately reach zero when sulfur is completely oxidized. For the given measurement, the surface can be expected completely regenerated after 20 cycles, as the charge reaches a constant value of about $-165\ \mu C/cm^2$ here (red dashed line). This is consistent with observations of Sung et al., who found the same surface being sulfur free after cycling 20 times to 1.2 V [73]. Consequently, for the presented measurement the value of $-165\ \mu C/cm^2$ can be assigned to ORR and will therefore be subtracted from the charges of every previous cycle to determine the sulfur oxidative charges (grey shaded area). From these, the sulfur coverage changes are calculated assuming a 6 electron process and 241 $\mu C/cm^2$ per 1e surface redox reaction.

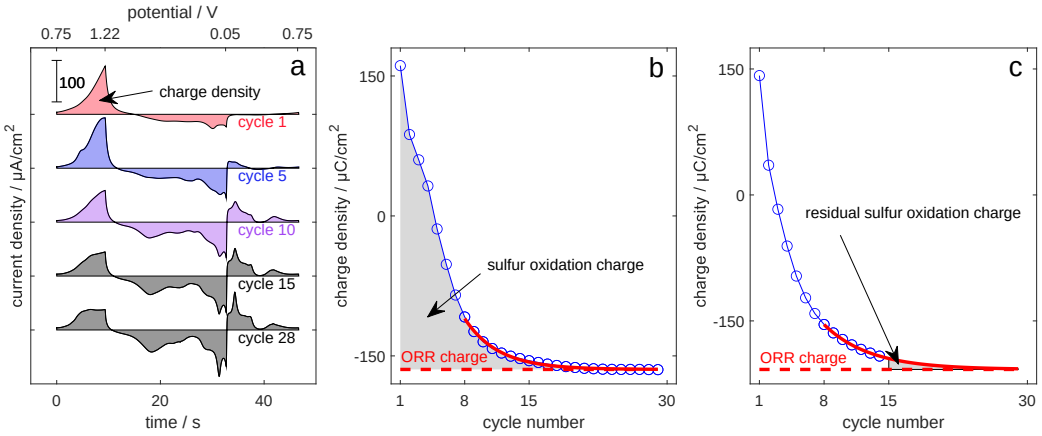

Figure SI 1.1: Procedure for coulometry that was used to determine the sulfur oxidative charge. In a), the current integration for selected cycles of an example measurement with 30 oxidation cycles is shown. b) shows further analysis of the obtained charges for the same measurement with no residual sulfur detectable. c) shows the analysis of a shorter measurement using 14 oxidation cycles with minor amounts of residual surface sulfur.

However, the majority of measurements were performed using only 14 oxidation cycles, so the charges obtained from coulometry do not always reach saturation and a minor residual sulfur coverage may be expected (see figure SI 1.1c). This coverage was estimated fitting an exponential function $f(x) = a \cdot exp(-b \cdot x) + c$ to the available data to estimate the charge evolution after the 14th cycle (solid red line). The charge corresponding to the residual sulfur coverage is then given by $\int (f(x) - c)\, dx$ from the 15th cycle $\rightarrow \infty$ (grey shaded area). The c-value (dashed red line) of the fit can be directly assigned to the oxygen reduction charge. Consequently, the sulfur oxidative charge per cycle is given by the difference of the corresponding integrated charge and the c-value. This principle was also applied to the measurement with 30 oxidation cycles (see figure SI 1.1b, solid red line), showing the exponential fit is a sufficiently good approximation to describe the charge evolution. For this fit, best agreement was obtained using all cycles ≥ 8, so the same range was also used for fitting the measurements containing only 14 oxidation cycles. Including more or less cycles for the fit leads to small deviations in the results, which are shown as errors in figure 4 (main publication).
The residual sulfur coverage, obtained using the outlined method, is in the region between $1 - 4\%$, depending on the measurement. This is consistent with the residual sulfur coverage of $0 - 2.5\%$ we obtained by analysing the hydrogen oxidative charge (see SI 1.2).

SI 1.2 DETERMINING RESIDUAL SULFUR BY ANALYSING THE HYDROGEN OXIDATIVE CHARGE

For comparison, the residual sulfur coverage was also estimated by analyzing the hydrogen oxidative charge Q_H^S. Sulfur effectively suppresses hydrogen adsorption by blocking the available surface sites. This is relevant, especially for the low coverage regime ($\Theta_S \leq 0.1$ ML), where a relation of one sulfur atom blocking a number of $\epsilon = 8 \pm 1$ [74] or 10 ± 1 [73] surface sites was found. The coverage of coadsorbed hydrogen, determined from the corresponding hydrogen oxidative charge, can therefore directly be related to the sulfur coverage Θ_S on a partly blocked surface [57, 71, 75]. With Q_H^0 being the hydrogen oxidative charge of the clean surface, the sulfur coverage can be estimated using:

$$\Theta_S = \left[\frac{Q_H^0 - Q_H^S}{Q_H^0} \right] \cdot \frac{1}{\epsilon} \,. \tag{7.1}$$

After each sulfur oxidation cycle, Q_H^S was determined by integrating the current of the subsequently positive-going scan from 0.05 V to 0.36 V (see figure SI 1.2a). As baseline, a simple double layer approximation was used, assuming a constant double layer capacitance that was estimated from the current at potential of zero charge in perchloric acid (see figure 4a, main publication). The hydrogen oxidative charge Q_H^0 was determined the same way, analysing the CV of a sulfur free surface (see figure SI 1.2b). A charge of $Q_H^0 = 213\ \mu C/cm^2$ was obtained, which is little less than one would expect for a monolayer of electrons (241 $\mu C/cm^2$ [76]). Figure SI 1.2c) shows the evolution of Q_H^S for the cycles 6-14 of five individual measurements. The charges Q_H^S are increasing with every cycle and almost reach the value of the sulfur free surface (black line) after 14 cycles. Figure SI 1.2d) shows the corresponding sulfur coverages, calculated using equation 7.1 with $\epsilon = 9$. Using this approach, we would expect a residual sulfur coverage of only $0 - 1\%$ after 14 cycles, depending on the single measurement.

This approach however ignores the continuous surface roughening (increasing peak at 0.13 V [66, 76]) and the related increase of the electrochemical surface area (ECSA) when sulfur is oxidatively desorbed. Björling et al. found an ECSA increase that stayed well below 10% when reordering a surface by cycling to potentials as high as 1.39 V. The related peak at 0.13 V (A4) reached a saturation charge of about 80 $\mu C/cm^2$ [76]. We can expect the surface reordering after 14 cycles of sulfur oxidation being much less advanced, as the A4 peak for our measurements has a total charge of only $20 - 30\ \mu C/cm^2$, depending on the measurement. However, assuming a maximum ECSA increase of 10 %, would lead to a slightly higher Q_H^0 of about 234 $\mu C/cm^2$. Further assuming $\epsilon = 7$ provides a good approximation for the maximum expectable sulfur coverage, as indicated with the positive-going error bars in figure SI 1.2d). For the negative-going error bars a value of $\epsilon = 11$ was used. Consequently, the residual sulfur coverage for all measurements is expected within a range of $0 - 2.5\%$ after the 14th cycle, as indicated by the black bar in figure SI 1.2d). Note this approximation relies on the site-blocking capabilities of sulfur, which are still under discussion. The findings are however are in good agreement with the residual sulfur coverage of $1 - 4\%$ found from coulometry of the sulfur oxidative charge (see SI 1.1).

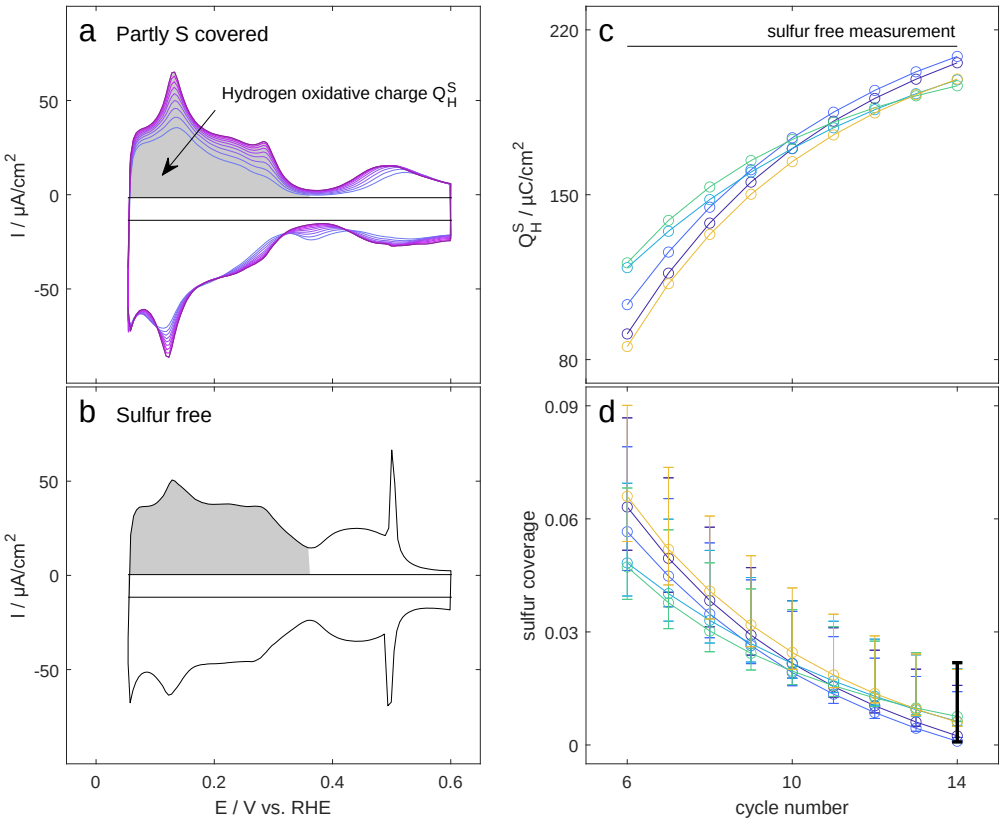

Figure SI 1.2: Coulometry of the hydrogen oxidative charges to determine the residual sulfur coverage. Panel (a) shows the CV, double layer approximation (solid black lines), and hydrogen oxidative charges (Q_H^S, greyed area) for cycles 6-14 of an example measurement. Panel (b) shows the same for a sulfur free surface. Panel (c) shows the evolution of hydrogen oxidative charges for the cycles 6-14 of five individual measurements. In Panel (d) the corresponding sulfur coverages are given.

8

MEASUREMENT OF SURFACE DIFFUSION

First proof-of-principle studies were performed on measuring the surface diffusion of chemisorbed sulfur on the Pt(111) electrode in 0.1 M H_2SO_4.
A brief overview over the measurement technique and first results are described in section 8.1 [LK2]. We here show the feasibility of the *in situ* LOD methodology to obtain quantitative surface diffusion data at electrochemical interfaces. The observed S_{ad} surface diffusion rates are at least an order of magnitude faster than under UHV conditions and show a strong dependency on the applied potential and on the coverage of adsorbates Θ.
In section 8.2 [LK3], we focus on the interpretation of LOD signals, which can in certain cases differ from a single exponential decrease, making the determination of quantitative diffusion rates more difficult. The temporal evolution of LOD signals is discussed on basis of S_{ad} diffusion measurements and additional numerical simulations of the equilibration of adsorbate gratings. We could demonstrate a strong influence of adsorbate-adsorbate interactions and high coverage modulation depths to the LOD signal evolution. This allowed us to qualitatively describe S_{ad} surface diffusion over a wide coverage range, reaching from fastest diffusion rates at low coverages up to rather immobile adlayer phases with low sulfur mobility at high coverages. Furthermore, the findings allowed us to develop approaches required for extracting quantitative surface diffusion rates.

This chapter is based on an article to be published in *ACS Measurement Science Au* [LK2] (in press), available under `https://doi.org/10.1021/acsmeasuresciau.2c00066` and reprinted with permission from Lasse Kattwinkel and Olaf M. Magnussen. Copyright © XXXX The Authors.
L. Kattwinkel and O. M. Magnussen, "Measurement of surface diffusion at the electrochemical interface by in situ linear optical diffraction," ACS Measurement Science Au, in press. (2023).

It is further based on an article to be published in *The Journal of Chemical Physics* [LK3] (submitted manuscript).
L. Kattwinkel and O. M. Magnussen, "Influence of coverage on adsorbate diffusion measurements at electrode surfaces by in situ linear optical diffraction," The Journal of Chemical Physics, submitted manuscript. (2023).

ACS MEASUREMENT SCIENCE Au
AN OPEN ACCESS JOURNAL OF THE AMERICAN CHEMICAL SOCIETY

pubs.acs.org/measureau Letter

Measurement of Surface Diffusion at the Electrochemical Interface by In Situ Linear Optical Diffraction

Lasse Kattwinkel and Olaf M. Magnussen*

Cite This: https://doi.org/10.1021/acsmeasuresciau.2c00066 Read Online

ACCESS | Metrics & More | Article Recommendations | Supporting Information

ABSTRACT: A new in situ method for measuring the surface diffusion rates of adsorbates on electrode surfaces in electrolyte solution is presented. The method is based on the generation of a periodic spatial modulation of the adsorbate coverage via interfering laser pulses and subsequent monitoring of the diffusion-induced decay of this pattern using the optical diffraction signal of a second laser. Proof-of-principle measurements of the surface diffusion of adsorbed sulfur on Pt(111) electrodes in 0.1 M H_2SO_4 indicate potential- and coverage-dependent diffusion constants that are significantly higher than those of sulfur on Pt(111) under vacuum conditions.

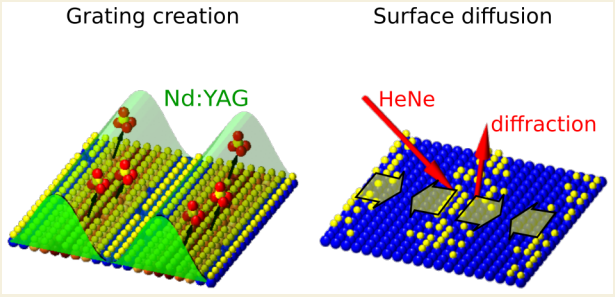

KEYWORDS: *surface diffusion, electrochemical interface, linear optical diffraction, in situ LOD, Pt(111) electrode, chemisorbed sulfur*

Diffusion of adsorbed species at solid−liquid interfaces plays a major role in many processes, such as crystal growth or electrocatalysis. Quantitative data on such interfacial diffusion are therefore essential for understanding and optimizing these processes. Surface diffusion on solids under vacuum conditions has been extensively studied using field electron[1−3] and field ion microscopy,[2−4] scanning probe microscopy,[2,3,5] or profile evolution techniques, where diffusion can be traced optically[2,3,6−12] or by electron microscopy.[2,3,13] In contrast, only a few studies on surface diffusion at the solid−liquid interface exist, predominantly due to the lack of suitable experimental methods. These studies were based on the direct observation of adsorbate motion by electrochemical video-rate scanning tunneling microscopy (STM),[14,15] on STM measurements of the fluctuations of atomic steps[16−18] or adatom island shapes,[17,19] and on nuclear magnetic resonance spectroscopy.[20] Because these studies are restricted to the temperature window of liquid water, where the adsorbate surface mobility is high, they are often limited to model systems with slow diffusion rates.

To measure faster diffusion rates, we introduce here an in situ profile evolution technique, where diffusion is traced using linear optical diffraction (LOD). This method has been extensively used for studies of adsorbate diffusion under ultrahigh vacuum (UHV) conditions, e.g., of CO and H on Pt(111) and Ni(*hkl*).[6−12] In the LOD, a density grating within an adsorbate layer is formed by localized thermal desorption, induced by a temperature grating that is generated using two interfering beams of a pulsed laser. The subsequent evolution of the adsorbate density distribution is then probed by diffraction of a continuous wave laser beam at the grating. From the exponential decrease of the optical diffraction intensity, the surface diffusion coefficient can be extracted.[21,22] This way, diffusion rates can be measured over many orders of magnitude (10^{-7}−10^{-16} cm^2/s).[21]

We here show that LOD is also suited for in situ studies of adsorbate diffusion at the interface between solid electrodes and liquid electrolytes. The optical setup and electrochemical cell is shown in Figure 1 (for more details, see Supporting Information, section 1). The adsorbate coverage grating is created by the beam of a frequency doubled (532 nm), 10 Hz, s-polarized Nd:YAG laser (Continuum Surelite EX), which is split up and brought to interference at the adsorbate covered sample surface under an angle of θ = 17.9°. The resulting grating has a periodicity of $\Lambda = \lambda/(2\sin(\theta)) = 650$ nm[23] and is probed via a 5 mW p-polarized He−Ne laser (632 nm, Thorlabs HNL050L-EC) under an incident angle of 46.9°. Its first-order linear diffraction signal, which reflects the modulation amplitude of the adsorbate distribution, is then emitted almost normal to the surface and measured by a PMT detector (Hamamatsu H11901-01). To compensate intensity fluctuations of the laser beam, its incident intensity is monitored using a photodiode (Thorlabs DET36A/M), located directly at the laser output. An identical photodiode is used to monitor the optical reflectance, which provides information about adsorbate coverage changes during the

Received: November 18, 2022
Revised: December 21, 2022
Accepted: December 22, 2022

https://doi.org/10.1021/acsmeasuresciau.2c00066
ACS Meas. Sci. Au XXXX, XXX, XXX−XXX

ACS Measurement Science Au pubs.acs.org/measureau Letter

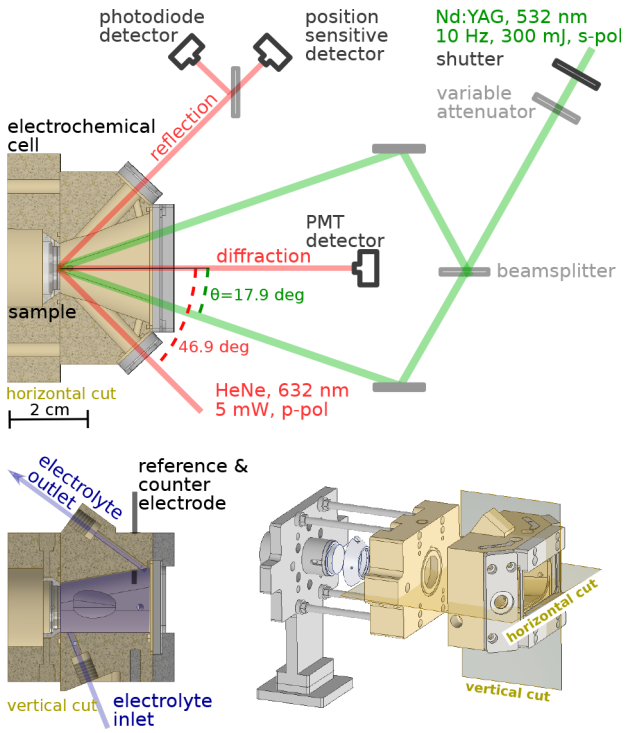

Figure 1. Optical setup and electrochemical cell for in situ LOD measurements of surface diffusion in electrochemical environment.

measurement. An additional position-sensitive detector (Thorlabs PDP90A) allows precise cell alignment and monitoring of the beam pointing stability.

The single crystal sample is located within a newly developed electrochemical cell made of PEEK. An inlet and outlet allow exchanging the electrolyte volume of 10 mL as well as measurements under electrolyte flow. For the optical measurements, the laser beams pass through fused silica windows. These are arranged perpendicular to the probe beam to allow polarization-dependent studies.

Proof-of-principle in situ LOD studies of adsorbate diffusion were performed for sulfur on Pt(111) in 0.1 M H_2SO_4. Chemisorbed sulfur (S_{ad}) is known as a strong catalyst poison and stable over a wide potential range, up to potentials of about 0.8 V/RHE,[24] where oxidation to SO_4^{2-} commences. The onset of oxidation strongly depends on temperature and shifts to lower potentials with higher temperature.[25,26] Furthermore, multiple oxidation cycles of at least 1.2 V are necessary to completely remove chemisorbed S_{ad}.[26] Despite its high relevance to catalyst and fuel cell poisoning, S_{ad} diffusion at Pt(111) electrodes has not been studied so far, and only a few studies exist under vacuum conditions.[5,27,28]

In the experiments, the Pt(111) single crystal sample was first annealed in an induction oven. Then approximately 1 monolayer (ML) S_{ad} was adsorbed by 5 min immersion into 10 mM Na_2S solution, followed by extensive rinsing with ultrapure water and transfer into the cell filled with deaerated electrolyte solution.

The measurement procedure consisted of four steps, schematically shown in Figure 2A: (I) creation of an adsorbate coverage modulation, (II) further coverage reduction, (III) diffusion-induced decay of the previously created coverage modulation, and (IV) determination of the average adsorbate coverage. Figure 2B,C shows the diffraction signal (blue) and the relative reflectance change $\Delta R/R$ (red) as well as the electrode potential (blue) and current density (red) during these steps.

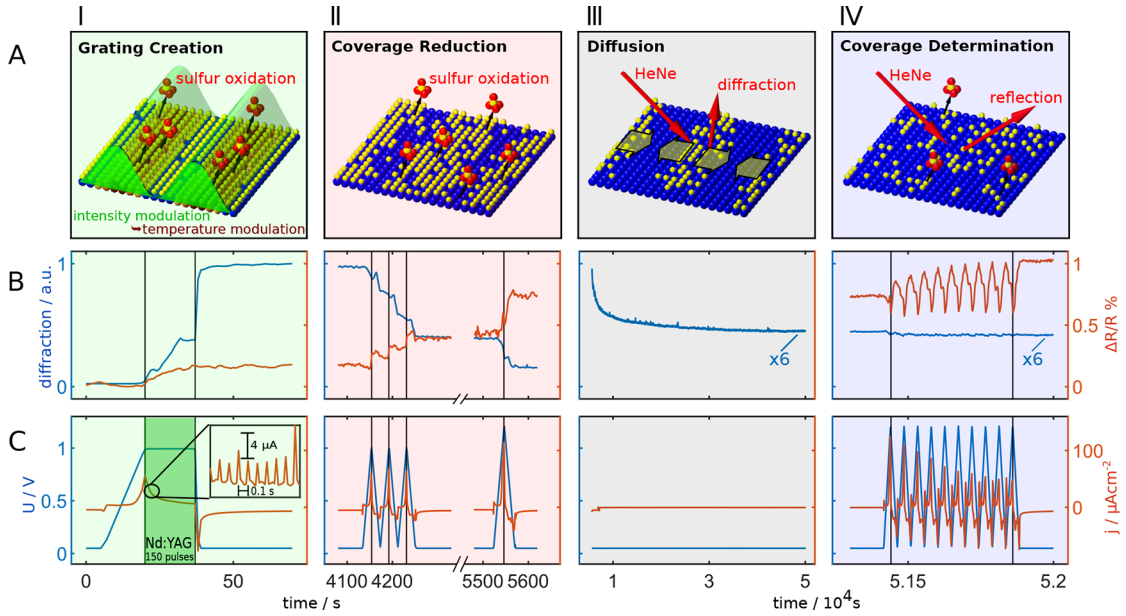

Figure 2. (A) Schematic sketch illustrating the four steps (I–IV) of the in situ LOD measurements, (B) corresponding optical diffraction (blue) and reflectance (red) signal changes, and (C) the potential (blue) and electrochemical current density (red) during a typical measurement. In step I, an adsorbate grating is formed by local sulfur oxidation induced by irradiation with two superimposed beams of the nanosecond Nd:YAG laser. Current spikes due to laser-induced sulfur oxidation are illustrated in the inset. Then, the average adsorbate coverage is further reduced by potential cycles into the sulfur oxidation regime (II), before the actual diffusion measurement by diffraction of the HeNe laser beam at the adsorbate lattice is performed (III). Finally, the average adsorbate coverage in the diffusion measurement is determined by full oxidation of the residual adsorbed sulfur (IV). Note that different time scales in the four sections were used.

https://doi.org/10.1021/acsmeasuresciau.2c00066
ACS Meas. Sci. Au XXXX, XXX, XXX−XXX

In step I, the interference of the Nd:YAG laser beams create a periodic intensity pattern and thus a spatial temperature modulation on the sample. At the same time, the electrode potential is increased to the onset of sulfur oxidation (≈1 V). Because S_{ad} oxidation is temperature-dependent,[25,26] its rate is locally increased in the areas of higher temperature and a periodic S_{ad} grating is created. The enhancement of the oxidation rate by the laser manifests as small current spikes that occur simultaneously with the laser pulses (Figure 2C, inset). Quantitative interpretation of these current spikes is difficult, however, because of the highly nonlinear dependence of the current on the laser intensity. As the S_{ad} is oxidized to SO_4^{2-}, no sulfur readsorption from the electrolyte can occur. This is an advantage as compared to thermal desorption of S_{ad} into the liquid, where readsorption may partially refill the formed grating. However, also laser-independent and thus spatially homogeneous sulfur oxidation occurs in this potential range. Potential and laser pulse energies must therefore be chosen carefully to create an adsorbate grating with sufficient modulation depth, without lowering the average S_{ad} coverage too much or damaging the Pt surface (see Supporting Information, section 5).

The formation of the grating can be clearly observed in the diffraction signal, which is continuously increasing during application of the Nd:YAG laser pulses. Sufficiently strongly modulated S_{ad} gratings could only be achieved by multiple (50−300) pulses. Unfortunately, the increase in signal with number of pulses was not fully reproducible, probably because of small positional fluctuations in the interference patterns of the individual pulses. We therefore chose the number of pulses on the basis of the diffraction signal amplitude. After the initial grating formation, the potential is changed back from the oxidative regime to the double layer or hydrogen adsorption region. This potential change results in a pronounced increase of the diffraction signal. We attribute this increase to the desorption of oxygenated species that were previously adsorbed on Pt lattice sites are freed from S_{ad} by the grating creation process. As the optical diffraction signal originates from differences in the local reflectance of the surface and the difference between bare (or SO_4^{2-} covered) and the S_{ad} covered Pt(111) electrode is larger than that between Pt(111) covered by oxygenated species and by S_{ad},[24] the desorption of oxygenated surface species will increase the grating contrast.

In step II, the average sulfur coverage can be further reduced by potential cycling, as evidenced by the increase in $\Delta R/R$ already described in ref 24. This allows studying the S_{ad} diffusion at different coverages. The coverage reduction is controlled by the upper potential limit or the number of cycles and can be directly monitored by the change in $\Delta R/R$. However, the decrease in S_{ad} coverage also leads to a strong decrease of the diffraction signal.

Step III is the actual measurement of the surface diffusion process. The latter results in a gradual decay of the coverage profile until the coverage is uniform. The corresponding decrease in the amplitude of the adsorbate grating is determined from the change in the diffraction signal. If the diffusion constant D is coverage-independent, the diffraction signal intensity I follows an exponential decay (see Supporting Information, section 2):

$$I(t) = I(t=0)\cdot\exp\left(\frac{-8\pi^2 D}{\Lambda^2}t\right) \quad (1)$$

Thus, D can be directly obtained from the decay's time constant. If D is coverage-dependent, there is no simple expression describing the diffraction signal and a multi- or non-exponential decay is expected.[22] However, eq 1 remains a sufficiently good approximation for a grating with a shallow coverage modulation, where D can be assumed to be rather constant.[6,7] This is usually the case after sufficiently long times, when the coverage distribution approaches equilibrium, as can be observed in the example in Figure 2B, III (see Supporting Information, section 4). Here, the diffraction signal can be described by a single exponential decay, after the initially fast decay of the signal has subsided.

In the last step (IV) of the experiment, the average coverage is determined by oxidative stripping of the remaining S_{ad} via potential cycles and analysis of the corresponding changes in the optical reflectance signal (see Supporting Information, section 3). The relation between optical reflectance change and sulfur coverage was already investigated in a previous work[24] and is shown in the inset of Figure 3B. In some experiments, a small diffraction signal remained even after complete removal

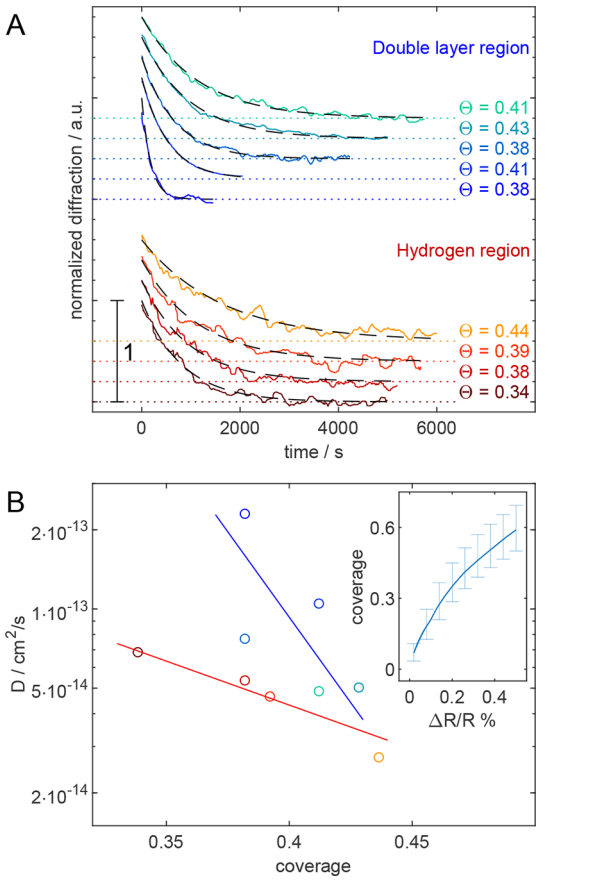

Figure 3. (A) LOD transients of S_{ad} diffusion on Pt(111) in the double layer (blue to green, U = 0.31 V) and hydrogen adsorption region (red to yellow, U = 0.17, 0.12, 0.14, 0.05 V) and corresponding exponential fits (black dashed line) at various S_{ad} coverages Θ. (B) Resulting diffusion constants as a function of S_{ad} coverage. The coverages were determined from the change in $\Delta R/R$ using the $\Delta R/R$−coverage relation plotted in the inset. Adapted with permission from ref 24. Copyright 2022 Elsevier Ltd.

https://doi.org/10.1021/acsmeasuresciau.2c00066
ACS Meas. Sci. Au XXXX, XXX, XXX−XXX

of the S_{ad} from the surface (see Figure 2B). This is attributed to minor laser-induced Pt surface modification.

Using the described methodology, we studied the coverage and potential dependence of S_{ad} surface diffusion on Pt(111) in 0.1 M H_2SO_4 in the hydrogen adsorption and double layer region. The selected measurements (see Supporting Information, appendix) are performed at coverages between 0.34 and 0.44 ML (error estimation is given in the Supporting Information, section 3). The decay of the diffraction signals (Figure 3A, colored lines) is well described by single exponential fits (dashed black lines), from which the diffusion constants were extracted via eq 1 (for more details, see Supporting Information, section 4).

In Figure 3B, the obtained diffusion constants are plotted against coverage for the two potential regimes. They are in the range of 2×10^{-14} to 2×10^{-13} cm^2/s. The scatter in the data largely results from the limited accuracy of the coverage measurement, which is about ±0.02 ML. The error in D originating from the exponential fit is smaller than 6% (95% confidence interval) and can thus be neglected. In both potential regions, the S_{ad} diffusion is faster at lower coverages, although the effect is stronger in the double layer than in the hydrogen adsorption region (a factor 20 per 0.1 ML coverage change compared to a factor 2.2 per 0.1 ML, according to a linear regression). Furthermore, diffusion in the double layer region is faster than diffusion in the hydrogen region at least at lower coverages. This suggests that adsorbed hydrogen inhibits the S_{ad} surface diffusion by blocking available surface sites. The measured diffusion rates are about an order of magnitude higher than those found by Renisch et al. for tracer diffusion of S_{ad} on Pt(111) under UHV conditions.[5] Extrapolating the coverage dependence observed in our studies to the tracer diffusion regime, this difference would be even several orders of magnitude larger. Although minor laser-induced modification of the Pt substrate is observed for some measurements in the double layer region (see Supporting Information, section 5), such modification cannot explain these findings because it should increase the density of defects which usually inhibits surface diffusion.[3] Thus, our observations indicate a pronounced influence of the electrochemical environment on the surface diffusion process.

In summary, we introduced in situ linear optical diffraction as a new method for measuring surface diffusion in electrochemical environment and demonstrated its feasibility by measuring the diffusion of S_{ad} on Pt(111) in 0.1 M H_2SO_4. The measured diffusion constants are close to the upper limit of what can be measured by direct microscopic methods, such as video-rate STM. However, in situ LOD, in principle, allows one to measure even much faster diffusion processes. Already the current experimental setup would allow decay constants to be measured in the range of several seconds, which would enable quantitative determination of diffusion constants that are up to 3 orders of magnitude higher than those reported in this work. Several orders of magnitude more are obtainable by increasing the lattice spacing of the adsorbate grating, which would require modification of the incident angles and the electrochemical cell. Therefore, in situ LOD allows the range of surface diffusion measurements in electrochemical environment to be extended from low-mobility model systems to systems of high practical relevance, e.g., in electrocatalysis. Furthermore, the general approach may have applications beyond surface diffusion measurements. For example, the subsequent adsorption of reactive species into an adsorbate grating (e.g., the adsorption of OH in a grating of adsorbed CO) could allow the rate of surface reactions at electrochemical interfaces to be quantitatively measured.

■ ASSOCIATED CONTENT

Supporting Information

The Supporting Information is available free of charge at https://pubs.acs.org/doi/10.1021/acsmeasuresciau.2c00066.

In situ LOD setup and cell, simple model for the adsorbate grating evolution, sulfur coverage determination from optical reflectance, temporal evolution of the diffraction signal, influence of grating creation on the platinum surface, measurement data (PDF)

■ AUTHOR INFORMATION

Corresponding Author

Olaf M. Magnussen − *Institut für Experimentelle und Angewandte Physik, Christian-Albrechts-Universität zu Kiel, 24118 Kiel, Germany;* orcid.org/0000-0003-4900-0880; Email: magnussen@physik.uni-kiel.de

Author

Lasse Kattwinkel − *Institut für Experimentelle und Angewandte Physik, Christian-Albrechts-Universität zu Kiel, 24118 Kiel, Germany;* orcid.org/0000-0001-5360-4949

Complete contact information is available at: https://pubs.acs.org/10.1021/acsmeasuresciau.2c00066

Author Contributions

CRediT: **Lasse Kattwinkel** conceptualization (equal), formal analysis (lead), investigation (lead), methodology (lead), software (lead), visualization (lead), writing-original draft (lead); **Olaf M. Magnussen** conceptualization (equal), funding acquisition (lead), supervision (lead), writing-review & editing (lead).

Notes

The authors declare no competing financial interest.

■ ACKNOWLEDGMENTS

We gratefully acknowledge financial support by the Struktur- und Exzellenzbudget des Landes Schleswig-Holstein.

■ REFERENCES

(1) DiFoggio, R.; Gomer, R. Diffusion of hydrogen and deuterium on the (110) plane of tungsten. *Phys. Rev. B* **1982**, *25*, 3490−3511.

(2) Gomer, R. Diffusion of adsorbates on metal surfaces. *Rep. Prog. Phys.* **1990**, *53*, 917.

(3) Barth, J. Transport of adsorbates at metal surfaces: from thermal migration to hot precursors. *Surf. Sci. Rep.* **2000**, *40*, 75−149.

(4) Lovisa, M. F.; Ehrlich, G. Quantitative determinations of the temperature dependence of diffusion phenomena in the FIM. *Surf. Sci.* **1991**, *246*, 43−49.

(5) Renisch, S.On the diffusion of adsorbed particles on single crystal surfaces: dynamical investigations with the scanning tunneling microscope. Ph.D. thesis, FU Berlin, 1999.

(6) Ma, J.; Xiao, X.; DiNardo, N. J.; Loy, M. M. T. Diffusion of CO on Pt(111) studied by an optical diffraction method. *Phys. Rev. B* **1998**, *58*, 4977−4983.

(7) Xiao, X.-D.; Xie, Y.; Shen, Y. R. Coverage dependence of anisotropic surface diffusion: CO/Ni(110). *Phys. Rev. B* **1993**, *48*, 17452−17462.

https://doi.org/10.1021/acsmeasuresciau.2c00066
ACS Meas. Sci. Au XXXX, XXX, XXX−XXX

(8) Zheng, C. Z.; Yeung, C. K.; Loy, M. M. T.; Xiao, X. Step effects and coverage dependence of hydrogen atom diffusion on Pt(111) surfaces. *Phys. Rev. B* **2004**, *70*, 205402.
(9) Zheng, C. Z.; Yeung, C. K.; Loy, M. M. T.; Xiao, X. Quantum diffusion of H on Pt(111): step effects. *Phys. Rev. Lett.* **2006**, *97*, 166101.
(10) Zhu, X. D.; Lee, A.; Wong, A.; Linke, U. Surface diffusion of hydrogen on Ni(100): an experimental observation of quantum tunneling diffusion. *Phys. Rev. Lett.* **1992**, *68*, 1862−1865.
(11) Lee, A.; Zhu, X. D.; Deng, L.; Linke, U. Observation of a transition from over-barrier hopping to activated tunneling diffusion: H and D on Ni(100). *Phys. Rev. B* **1992**, *46*, 15472−15476.
(12) Cao, G. X.; Nabighian, E.; Zhu, X. D. Diffusion of hydrogen on Ni(111) over a wide range of temperature: exploring quantum diffusion on metals. *Phys. Rev. Lett.* **1997**, *79*, 3696−3699.
(13) von Oertzen, A.; Rotermund, H.H.; Nettesheim, S. Investigation of diffusion of CO absorbed on Pd(111) by a combined PEEM/LITD technique. *Chem. Phys. Lett.* **1992**, *199*, 131−137.
(14) Tansel, T.; Magnussen, O. M. Video STM studies of adsorbate diffusion at electrochemical interfaces. *Phys. Rev. Lett.* **2006**, *96*, 026101.
(15) Yang, Y.-C.; Magnussen, O. M. Quantitative studies of adsorbate dynamics at noble metal electrodes by in situ video-STM. *Phys. Chem. Chem. Phys.* **2013**, *15*, 12480−12487.
(16) Giesen, M.; Randler, R.; Baier, S.; Ibach, H.; Kolb, D. Step dynamics on Cu (100) and Ag (111) electrodes in an aqueous electrolyte. *Electrochim. Acta* **1999**, *45*, 527−536.
(17) Giesen, M. Step and island dynamics at solid/vacuum and solid/liquid interfaces. *Prog. Surf. Sci.* **2001**, *68*, 1−154.
(18) Baier, S.; Giesen, M. Determination of activation energies of mass transport processes on Ag(111) electrodes in aqueous electrolyte. *Phys. Chem. Chem. Phys.* **2000**, *2*, 3675−3680.
(19) Giesen, M.; Beltramo, G.; Dieluweit, S.; Müller, J.; Ibach, H.; Schmickler, W. The thermodynamics of electrochemical annealing. *Surf. Sci.* **2005**, *595*, 127−137.
(20) Babu, P.; Chung, J.-H.; Oldfield, E.; Wieckowski, A. CO surface diffusion on platinum fuel cell catalysts by electrochemical NMR. *Electrochim. Acta* **2008**, *53*, 6672−6679.
(21) Zhu, X. D. Optical diffractions as probes to surface diffusion of adsorbates. *Modern Physics Letters B* **1992**, *06*, 1217−1235.
(22) Xiao, X.-D.Surface diffusion studies by optical diffraction techniques. Ph.D. thesis, University of California, 1992.
(23) Eichler, H. J.; Hermerschmidt, A. In *Photorefractive materials and their applications 1: basic effects*; Günter, P., Huignard, J.-P., Eds.; Springer: New York, 2006; pp 7−42.
(24) Kattwinkel, L.; Magnussen, O. M. Optical reflectance studies on the oxidation of chemisorbed sulfur at the Pt(111) electrode. *Electrochim. Acta* **2022**, *434*, 141297.
(25) Sung, Y.-E.; Chrzanowski, W.; Wieckowski, A.; Zolfaghari, A.; Blais, S.; Jerkiewicz, G. Coverage evolution of sulfur on Pt(111) electrodes: from compressed overlayers to well-defined islands. *Electrochim. Acta* **1998**, *44*, 1019−1030.
(26) Zolfaghari, A.; Jerkiewicz, G.; Chrzanowski, W.; Wieckowski, A. Energetics of the underpotential deposition of hydrogen on platinum electrodes: II. presence of coadsorbed sulfur. *J. Electrochem. Soc.* **1999**, *146*, 4158−4165.
(27) Nilekar, A. U.; Greeley, J.; Mavrikakis, M. A simple rule of thumb for diffusion on transition-metal surfaces. *Angew. Chem.* **2006**, *118*, 7204−7207.
(28) Bernard Rodriguez, C. R.; Santana, J. A. Adsorption and diffusion of sulfur on the (111), (100), (110), and (211) surfaces of FCC metals: density functional theory calculations. *J. Chem. Phys.* **2018**, *149*, 204701.

https://doi.org/10.1021/acsmeasuresciau.2c00066
ACS Meas. Sci. Au XXXX, XXX, XXX−XXX

Measurement of Surface Diffusion at the Electrochemical Interface by In Situ Linear Optical Diffraction

Supporting Information

Lasse Kattwinkel and Olaf M. Magnussen

Contents

SI 2.1 *in situ* LOD SETUP AND CELL

The experimental setup was developed specifically for *in situ* LOD measurements in electrochemical environment. It consists of an optical table with the Nd:YAG and the HeNe laser, all optical components and detectors (see Figure SI 2.2), and a custom-designed electrochemical cell (see Figure SI 2.1). The cells' geometry is predominantly determined by the external optical beam path. The Nd:YAG beams are brought to interference on the sample surface under an angle of $\theta = 17.9°$ (within the cell). Assuming highly diluted acid with a refractive index of $n = 1.33$ as electrolyte, the wavelength $\lambda'_{Nd:YAG}$ within this medium is given by $\lambda'_{Nd:YAG} = \lambda_{Nd:YAG}/n = 400$ nm. The resulting grating has therefore a periodicity of $\Lambda = \lambda'_{Nd:YAG}/\left(2sin\left(\theta\right)\right) = 650$ nm [42]. The grating is probed using the first order diffraction signal of a HeNe laser with the wavelength of $\lambda'_{HeNe} = \lambda_{HeNe}/n = 476$ nm within the electrolyte. The condition for the first order interference maximum is $sin\left(\beta\right) + sin\left(\gamma\right) = \lambda'_{HeNe}/\Lambda$. Accordingly, the diffracted beam can be detected perpendicular to the surface ($\beta = 0°$) by using an incident angle of $\gamma = 46,9°$. To simplify the cell alignment and enable also polarization dependent measurements, the probe laser beam should pass all windows perpendicularly. Therefore, we chose a cell design with 3 windows, a big front window for the Nd:YAG beams and the diffracted HeNe beams and two smaller side windows for the incident and reflected HeNe beam.

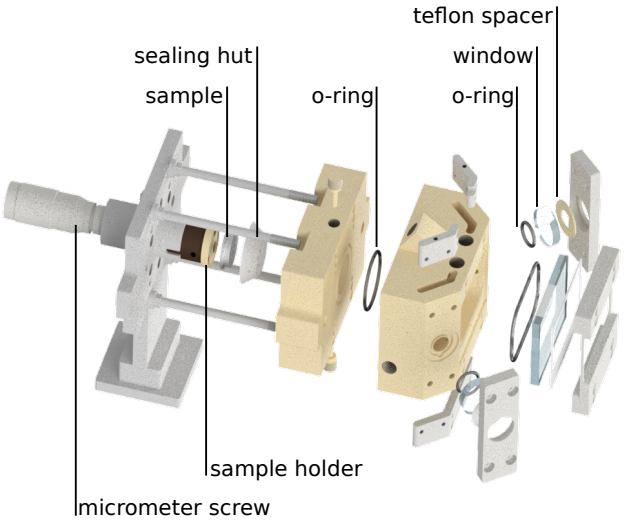

Figure SI 2.1: Electrochemical cell, disassembled into its single parts.

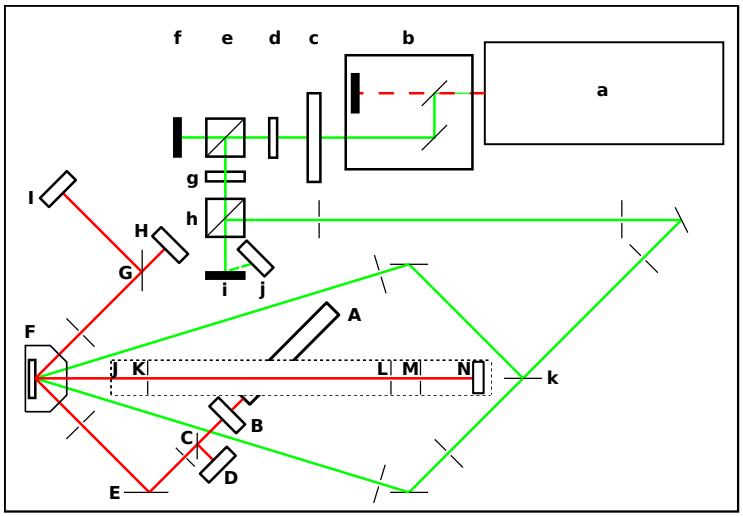

a) Nd:YAG laser
b) infrared separation
c) shutter
d) half wave plate
e) beamsplitter (pol. dependent)
f) beam dump
g) nd filter
h) beamsplitter (pol. dependent)
i) beam dump
j) Si detector (pulse acquisition)
k) beamsplitter (50:50)

A) HeNe laser
B) shutter
C) beamsplitter (10:90)
D) Si detector (HeNe monitor)
E) periscope
F) cell / sample
G) beamsplitter (90:10)
H) position sensitive detector
I) Si detector (reflection)
J) optical bench (covered)
K) iris
L) variable horizontal slit
M) variable vertical slit
N) PMT detector

(a)

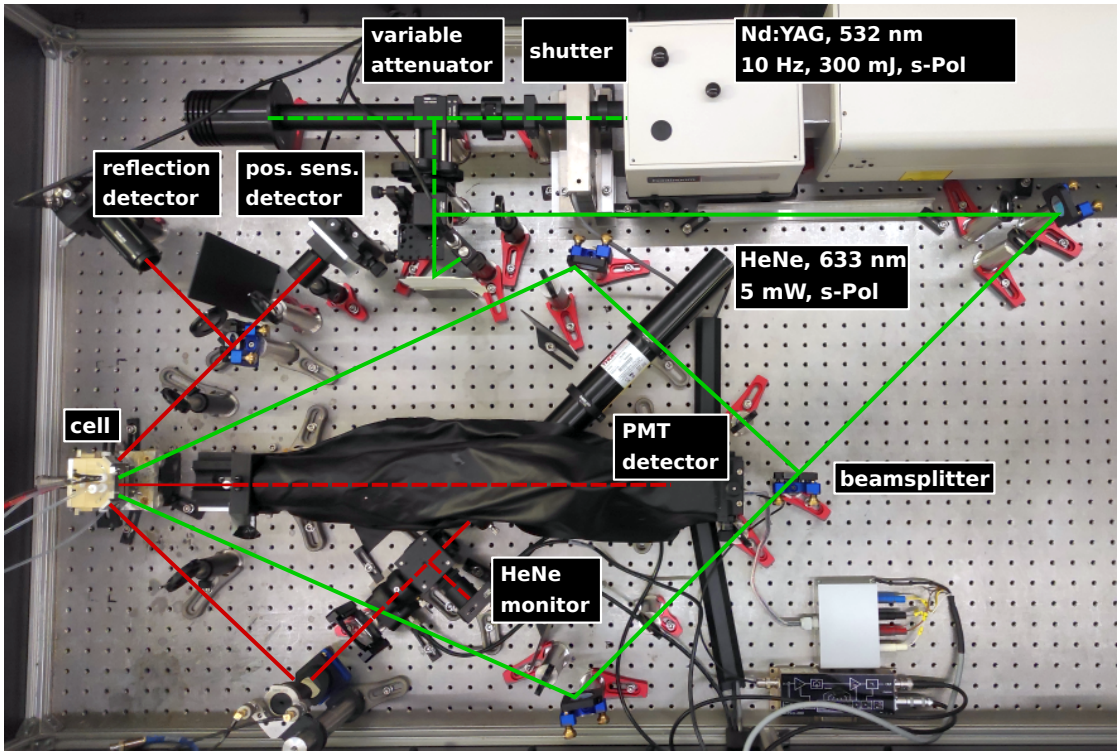

(b)

Figure SI 2.2: Scheme (a) and image (b) of the optical setup.

SI 2.2 SIMPLE MODEL FOR THE ADSORBATE GRATING EVOLUTION

In the following, a simple model for the adsorbate grating evolution and the corresponding first order linear diffraction signal will be discussed. The created adsorbate grating has some arbitrary, yet periodic shape. Its local coverage $\Theta(x,t)$ can therefore be described using a Fourier series [19–21]

$$\Theta(x,t) = \Theta_0 + \sum_{n=1}^{\infty} \Theta_n(t)\, cos\,(2n\pi x/\Lambda) \tag{8.1}$$

with Θ_0 being the average adsorbate coverage, Λ the periodicity of the grating, and $\Theta_n(t)$ describing the coverage modulation of the n-th harmonics of the grating. In the case that the optical reflectance R is linearly proportional to the coverage of adsorbates, the diffraction intensity for the n-th harmonic of the grating I_n is given by: [19–21]

$$I_n(t) \quad \sim \quad \Theta_n^2(t)\,. \tag{8.2}$$

For sulfur covered Pt(111), a linear relation was found between R and Θ over a wide range of sulfur coverage [LK1]. Deviations from this behavior were only found for coverages $\Theta \leq 0.3$ ML. However, even in the latter case a linear relationship is a good approximation for adsorbate gratings with small modulation amplitude, so that the system can be described well using equation 8.2.
Surface diffusion results in a gradual equilibration of the adsorbate distribution, i.e., a decay of the adsorbate grating. This process can be described by the one-dimensional diffusion equation:

$$\frac{\delta\Theta}{\delta t} = \frac{\delta}{\delta x}\left(D\left(\Theta(x,t)\right)\frac{\delta\Theta}{\delta x}\right) \tag{8.3}$$

with the diffusion coefficient $D(\Theta)$ generally being dependent on the coverage $\Theta(x,t)$. If the modulation amplitude of the adsorbate grating is small, D can be approximated by a constant value. In this case, the time evolution of an arbitrary grating can be calculated analytically by combining equation 8.1 and 8.3, resulting in: [21, 24]

$$\Theta_n(t) = \Theta_n(t=0)\cdot exp\left(\frac{-4\pi^2 n^2 D}{\Lambda^2}t\right) \tag{8.4}$$

with $\Theta_n(t=0)$ being the initial coverage modulation of the n-th harmonic. As the diffraction signal $I_n(t)$ is proportional to $\Theta_n^2(t)$ (see equation 8.2), it can be described by: [21, 24]

$$I_n(t) = I_n(t=0)\cdot exp\left(\frac{-8\pi^2 n^2 D}{\Lambda^2}t\right)\,. \tag{8.5}$$

The time evolution of the first order (n=1) diffraction signal, which is measured in linear optical diffraction, is therefore given by:

$$I_1(t) = I_1(t=0)\cdot exp\left(\frac{-8\pi^2 D}{\Lambda^2}t\right)\,. \tag{8.6}$$

Thus, the diffusion constant D can be determined from the exponential decay of the intensity over an arbitrary time interval from $t_1 \geq 0$ to $t_2 > t_1$.

SI 2.3 SULFUR COVERAGE DETERMINATION FROM OPTICAL REFLECTANCE

At the end of every measurement, the S_{ad} coverage is determined by performing potential cycles into the regime of S_{ad} oxidation and analysis of the corresponding change in the optical reflectance signal.
As shown in Figure SI 2.3, the reflectance change is obtained from the difference in the averaged signal prior to and after the S_{ad} stripping. If necessary, an additional drift correction was applied beforehand to compensate fluctuations in the reflectance signal. As we showed in a previous work [LK1], the obtained reflectance change can be directly correlated with a sulfur coverage change, which equals the total sulfur coverage in this case. The inset of Figure 3B (main publication) shows an excerpt of the corresponding relation, using the previously published data. The error bars originate from uncertainties in the coulometric data on which this relation is based. These uncertainties are also responsible for the rather low absolute precision of the determined coverage, which we estimate as ± 0.1 ML. Note, that this systematic error affects all coverage values equally. The individual deviations of each coverage measurement are much smaller ($\approx \pm 0.02$ ML) and originate from drifts in the reflectance signal.

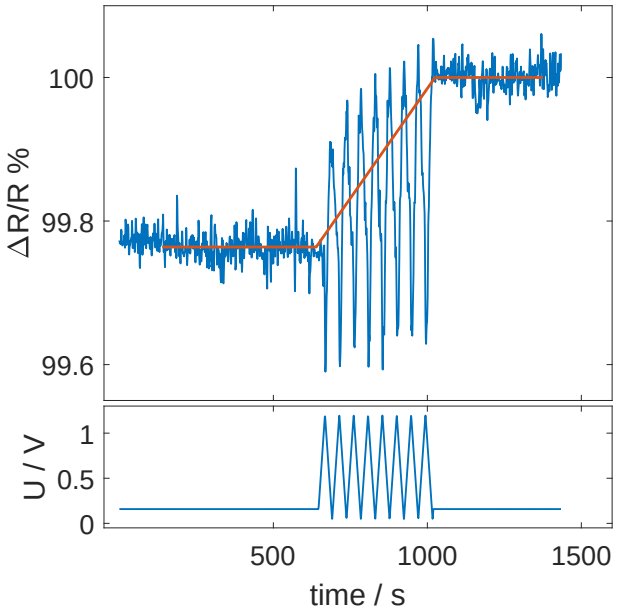

Figure SI 2.3: Optical reflectance change during oxidative stripping of S_{ad} by potential cycles in the last step (IV) of a typical experiment.

SI 2.4 TEMPORAL EVOLUTION OF THE DIFFRACTION SIGNAL

The diffraction signals of the diffusion measurements can be described by either a single-exponential (Figures A.2-A.3, measurements I-III,VIII) or a multi-exponential decay (Figures A.2-A.3, measurements IV-VII,IX). A non single-exponential diffraction signal was already reported for second harmonic diffraction studies of CO on Ni(110) in vacuum [24]. The authors analyzed, that force fitting such data with a single exponential leads to major errors in the extracted diffusion constants. The physical picture behind this behaviour was explained with the coexistence of several decay time constants, that were attributed to high coverage modulations of the gratings. Therefore, a faster diffusion at high coverages dominated the signal in the initial stages of the diffusion process. For proper data analysis, the authors proposed to either wait long enough for the coverage modulation to decrease or to directly generate gratings with small modulation amplitudes [21].
In the case of single-exponential decay, the diffraction signals were therefore analyzed as presented in Figure 3 (main publication). In the case of multi-exponential decay, the diffraction signals can be described using the sum of two exponential functions (see Figure SI 2.4, red dashed line). These measurements are only analyzed in the time range where the fast exponential function (purple line) already subsided (shaded in grey) and the diffraction signal thus is well described by a single-exponential decay. Following Ref. [24], the two types of measurements were

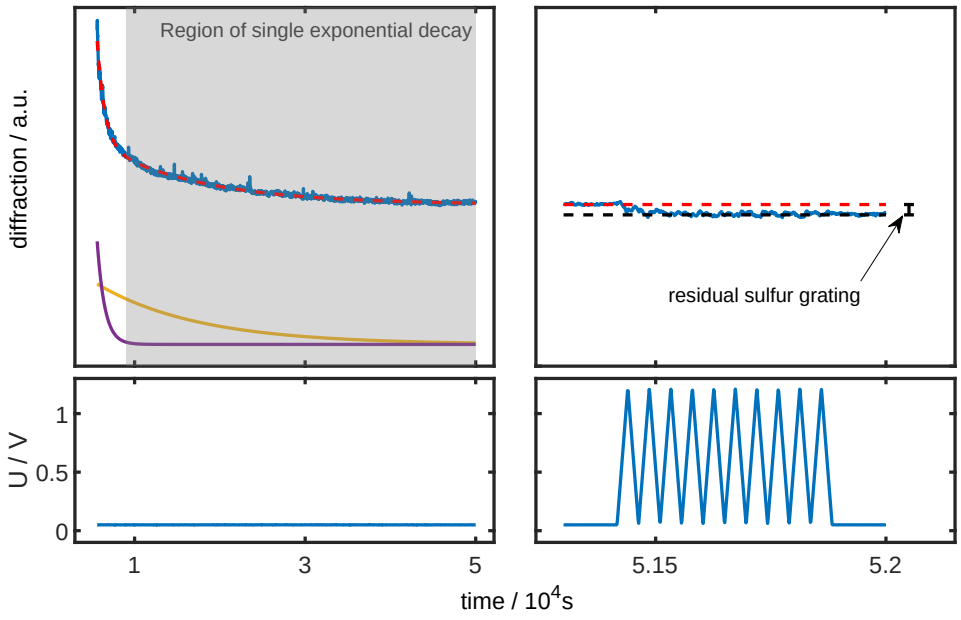

Figure SI 2.4: Example for a measurement exhibiting a multi-exponential decay of the diffraction signal (top panels, blue line). During the diffusion measurement (left panels), the signal can be fitted using the sum of two exponential functions (dashed red line, individual components shown underneath as purple and yellow line). During the coverage determination process (right panels), the diffraction signal slightly decreases (see dashed red and black lines), which can be associated to the oxidation of a small residual S_{ad} grating.

attributed to the decay of S_{ad} gratings with a low and with a high initial coverage modulation, respectively. The employed procedure thus ensures that comparable diffusion data is obtained from the two types of measurements.
The analysis was restricted to measurements in which the S_{ad} grating decayed almost completely (Figures A.2-A.3). This is the case if the diffraction signal exhibits only minor changes after oxidative S_{ad} desorption at the end of a measurement (see Figure SI 2.4, right). Only then, the data allowed to verify the presence of a single-exponential decay with well-defined time constant.

SI 2.5 INFLUENCE OF GRATING CREATION ON THE PLATINUM SURFACE

As atomic steps and lattice defects may influence surface diffusion [8, 9], it is important to ensure a flat sample surface. For the initial preparation, the Pt(111) sample was annealed in hydrogen atmosphere using an inductional oven. AFM measurements in ambient environment (Figure SI 2.5A) and electrochemical measurements (see figure SI 2.6A) indicate that this preparation results in an atomically flat surface with low defect density. However, also the grating creation process may damage the surface. In this case, one would expect a periodic accumulation of crystal defects (e.g. adatoms or vacancies) in the areas with high laser intensity or even a grating-like structure within the platinum substrate. Both should manifest in the form of an increased diffraction signal that remains permanently and cannot be removed by potential cycling. Specifically, the diffraction signal after complete S_{ad} oxidation at the end of the measurement would be higher compared to its value prior to the grating creation process (i.e., at the beginning of the experiment).

In many of the experiments, specifically 3 of 4 diffusion measurements acquired in the hydrogen region (Figure A.2), the diffraction signal almost completely retains its

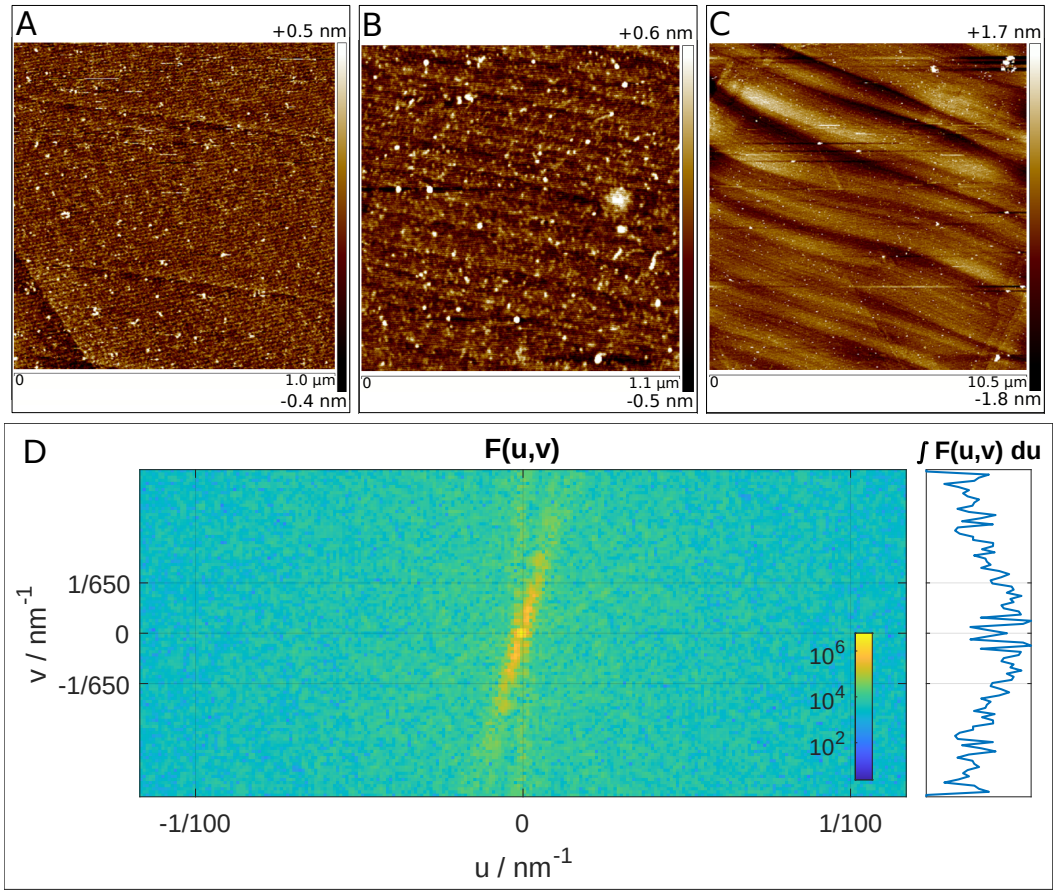

Figure SI 2.5: AFM images of the Pt(111) surface (A) prior to and (B, C) after creation and oxidative removal of an S_{ad} grating. (D) 2D Fourier transform of the image in (C) and its average value in horizontal direction, shown on a logarithmic scale. No residual grating structure (expected in horizontal direction with a periodicity of about 650 nm) can be detected.

initial value. To verify, that this implies the absence of laser-induced surface defects, we performed AFM characterization of a sample where no increase of the diffraction signal was found after oxidatively removing the S_{ad} grating (Figure SI 2.5B). Compared to the freshly annealed surface (Figure SI 2.5A), this surface appears more inhomogeneous, probably due to impurities deposited on the sample during transfer out of the electrolyte. However, no periodic structures with a periodicity of about 650 nm in the direction of the grating (horizontally) are visible. Also larger scale AFM images (Figure SI 2.5C) do not reveal any corresponding periodicity in the image or its 2D Fourier transform (Figure SI 2.5D), indicating that the grating formation procedure in such cases does not affect the Pt surface morphology.
However, in other experiments a significant residual diffraction signal is found (Figure A.3, V-VIII) and thus a laser induced roughening of the surface can be expected. Unfortunately, no AFM images were taken after these measurements, which precludes statements about the concrete morphology changes of the samples. Cyclic voltammograms recorded at the end of such a measurement (see figure SI 2.6C) are comparable to CVs recorded on sulfur covered samples without previous laser irradiation (see figure SI 2.6B). These findings suggest that the irradiation has a smaller or different influence on the surface morphology as the sulfur oxidation process itself.

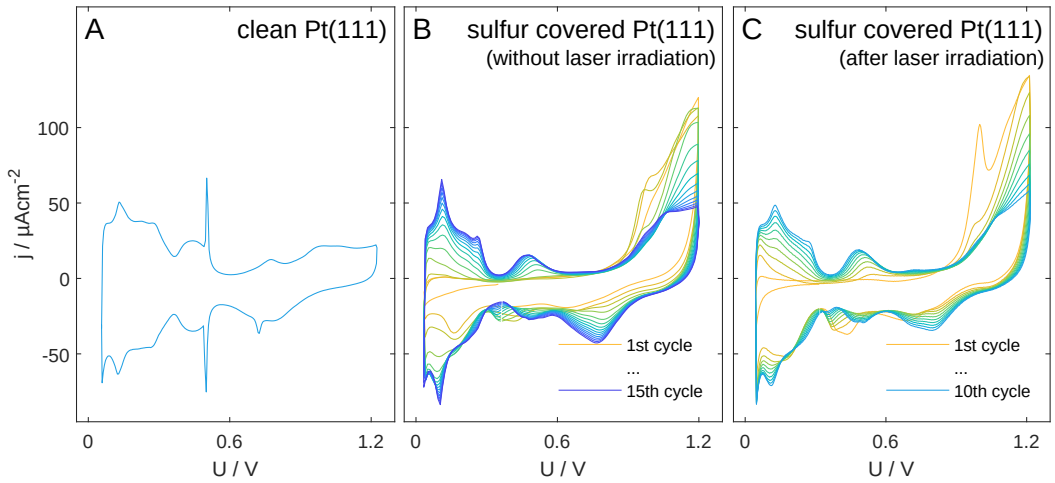

Figure SI 2.6: CVs of a freshly prepared Pt(111) crystal in 0.1 M H_2SO_4 for a clean (A) and sulfur covered (B) sample. In (C) typical CVs acquired during step IV at the end of a diffusion measurement (measurement VIII) are shown, from which the S_{ad} coverage is determined. All CVs were obtained in the *in situ* LOD electrochemical cell on the same Pt(111) electrode. (A) and (B) are adapted with permission from Ref. [LK1]. Copyright 2022 Elsevier Ltd.

Influence of coverage on adsorbate diffusion measurements at electrode surfaces by *in situ* linear optical diffraction

Lasse Kattwinkel[a] and Olaf M. Magnussen[a]

[a]*Institut für Experimentelle und Angewandte Physik, Christian-Albrechts-Universität zu Kiel, Leibnizstraße 19, Kiel, 24118, Germany*

ABSTRACT

In situ linear optical diffraction is a new method for studies of surface mass transport in electrochemical environment that is based on the equilibration of coverage gratings in an adlayer on the electrode surface. We here discuss the temporal evolution of the diffraction intensity on the basis of experimental data for sulfur adsorbates on Pt(111) electrodes in 0.1 M H_2SO_4 and simulations of the time-dependent diffusion profiles. At low and medium sulfur coverage, the decay of the signal exhibits two time scales, which can be explained by the influence of coverage dependent diffusion rates on the evolution of gratings with large coverage modulation. At high coverage, a further, ultra-slow decay process or even a complete termination of the decay are observed, which we attribute to the presence of high-density ordered adlayer phases with low sulfur mobility. These results provide insight into the approaches required for extracting quantitative surface transport rates from linear optical diffraction measurements.

Keywords: Sulfur, Surface diffusion, Pt(111) electrode, Interface structure, Optical diffraction

INTRODUCTION

Sulfur poisoning is well known to decrease the efficiency of platinum based catalysts or fuel cells. Despite the high relevance of this effect to upcoming hydrogen based energy storage and conversion systems, underlying fundamental processes like sulfur site blocking capabilities [73, 74], sulfur oxidative removal [57, 71, 72, 75, 77–86] and sulfur surface diffusion on Pt surfaces are still poorly understood. For the latter existed only few studies under vacuum conditions [37, 87, 88] but none in electrochemical environment. This lack of experimental data is due to the lack of suitable techniques for studying surface diffusion at electrochemical interfaces. Only a few experimental methods exist, such as electrochemical video-rate scanning tunneling microscopy (VSTM) [10, 30], which are restricted to rather small diffusion rates and largely limited to model systems.
Recently, our group adapted linear optical diffraction (LOD), a profile evolution technique where diffusion rates are determined by an all-optical approach, for *in situ* studies in electrochemical environment [LK2]. LOD measurements have been extensively used for measuring surface diffusion under ultrahigh vacuum

(UHV) conditions and allows measuring surface diffusion over many orders of magnitude [12–14, 24, 25, 41, 50]. We showed that the same principle can be applied also for studying the diffusion of adsorbates at the electrochemical interface. First proof-of-principle *in situ* LOD measurements were performed for the case of of sulfur diffusion on Pt(111) electrodes in 0.1 M H_2SO_4 solution and quantitative data for S_{ad} diffusion at coverages between 0.34 and 0.44 monolayers (ML) were acquired.
Here, we present a more detailed analysis of the diffusion behavior in this system, covering a wider range of S_{ad} coverages. We specifically address the temporal evolution of the diffraction signal measured in the *in situ* LOD experiments and compare it with numerical simulations. In combination, this provides a better understanding of the LOD signal evolution and, in particular, on the effect of coverage dependent surface diffusion rates.

EXPERIMENTAL

The newly developed *in situ* LOD methodology is already described in our previous publication [LK2] and will only be briefly summarized here. The experimental setup and measurement procedure is shown in figure 8.1. First, a periodic spatial coverage modulation is created within the sulfur adsorbate layer on the Pt(111) substrate. This is achieved by irradiating the sample at a potential close to sulfur oxidation regime with an s-polarized, frequency doubled, pulsed Nd:YAG laser beam, which is split up and brought to interference on the sample under an angle of $\theta = 17.9°$. The resulting intensity pattern (with a periodicity of $\Lambda = \lambda / (2sin(\theta)) = 650$ nm) [42] leads to spatially modulated heating of the Pt surface (figure 8.1b-I). Because S_{ad} oxidation is temperature dependent [56, 57], an increased sulfur oxidation yield is obtained in areas of higher temperature and a grating is created within the adsorbate layer. The grating is probed using the first order linear diffraction signal of a 5 mW HeNe laser. In addition, the optical reflectance is monitored to gather information about adsorbate coverage changes during the measurement. To allow diffusion measurements at various sulfur coverages, the coverage can be further reduced by potential cycling in a second step (figure 8.1b-II).
In the actual diffusion measurement the change of the first order diffraction signal intensity I with time is monitored at a fixed potential (figure 8.1b-III). As will be discussed in more detail below, I is directly related to the coverage modulation in the grating. Because of the gradual equilibration of the coverage modulation via surface diffusion, I decreases until a uniform coverage is reached. If the diffusion constant D is coverage independent, the diffraction signal follows an exponential decay [24] with

$$I(t) = I(t=0) \cdot exp\left(-\tau^{-1} \cdot t\right); \text{ with } \tau^{-1} \equiv \frac{8\pi^2 D}{\Lambda^2} \tag{8.7}$$

This expression is also valid for the decay of gratings with small coverage modulation, where D is approximately constant [14, 24]. In this case, a simple single exponential decay is observed, from which D can be directly extracted. At higher coverage modulation, a multi-exponential decay can be expected and interpretation of the signal is more difficult [21]. This case will later be discussed in greater

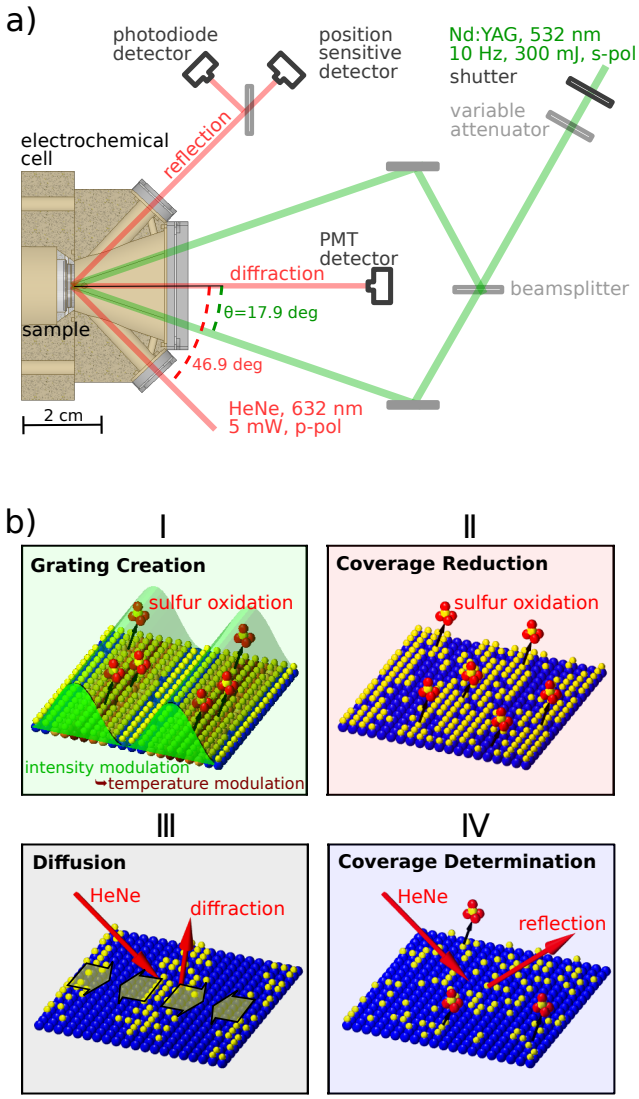

Figure 8.1: (a) Optical setup and electrochemical cell for *in situ* LOD measurements of surface diffusion in electrochemical environment. (b) Schematic illustration of the four main steps in the *in situ* LOD measurements. Adapted with permission from Ref. [LK2].

detail. At the end of every measurement (figure 8.1b-IV), the average coverage is determined by oxidative desorption of the remaining S_{ad} and analysis of the corresponding changes in the reflectance signal, as described in Ref. [LK2]. In the following, all coverages Θ will be given in respect to a full (1×1) monolayer (ML). All *in situ* LOD studies on S_{ad} diffusion on Pt(111) were carried out in 0.1 M H_2SO_4, made of ultrapure water (18 MΩcm) and 96% H_2SO_4 (Merck, Suprapur) with a $Hg/HgSO_4$ reference electrode (SI Analytics, ScienceLine Hg/Hg_2SO_4–, K_2SO_4 0,6 mol/l), a platinum wire as counter electrode, and an IVIUM CompactStat potentiostat. For easier comparison, all potentials are given with respect to the reversible hydrogen electrode (RHE) in the following. The sample preparation and characterization was performed as described in detail in Ref. [LK1]: Prior to each measurement, the Pt(111) single crystal sample with a diameter of 12 mm

(Mateck) was rinsed with ultrapure water, annealed using an induction oven, and cooled down to room temperature. The sample was then covered with a droplet of 10 mM Na_2S solution, prepared from ultrapure water (18 MΩcm) and sodium sulfide (Alfa Aesar, anhydrous granular). The whole process was performed in pure hydrogen atmosphere to prevent oxygen exposure, as the latter may influence the sulfur deposition process [56, 73]. After 5 minutes of deposition time, after which a fully covered monolayer of sulfur is expected [71, 72], the crystal was rinsed with ultrapure water to remove all residues of the Na_2S solution, and transferred into the electrochemical cell. The cell was then filled with deaerated H_2SO_4 electrolyte solution and rinsed with another 150 ml of electrolyte while keeping the sample at a potential in the double layer regime. The subsequent *in situ* LOD measurements follow the previously described approach with slight variations for each individual measurement (see appendix, figure A.3).

RESULTS AND DISCUSSION

Diffusion at low and medium coverages

The diffusion of S_{ad} on Pt(111) at medium coverages ($\Theta_{avg} = 0.38 - 0.43$) and a potential of 0.31 V/RHE was already investigated in Ref. [LK2]. In these studies, *in situ* LOD data were acquired, in which the diffraction signal $I(t)$ decays as shown in figure 8.2a. The $I(t)$ cannot be fitted by a single exponential decay. Rather, a sum of two exponential functions is necessary, namely a fast decay dominating the beginning of the measurement (dotted line) and a slower decay describing the long-time behavior (dashed line). The fast process can be attributed to the initial shape change of the coverage distribution in the grating. The slow process represents the final equilibration of the adsorbate distribution at low coverage modulation. Consequently, the slow long-term decay was employed in our previous publication for the determination of the diffusion constants D via equation 8.7. The D values obtained from this analysis are plotted against coverage in figure 8.2c) (blue triangles). They show that S_{ad} diffusion becomes faster towards low coverages by approximately a factor of 20 per 0.1 monolayer coverage change, according to a linear regression (blue line).

In the following, we focus on the initial fast decay of the diffraction signal. Comparable LOD signals exhibiting non-single or multi-exponential decay were already reported in previous studies. Xiao et al. found non-single exponential decay in second harmonic diffraction studies of CO on Ni(110) in vacuum at high coverage modulations [24]. This behavior was explained by the coexistence of several time constants, with faster diffusion dominating the signal in the initial stages of the diffusion process. This is consistent with model simulations of Verhoef et al., who found the LOD signal evolution being sensitive to adsorbate-adsorbate interactions [55]. Ma et al. reported multi-exponential decay for CO diffusion on a phosphor-contaminated Pt(111) surface [14]. They attributed this to the coexistence of two different diffusion channels, specifically diffusion over clean and diffusion over contaminated surface areas. Diffusion via a second channel (e.g. bulk diffusion through the electrolyte) would in principle also be possible in our measurements of S_{ad} diffusion, but can be ruled out by additional measurements, which are

presented at the end of this section.
We therefore consider the combined effects of a high initial coverage modulation and a strongly coverage-dependent S_{ad} diffusion as origin of the multi-exponential decay behavior. In this case, D cannot be assumed to be constant and thus equation 8.7 is not valid anymore. However, the diffusion process can be described by approximating the diffusion constant $D(\Theta)$ in the vicinity of the average coverage Θ_{avg} by a power series [21, 22]:

$$D(\Theta) = D(\Theta_{avg}) \left[1 + d_1(\Theta - \Theta_{avg}) + d_2(\Theta - \Theta_{avg})^2 + ...\right] . \tag{8.8}$$

The periodic coverage distribution can be described by a Fourier series with coefficients $\Theta_n(t)$. Employing the above approximation, the first two Fourier coefficients evolve in time as:

$$\frac{\delta\Theta_1(t)}{\delta t} = -\frac{\pi^2}{\Lambda^2} D(\Theta_{avg}) \left(\Theta_1(t) + \frac{1}{2} d_1 \Theta_1(t)\Theta_2(t) + ...\right) \tag{8.9}$$

$$\frac{\delta\Theta_2(t)}{\delta t} = -\frac{4\pi^2}{\Lambda^2} D(\Theta_{avg}) \left(\Theta_2(t) + \frac{1}{4} d_1 \Theta_1(t)^2 + ...\right) . \tag{8.10}$$

While these differential equations cannot be solved analytically, they clearly indicate multi- or non-exponential decay unless $d_1\Theta_2(t) << 1$ [21, 22]. However, for a strong dependence of D on coverage, d_1 will be large and significant deviations from a single exponential decay can be expected.
As the LOD signal evolution for gratings with high coverage modulation cannot be described analytically, it was further investigated using numerical simulations. Technical details for these simulations are given in the supporting information, section SI 3.1. All simulations were performed using a coverage-dependent diffusion constant $D(\Theta)$ (figure 8.2b, top right panel). $D(\Theta)$ is based on the experimental values at coverages between 0.38 and 0.43, which were extrapolated to the coverage range of $0.3 - 0.5$ using the result of the linear regression (figure 8.2c, blue line). For simplicity, $D(\Theta)$ was kept constant for coverages below 0.3 and above 0.5. However, the exact dependence of D on Θ does not significantly influence the following analysis. In figure 8.2b the temporal and spatial coverage evolution (insets, right hand side) is shown for three sinusoidal gratings with the same average coverage ($\Theta_{avg} = 0.4$), but different initial coverage modulations with varying modulation depths $\Delta\Theta = \Theta_1(t = 0)$. The corresponding temporal evolution of the diffraction intensities are plotted on the left hand side. The LOD signal of the grating with $\Delta\Theta = 0.1$ (orange line) shows a perfect single exponential decay (corresponding fit indicated by a dashed line). In contrast, the signal of the grating with $\Delta\Theta = 0.2$ (red line) already differs slightly from such a decay. In the beginning the signal decreases faster than the single exponential fit, in the end the decrease is delayed. A similar but much more pronounced behavior can be observed for the grating with the highest coverage modulation, $\Delta\Theta = 0.4$ (brown line). In this case, the LOD signal can obviously not be fitted anymore by a single exponential function. However, fits by a sum of two exponential functions with different time constants, denoted double-exponential decay in the following, provide an excellent description.
The plots illustrating the temporal evolution of the coverage distribution (bottom inset right side) show the origin of the two time scales in the decay behavior. Between the initial distribution at $t = 0$ (black line) and the grating at time t_1,

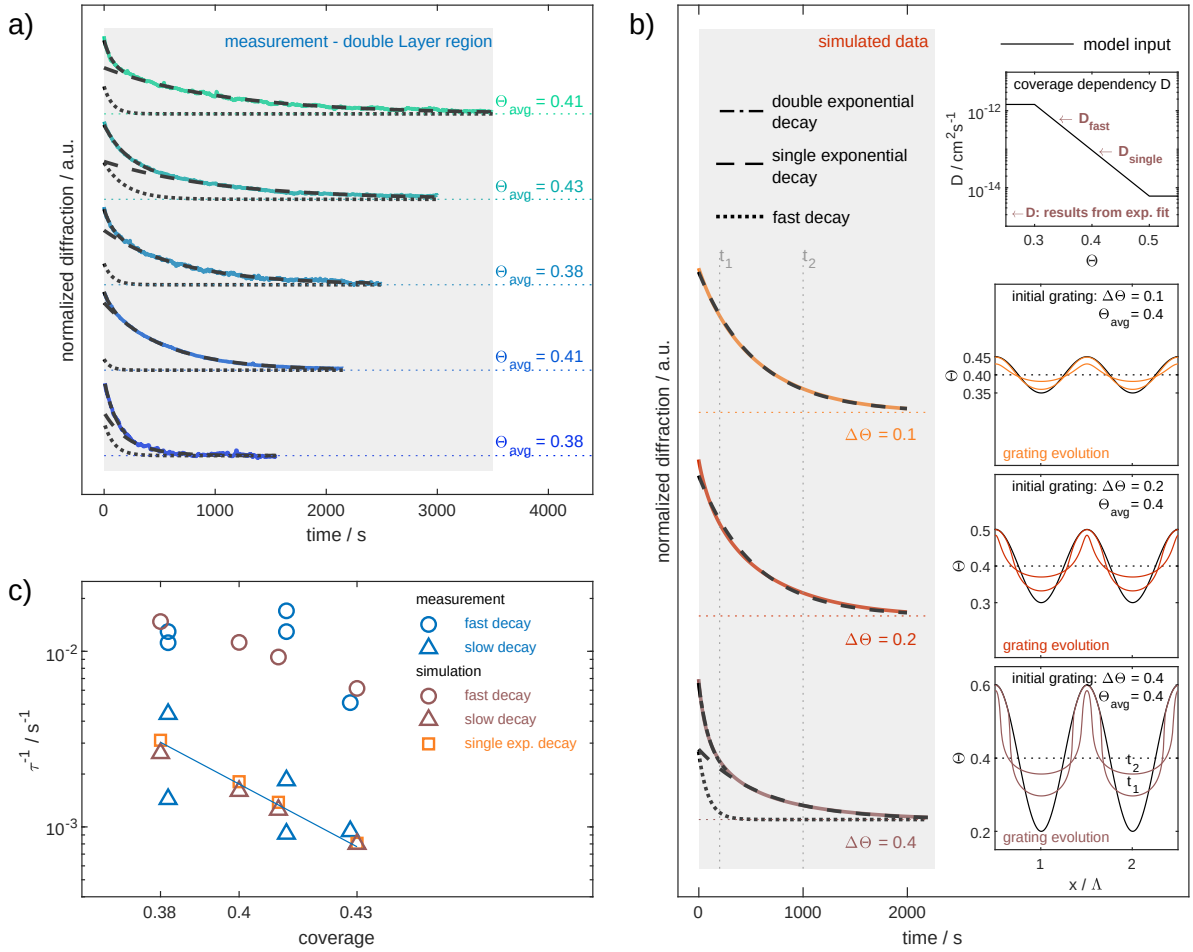

Figure 8.2: Temporal evolution of diffraction intensity during grating equilibration. (a) Experimental data obtained from *in situ* LOD measurements of S_{ad} diffusion on Pt(111) at a potential of 0.31 V and different S_{ad} coverages (colored lines). Black lines show fits by a double-exponential decay (dashed-dotted) and it's fast (dotted) and slow (dashed) component. (b) Simulated data for $\Theta_{avg} = 0.40$ with different initial coverage modulations $\Delta\Theta$ and a given coverage dependence of the diffusion rate $D(\Theta)$ (top right). Shown are simulated intensity curves (left, colored lines), single-exponential ($\Delta\Theta = 0.1$ and 0.2) and double-exponential ($\Delta\Theta = 0.4$) fits (left, black lines), and the corresponding evolution of the coverage distribution (right). (c) Comparison of the decay rates τ^{-1} obtained from the fits of the experimental data and the simulations at $\Delta\Theta = 0.1$ (single exp. decay) and $\Delta\Theta = 0.4$ (double exp. decay).

where the fast decay has almost subsided, mass transport predominantly occurs within the low coverage region were the diffusion rate is much faster than in the high-coverage regions. Therefore, the coverage is this region increases with a higher rate in the beginning of the diffusion process, leading to a fast decrease of the gratings 1st harmonic modulation amplitude $\Delta\Theta_1$. If the optical reflectance is proportional to the coverage, the diffraction intensity of the first order LOD signal $I_1(t)$ is proportional to $\Delta\Theta_1^2(t)$ (see supporting information, section SI 3.1). Consequently, the fast initial mass transport in the low coverage region directly leads to the initial fast decay of the diffraction signal.

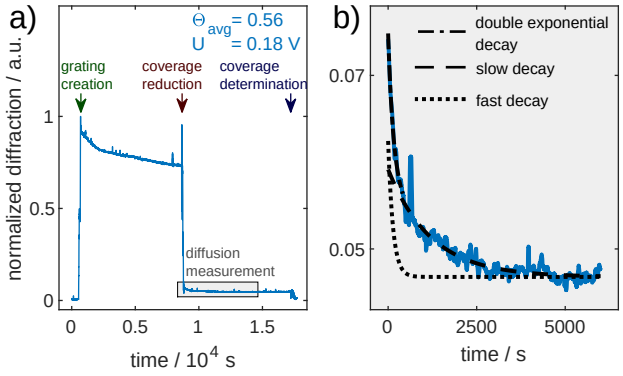

Figure 8.3: (a) *In situ* LOD measurement with a large time span between the initial grating creation (green arrow) and the actual diffusion measurement (shaded grey), performed after coverage reduction by potential cycling (red arrow). (b) Magnified view of the diffusion measurement in (a), showing that the decay involves two time scales.

For further analysis, simulated LOD signals for different average coverages Θ_{avg} in the range of the experimentally studied coverages were fitted using either a single-exponential function ($\Delta\Theta = 0.1$), or a double-exponential function ($\Delta\Theta = 0.4$). From these fits, the decay rates τ^{-1} were determined, which are given in table 8.1 and plotted against average coverage Θ_{avg} in figure 8.2c. Here, the simulation results are compared with the decay rates of the experimental data from figure 8.2a. The simulation results for $\Delta\Theta = 0.4$ agree well with the experimental values of the fast (circles) and slow decay (triangles). Also the simulation results for $\Delta\Theta = 0.1$ (squares) are in good agreement with the slow decay in the experimental data. In addition, the diffusion rates obtained from the slow decay via equation 8.7 (see table 8.1) are in good agreement with $D\left(\Theta_{avg}\right)$, justifying the extraction of the coverage-dependent diffusion constants from these data. In contrast, diffusion constants calculated in the same way from the fast decay are more difficult to interpret. These are much slower than the fastest occurring diffusion rates employed in the simulations (i.e., $D\left(\Theta \leq 0.3\right) = 1.5 \cdot 10^{-12}$ cm^{2}s^{-1}). This finding can be explained, by considering that the extracted D corresponds to diffusion within the area that is predominantly involved in the mass transport process and is determined by the effective coverage within that area. In the fast diffusion process, adsorbates are mainly redistributed from areas of medium coverage to areas of low coverage (see figure 8.2b, bottom right) and the effective coverage will be somewhere in between those. Therefore, the diffusion constants extracted via equation 8.7 from the initial fast decay merely provide a lower limit for the highest $D\left(\Theta\right)$ values in the studied system.

The above results indicate that fitting the LOD data with a double-exponential function and assigning the slower exponential decay to diffusion at the average coverage, does in principle lead to accurate results. However, this behavior can only be expected, if the effective coverage driving the diffusion process is close to the average coverage. This is true for gratings with shallow modulation depth $\Delta\Theta$, which thus should be favoured for most accurate results, as already proposed in LOD studies under UHV conditions [24]. It is explicitly not the case, if the equilibration of the coverage distribution is entirely limited by slow diffusion rates in

specific areas (see next section). Although the direct creation of reproducible grating structures with small $\Delta\Theta$ by the nanosecond laser is challenging in electrochemical environment, an alternative procedure is given by a two-step grating preparation. Here, firstly a high $\Delta\Theta$ modulation is created, which is then reduced by potential cycling. The scatter in the extracted diffusion constants from gratings prepared this way (see [LK2], measurements in hydrogen region) was much lower than in directly created S_{ad} gratings, used in the experiments presented here. Considering that S_{ad} oxidation is more effective at high coverages [LK1], it is likely that the two-step procedure predominantly reduces the high S_{ad} coverage areas, resulting in a smaller $\Delta\Theta$.

Although the coverage dependence of D satisfactorily explains the observation of two time constants in the decay, the coexistence of two different diffusion pathways can in principle not be excluded. In particular, diffusion through the adjacent electrolyte is possible [89, 90], other than for measurements under UHV conditions. For the strongly chemisorbing S_{ad}, this would only be expected after adsorbate grating creation, where sulfur species may be desorbed, diffuse in the solution and subsequently readsorb on the electrode. However, such solution-mediated diffusion cannot account for the initial fast decay, as the latter was observed also in experiments with large time intervals between grating creation by the laser irradiation and the actual diffusion measurement (figure 8.3). Here, a double-exponential decay with a fast initial decay (rate $7.2 \cdot 10^{-3}$ s^{-1}) is observed after a coverage reduction that was performed more than two hours after the laser-induced desorption. This rules out that the fast decay originates from solution-mediated diffusion of thermally desorbed sulfide. The latter also seems unlikely, considering that our grating preparation procedure removes S_{ad} via oxidation to sulfate ions [LK1].

Θ_{avg}	$D\left(\Theta_{avg}\right)$ cm^2s^{-1}	τ_{single}^{-1} $\left(10^3 s\right)^{-1}$	τ_{fast}^{-1} $\left(10^3 s\right)^{-1}$	τ_{slow}^{-1} $\left(10^3 s\right)^{-1}$	D_{single} cm^2s^{-1}	D_{fast} cm^2s^{-1}	D_{slow} cm^2s^{-1}
0.38	1.6e-13	3.1	14.8	2.6	1.6e-13	7.9e-13	1.4e-13
0.40	9.4e-14	1.8	11.3	1.6	9.5e-14	6.0e-13	8.6e-14
0.41	7.1e-14	1.4	9.4	1.2	7.2e-14	5.0e-13	6.7e-14
0.43	4.1e-14	0.8	6.2	0.8	4.2e-14	3.3e-13	4.3e-14

Table 8.1: Results of the LOD simulations for different average coverages Θ_{avg}. Shown are the decay rates τ_{single}^{-1} and the corresponding diffusion rates D_{single} obtained from a single-exponential fit of simulations performed at $\Delta\Theta = 0.1$ as well as the rates of the fast and slow decay, τ_{fast}^{-1} and τ_{slow}^{-1}, determined from a double-exponential fit of simulations performed at $\Delta\Theta = 0.4$, and the corresponding diffusion rates, D_{fast} and D_{slow}, that are calculated from the decay rates via equation 8.7. For comparison, also the exact diffusion rate $D\left(\Theta_{avg}\right)$ at the average coverage is given.

Diffusion at high coverages

The data in figure 8.2c already indicates a slower diffusion rate with increasing coverage. To further investigate this behavior, additional *in situ* LOD measurements were performed at S_{ad} coverages close to 0.5 and higher. In these studies, an unusual temporal evolution at long time scales was observed, which was studied in more details and is discussed in the following.
As an example, figure 8.4a shows an *in situ* LOD measurement with an average S_{ad} coverage of 0.64. Here, the decay of the diffraction signal after grating creation (magnified in figure 8.4b) is initially similar to that found in the measurements at low/medium coverages. However, the diffraction signal remains constant after $t_{end} = 1500$ s, even though subsequent oxidative desorption of the remaining S_{ad} (purple arrow) leads to another strong decrease in the diffraction signal. The latter reveals that a surface grating was still present at this time and apparently could not be further dissolved by surface diffusion. We propose that this stability of the grating results from the coexistence of different S_{ad} phases on the surface. In figure 8.4c (right panels) the known adlayer phases of sulfur on Pt(111) [56, 73] and the corresponding S_{ad} coverages are shown. Specifically, at high coverage ordered close-packed $c(2 \times 2)$ and (1×1) phases exist and attractive sulfur-sulfur interactions were reported [91]. Based on this phase behavior and assuming a negligible S_{ad} surface mobility in the $c(2 \times 2)$ and (1×1) phases, we propose for the high coverage regime a grating evolution as shown schematically on the left hand side of figure 8.4c. Here, mass transport is largely restricted to surface areas with $\Theta < 0.5$. In contrast, areas with $\Theta > 0.5$ are covered by a mix of immobile $c(2 \times 2)$ and (1×1) islands and can only contribute to the surface transport by detachment of S_{ad} at boundaries to low-coverage areas. The decay of the diffraction intensity between t_0 and t_{end} is then predominantly determined by transport from medium coverage to low coverage areas of the grating, which is supported by the similar rate of the measured exponential decay as compared to that measured at $\Theta \approx 0.4$ (see previous section). At time t_{end} (red line) the diffusion-driven equilibration has led to coverages between about $0.5 - 1.0$ on the entire surface, leading to a stable residual grating in which surface transport has effectively terminated.
The same scenario can also explain *in situ* LOD measurements at slightly lower coverages, where a complete dissolution of S_{ad} gratings can still be observed. Figure 8.5a shows such a measurement with a S_{ad} coverage of $\Theta_{avg} = 0.48$, recorded over a time period of about 20 hours. Clearly, three rates that differ by orders of magnitude ($\tau_1^{-1} = 15.1 \cdot 10^{-3}$ s^{-1}, $\tau_2^{-1} = 1.3 \cdot 10^{-3}$ s^{-1}, $\tau_3^{-1} = 0.03 \cdot 10^{-3}$ s^{-1}) govern the decay of the diffraction intensity.
To qualitatively explain this behavior, we carried out additional numerical simulations, in which we implemented the low mobility within the high-coverage S_{ad} phases into the model used for describing the medium coverage diffusion behavior (figure 8.5c, right). We note that the detachment of S_{ad} from the edges of $c(2 \times 2)$ and (1×1) covered areas cannot be described by a simple diffusion model based on differential equations. In order to still allow for transport from areas with $\Theta \geq 0.5$ into areas of lower coverage, the diffusion constant $D(\Theta)$ at $\Theta > 0.5$ was set merely to a much lower value ($3 \cdot 10^{-17}$ cm^{2}s^{-1}) than that of $D(\Theta = 0.5)$ rather than to 0. Because of this approximation, no quantitative modelling of the data

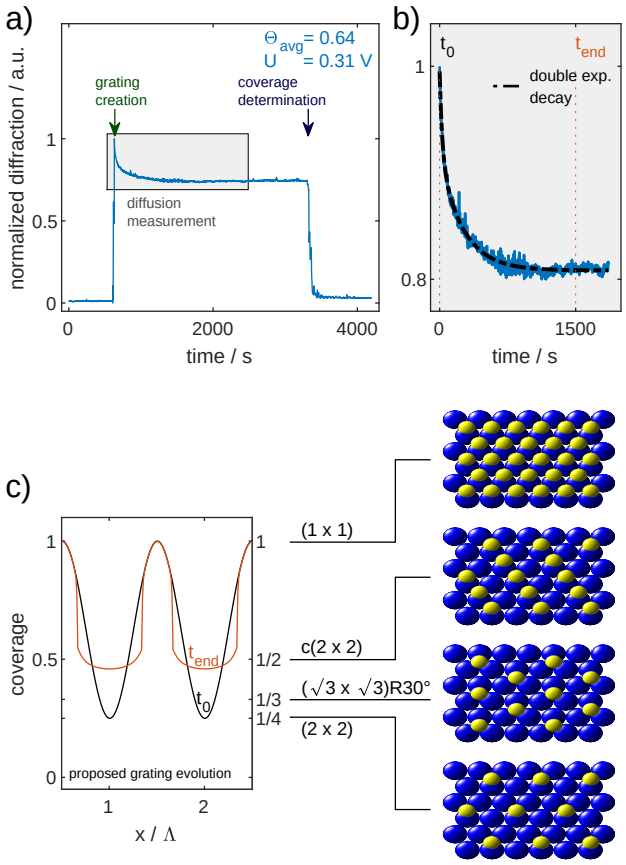

Figure 8.4: (a) *In situ* LOD measurement at high S_{ad} coverage ($\Theta_{avg} = 0.64$), where the diffusion process (magnified in (b)) leads only to incomplete decay of the adsorbate grating. (c) Schematic illustration of the evolution of a high-coverage grating in the presence of the stable sulfur adlayer phases, shown on the right hand side.

in figure 8.5a was attempted. However, simulations employing a grating with an average coverage $\Theta_{avg} = 0.48$ and a initial coverage modulation $\Delta\Theta = 0.56$ can indeed reproduce a decay with three significantly different decay rates (figure 8.5b). The corresponding temporal evolution of the simulated grating is illustrated in figure 8.5c (left panel) for three characteristic times (marked in figure 8.5b). In the initial stages ($t_0 < t < t_1$), the evolution is dominated by S_{ad} redistribution from areas of medium coverage to areas of low coverage. In accordance with that, the LOD signal is in this time regime well-described by a double-exponential decay with similar fast and slow rate as observed already at medium coverages (see previous section). The high coverage areas remain largely unaffected by the diffusion process. On longer time scales ($t > t_1$), this leads to a separation into distinct high coverage (≥ 0.7) and low coverage (≤ 0.4) areas, in which the coverage is rather uniform. The long-term decay is thus governed by transport at the edge of these areas, i.e., by the detachment rate at the edges of the high-density adlayer phases, rather than by surface diffusion.

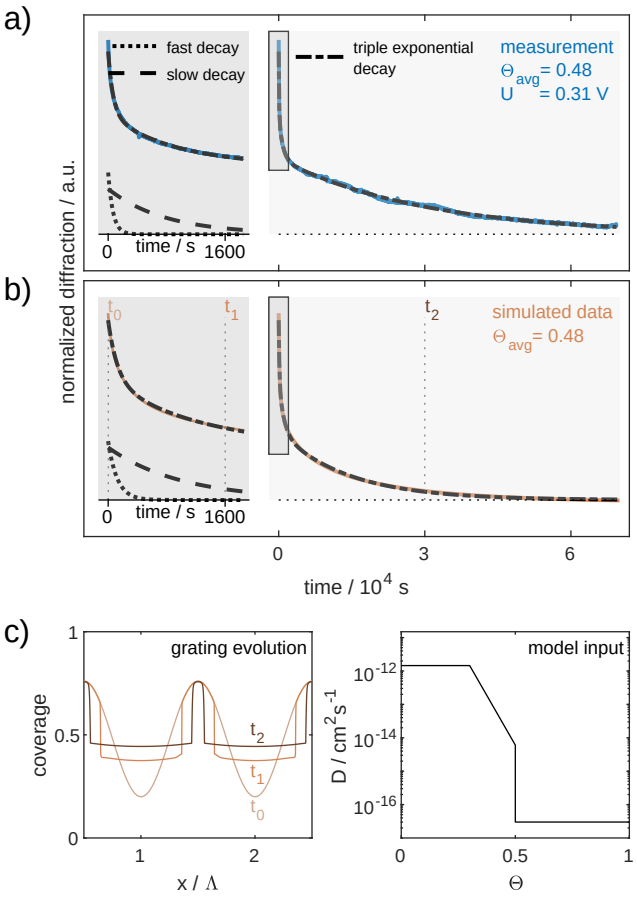

Figure 8.5: (a) Long-term *in situ* LOD measurement (blue line) at high S_{ad} coverage ($\Theta_{avg} = 0.48$), showing decay of the adsorbate grating on three different time scales. (b) Simulated LOD signal, obtained for a $D(\Theta)$ dependence with very low D for $\Theta > 0.5$ (c, right), which qualitatively reproduces the observed triple-exponential decay. The corresponding evolution of the coverage distribution is shown on the left hand side of (c).

CONCLUSIONS

As shown by our experimental studies and simulations, *in situ* LOD allows to quantitatively measure surface diffusion rates in electrochemical environment - but care has to be taken in the experimental data acquisition and interpretation. In particular, a coverage dependent adsorbate diffusion can strongly influence the temporal evolution of the diffusion profile and thus the decay of the diffraction intensity. We showed that this can lead to the emergence of two different time scales, of which only the slower long-term behavior has a simple physical interpretation, namely gives the diffusion rate at the average coverage. In contrast, the fast initial decay corresponds to a coverage redistribution that, at most, provides a lower limit for the fastest transport rates in the system. In principle, more detailed information on the latter process could be obtained by LOD measurements of higher diffraction orders [55]. However, the intensity of the diffraction peaks strongly decreases with the order [20], making such measurements technically difficult.
Furthermore, the presence of high-coverage adlayer phases that consist of attrac-

tively interacting adsorbates with low surface mobility can lead to additional phenomena. Specifically, an ultra slow decay may result, which is not determined by surface diffusion but by the rate of detachment from high-coverage areas. In extreme cases, this effect may even result in coverage gratings that are stable in time. This may pave the way to *in situ* LOD studies that go beyond measurements of surface diffusion. For example, such stable gratings could possibly be used in subsequent experiments for further reactions with electrolyte species, perhaps even for measuring the propagation rates of local reaction fronts in inhomogeneous surface reactions.

ACKNOWLEDGEMENTS

We gratefully acknowledge support by the Struktur- und Exzellenzbudget des Landes Schleswig-Holstein.

DATA AVAILABILITY

The data that support the findings of this study are available from the corresponding author upon reasonable request.

AUTHOR DECLARATIONS

The authors have no conflicts to disclose.

Influence of coverage on adsorbate diffusion measurements at electrode surfaces by *in situ* linear optical diffraction

Supporting Information

Lasse Kattwinkel and Olaf M. Magnussen

Contents

SI 3.1 NUMERICAL SIMULATIONS

For all simulations, firstly the spatial and temporal coverage evolution $\Theta(x,t)$ for a predefined initial coverage $\Theta(x,t=0)$ and diffusion coefficient $D(\Theta)$ was calculated. In these calculations the one-dimensional diffusion equation

$$\frac{\delta\Theta}{\delta t} = \frac{\delta}{\delta x}\left(D\left(\Theta(x,t)\right)\frac{\delta\Theta}{\delta x}\right) \tag{8.11}$$

was solved using MATLABs pdepe solver, starting with an initial coverage modulation

$$\Theta(x,t=0) = \Delta\Theta \cdot cos\left(\frac{2\pi x}{\Lambda}\right) + \theta_{avg}\ . \tag{8.12}$$

In the numerical calculation a mesh point density of 10^2 to 10^3 Λ^{-1} (depending on the simulation) and time intervals of $\Delta t = 1$ s were used. Increasing the number of mesh points or decreasing the time intervals had no significant influence on the calculations.
Subsequently, the diffraction intensity $I(t)$ was calculated for the obtained coverage distribution $\Theta(x,t)$ within the grating. As a first step, the time-dependent Fourier coefficients $\Theta_n(t)$ describing the grating

$$\Theta(x,t) = \Theta_{avg} + \sum_{n=1}^{\infty}\Theta_n(t)\,cos\left(2n\pi x/\Lambda\right) \tag{8.13}$$

were calculated using fast Fourier transform (FFT). Assuming a linear relation between the optical reflectance R and the coverage of the adsorbates Θ, the diffraction intensity for the n-th harmonic of a grating $I_n(t)$ is given by: [19–21]

$$I_n(t) \quad \sim \quad \Theta_n^2(t)\ . \tag{8.14}$$

Accordingly, the first order linear diffraction intensity was calculated by taking the square of the first order Fourier coefficient $I_1 = \Theta_1^2(t)$. The obtained diffraction intensity was then normalized by the intensity at $t = 0$.
The self consistency of the outlined modeling procedure was tested by simulating the decay of a sinusoidal coverage modulation for a coverage independent diffusion coefficient D_1. For this diffusion coefficient exists an analytical solution for equation 8.11, given by a single exponential decay. As expected, also the numerical calculated evolution of the diffraction signal precisely follows this decay. Extracting the diffusion constant from the single exponential decay (using equation 1, main publication), accurately leads to the diffusion constant D_1 which was used as model input. With the self consistency of the modeling procedure assured, the described procedure was used for all simulations presented in the publication.
In the case of the S_{ad} covered Pt(111) surface, the presumed linear relation between optical reflectance R and the coverage Θ of adsorbates is only approximately valid [LK1]. Thus, the usage of equation 8.14 for simulating the diffraction intensity may lead to minor inaccuracies. These were investigated by converting the calculated coverage distribution $\Theta(x,t)$ to a distribution of the optical grating contrast $R(x,t)$ using the $R(\Theta)$-relation from Ref. [LK1]. Analogous to the already

described procedure, the evolution of the diffraction intensity $I_1(t)$ was then obtained by squaring the first order fourier coefficient $R_1(t)$ of the grating contrast evolution $R(x,t)$.
The results for both modeling procedures are compared in table SI 3.2, which reproduces the calculation results presented in table 1 of the main publication and compares those with the results for the non-linear $R(\Theta)$-relation (given in red). While the τ^{-1}-values for the slow- and the single-exponential decay are almost identical, the values for the fast decay τ_{fast}^{-1} are slower, if the non-linear $R(\Theta)$-relation is taken into account. This behavior is directly related to the form of the $R(\Theta)$-relation, which shows deviations from a linear behavior only at small coverages, specifically a smaller change in reflectance with coverage [LK1]. Consequently, the deviation mainly affects the fast decay, which reflects the initial diffusion process at low coverages. The weaker dependence of reflectance with coverage here leads to a slower decay of the diffraction intensity and thus smaller τ_{fast}^{-1}-values. As no qualitative difference is observed and quantitative interpretation of the fast decay process is *per se* difficult, the non-linearity of $R(\Theta)$ is not relevant. More important, the effect is negligible for the slow decay and thus the extracted diffusion values at coverages of about $\Theta \approx 0.4$.

Θ_{avg}	$D(\Theta_{avg})$ $cm^2 s^{-1}$	τ_{single}^{-1} $(10^3 s)^{-1}$	τ_{fast}^{-1} $(10^3 s)^{-1}$	τ_{slow}^{-1} $(10^3 s)^{-1}$
0.38	1.6e-13	3.1 (3.1)	14.8 (12.2)	2.6 (2.8)
0.40	9.4e-14	1.8 (1.9)	11.3 (9.2)	1.6 (1.6)
0.41	7.1e-14	1.4 (1.4)	9.4 (7.5)	1.2 (1.2)
0.43	4.1e-14	0.8 (0.8)	6.2 (4.9)	0.8 (0.8)

Table SI 3.2: Results of the LOD simulations already presented in table 1 (main publication) with additional values (highlighted red) from identical simulations where the non-linear $R(\Theta)$-relation was taken into account.

Part IV

SUMMARY, CONCLUSIONS AND OUTLOOK

9 CONCLUSIONS AND OUTLOOK

We have presented proof-of-principle studies (sections 8.1 - 8.2) on the measurement of surface diffusion via LOD, which could, for the first time, be applied in electrochemical environment. We have shown that in this environment, the creation of adsorbate coverage modulations can be realized by laser enhanced oxidative desorption of the adsorbates (section 8.1). The equilibration of such gratings can be observed by linear optical diffraction, similar to measurements in vacuum, and diffusion rates can be determined by analysing the signals' decay.
The first proof-of-principle measurements were performed on sulfur diffusion on the Pt(111) surface, which was chosen as model system due the high influence of chemisorbed sulfur to the optical reflectance (section 7.1). Consequently, the created gratings develop a strong optical contrast and are relatively easy to detect. Potential and coverage dependent diffusion rates for S_{ad} could be measured and a significant deviation to the diffusion rates at surfaces in vacuum was found. However, for creating adsorbate coverage modulations multiple (50-300) laser pulses were necessary. This strongly indicates that laser enhanced oxidative desorption is only moderately effective for chemisorbed sulfur, probably due to the strong sulfur-platinum bond. Furthermore, we found strong sulfur-sulfur adsorbate interactions, which influence the LOD signal evolution and thus complicate the interpretation of LOD signals (section 8.2).
In the following, the implications of these very first findings for future enhancements of the *in situ* LOD methodology will be discussed (section 9.1). This will lead us to a brief discussion on different variations of the developed methodology. Finally, in section 9.2 we will shed light on further scientifically interesting systems for upcoming *in situ* LOD studies.

9.1 FURTHER PROPOSALS OPTIMIZING THE EXPERIMENTAL SETUP

In order to propose specific improvements for the presented *in situ* LOD methodology, the measurement procedure will be first recalled and light will be shed explicitly on encountered difficulties. Therefore, we will differentiate between the grating creation process (section 9.1.1), and the detection of adsorbate gratings (section 9.1.2), which also includes the actual *in situ* LOD measurements.

9.1.1 *Grating creation*

We will first recall the grating creation mechanism. For an effective creation of adsorbate gratings, the surface species should be oxidatively desorbed, and thus permanently removed from the surface (see section 4.4). This can be achieved by holding the electrode close to the potential where the adsorbates get oxidized, while, at the same time, the laser induces a periodic temperature modulation on the sample. In areas of increased temperature, also the oxidative desorption rate of

adsorbates will increase which leads to the formation of an adsorbate grating. In proof-of-principle diffusion measurements of chemisorbed sulfur on Pt(111), such a laser enhanced oxidative desorption mechanism could indeed be observed (see section 8.1). Complementary, if the electrode is held at lower potentials, e.g., in the double layer regime, grating creation was not possible. This strongly indicates that grating creation by redistribution of adsorbates (see section 4.4) can be largely neglected for this system. However, also the efficiency of laser induced oxidative desorption seems to be only moderate, as the usage of multiple laser pulses is necessary to create detectable adsorbate gratings. Thereby, creation of reproducible grating structures is hard to achieve, probably due to positional fluctuations in the interference patterns between subsequent pulses (see sections 4.1.1 and 8.1). Consequently, in order to enhance reproducibility, either the number of pulses necessary to create detectable grating structures have to be reduced or the positional fluctuation between single pulses have to be minimized. Also deviations in the pulse energies between subsequent pulses can be (partly) held accountable for the limited reproducibility of created gratings. S_{ad} gratings were created using pulse energies between 37 mJ and 44 mJ. Smaller energies lead to no detectable grating structures and higher energies already induced permanent structures within the platinum surface. The usable power range where S_{ad} gets oxidatively desorbed without permanent substrate damage is therefore rather small. In comparison, the power fluctuations between single pulses laser pulses are typically on the order of $\pm$ 0.5 mJ (standard deviation), respectively $\pm$ 2 mJ (maximum deviation). If multiple pulses are necessary for the grating creation process, these fluctuation are clearly one reason for the limited reproducibility of the grating creation process. The second, probably even more important reason is the already discussed positional fluctuation between subsequent pulses (section 4.1.1).

As already discussed in sections 5.1.2 and 5.3.2, also the modulation amplitudes of created adsorbate gratings (later denoted grating strength) probably strongly differ over the whole illuminated sample. This mainly results from spatial inhomogeneities in the energy density of the Nd:YAG laser beam, which is merely a perfectly shaped flattop. Although the spatial energy density of the Nd:YAG beam was only measured for its fundamental wavelength of 1064 nm (see figures 5.2 and 5.5a), these data imply that fluctuations in the spatial energy density are rather in the double-digit percentage range. Taking into account that S_{ad} oxidative desorption could only be achieved in a relatively small energy range, leads us to the conclusion that the created grating structures should differ significantly in strength over the whole illuminated sample. These local changes could actually be observed by slightly changing the probed area, which directly lead to changes in the LOD diffraction signal strength. If the probed area is sufficiently small, the local grating strength can be assumed homogeneously and the LOD signal will evolve as described in section 4.3. However, if the probed area contains grating structures that differ significantly from each other, LOD signal interpretation will become impossible for system with strong adsorbate-adsorbate interactions. To avoid such behaviour, a relatively small probe beam of 0.8 mm in diameter was used. However, in some cases, it might be useful to illuminate larger areas, e.g., for enhancing the LOD signal strength (see section 4.2). In these cases the Nd:YAG spatial energy density should be smoothed using additional beam shaping techniques. Beyond the

influence to the LOD signal, local fluctuations in grating strength also imply local fluctuations in the average adsorbate coverage. It should therefore be more accurate to determine the local adsorbate coverage via the optical reflectance change of the probed area, rather than to determine the average coverage from the whole sample by coulometry.

In the following, the above findings will be generalized in order to point out the prerequisites for the creation of detectable adsorbate gratings of different adsorbate-substrate systems. It will be assumed that grating creation is in principle possible via laser enhanced oxidative desorption of adsorbates, I) with at least 100 pulses necessary, or II) with only a single laser pulse necessary. Further differentiation is made between systems with a) slow diffusion rates or b) fast diffusion rates.
The performed proof-of-principle measurements on S_{ad} diffusion (sections 8.1-8.2) can be assigned to case (Ia), in which multiple pulses are necessary to create adsorbate gratings and diffusion rates are rather small. Independent from the above mentioned problems, the detectable diffusion rate is in this case limited by the time necessary to create detectable gratings. It is therefore mainly restricted by the repetition rate of the laser (10 Hz) and the number of pulses necessary for grating creation. Referring to equation 4.21, the half decay time of the LOD signal $t_{1/2}$ is given by:

$$t_{1/2} = \frac{ln\,(2)\,\Lambda^2}{8\pi^2 D}\,. \tag{9.1}$$

Assuming 100 laser pulses with 10 Hz repetition rate are necessary for grating creation, then the detectable LOD half decay time is limited to at least $t_{1/2} \geq 10$ s. For the current setup the detectable diffusion rate is then restricted to $D_{max} \leq 3 \cdot 10^{-12}$ cm^{2}s^{-1}. Increasing the grating constant to 5 μm by reducing the incident angles of the Nd:YAG beams to $\theta = 2.3°$ (see equation 4.4) would increase the detectable diffusion coefficient to $D_{max} \leq 2 \cdot 10^{-10}$ cm^{2}s^{-1}. However, this would require significant changes in the current optical setup and the electrochemical cell (see end of this section).
In case (Ib), where many laser pulses are necessary for grating creation but diffusion is faster than D_{max}, measurements are much more challenging. Let us first assume the grating dissolution is faster than the time between subsequent pulses, but a tiny LOD signal change can still be observed at each pulse. Then repeated measurements can be performed, where the LOD signal to noise ratio is further enhanced by averaging over the single measurements. However, if grating creation by single pulses leads to no detectable LOD signal change, either the repetition rate of the laser or the oxidative desorption rate per pulse has to be increased. Using the current approach, the oxidative desorption rate is dependent on the electrode potential and the laser-induced temperature change at the interface and thus on the laser power. Both parameters can only be varied in a narrow range, which may not be sufficient to fundamentally increase the oxidative desorption rate. In an alternative approach, the laser wavelength could be tuned to match the adsorption bands of the adsorbate-substrate system. Possibly, the local energy intake could thus be strongly enhanced without damaging the substrate itself. This principle was already demonstrated for the creation of monolayer gratings of Rhodamine 6G dye molecules on Si substrates [19]. These molecules are strongly absorbing at

$\lambda = 532$ nm, so that gratings in aerial environment could be successively created with the developed setup using single laser pulses of only 10 mJ pulse energy. However, both approaches, tuning the laser wavelength and increasing the laser repetition rate, would require massive changes in the current setup, specifically a change of the laser system for grating creation.
For systems where single pulses are sufficient to create detectable adsorbate gratings (IIa-b), *in situ* LOD measurements are rather straightforward. In these cases, the laser induced intensity modulation on the surface can even be tuned to gain further control on the gratings' shape (see section 4.1.1). The measurement range is then only limited by the LOD signal to noise ratio, which massively decreases for faster acquisition rates due to the shorter detector integration times. In these cases, appropriate methods to additionally enhance the SNR should be considered (see section 4.2). As already mentioned above, also the grating constant can be increased to decelerate the gratings' equilibration (see equation 9.1). Due to the increased detector integration times, this leads to enhanced signal to noise ratios and thus allows the measurement of much faster diffusion rates.

9.1.2 *Grating detection*

Let us now revisit the challenges we have encountered during *in situ* LOD measurements, that are related to the detection of adsorbate gratings and the measurement of surface diffusion. Again, we will first describe the corresponding measurement processes and then propose possible solutions for the encountered difficulties.
After grating creation, the first order linear diffraction signal is monitored to probe the relaxation of the adsorbate grating. From the signal decay, the diffusion rate of adsorbates can be easily determined if a) adsorbate-adsorbate interactions are negligibly small (at low adsorbate coverages) or b) if adsorbate-adsorbate interactions are largely constant within the studied coverage range (for gratings with shallow modulation depth). In both cases, the LOD signal develops a single exponential decay, from which the diffusion constant can be derived from (see section 4.3). However, in first proof-of principle measurements, sulfur gratings with presumably greater modulation depth were investigated, resulting in a multi-exponential decay of the LOD signal (section 8.2). We showed that this behaviour can be related to the strong sulfur-sulfur interactions within the system. Still, determining the diffusion rate was possible by analysing the LOD signal after an appropriate time, when the diffusion related relaxation of the initial grating already lead to a strong decay of the gratings' modulation depth. The subsequent single exponential decay of the LOD signal could thus be used to determine the sulfur diffusion rate.
In order to probe gratings with shallow modulation depth, much weaker LOD signals need to be detected (see section 4.2). In this respect, the performed measurements benefited from the strongly chemisorbing sulfur, which induces rather high reflectance changes on Pt(111) that lead to comparably strong LOD signals ($\Delta R/R \approx 1.2\%$ for S_{ad} adsorption of a complete monolayer, probed at $\lambda = 632$ nm, see section 7.1). However, probing less strongly bound adsorbates like CO on Pt(111) ($\Delta R/R \approx 0.3\%$ [92]) could require the usage of addition methods to increase the LOD signal to noise ratio. The most commonly used methods to

increase SNR were already presented in section 4.2. These can be easily applied also in the developed setup.

To further increase the LOD signal strength itself, the probe wavelength could be specifically tuned to the adsorbate-substrate system. Already early UV-Vis measurements by Molina and Parsons showed, that the optical reflectance of platinum electrodes is strongly dependent not only on the adsorbed species but also on the probe wavelength [93] (see section 2.2). Thus, by probing the grating at a wavelength where the adsorbate-substrate compound has strong absorption bands, the LOD signal strength could potentially be significantly increased. In special cases, even fluorescence could be stimulated selectively for certain adsorbates. In these cases, the wavelength of the fluorescent emission would differ from the diffuse scattering background. By appropriate filtering, the diffuse scattering could thus be be massively reduced in order to enhance the SNR. However, all the above proposals require either a single tunable laser or multiple probe lasers to cover the different wavelengths ranges. We already note that in an alternative approach, where the grating equilibration is monitored with a microscopy setup, also incoherent light sources could be used to probe the grating (see end of this subsection). In both cases, probing the sample with different wavelengths could even be used to differentiate between diffusion of two different species (a,b) within the same system, provided these have a different adsorption cross-section dependency on the wavelength. Let us therefore assume such a grating is probed with two distinct wavelengths $\lambda_{1,2}$, and the corresponding LOD signals $I_{1,2}$ for both wavelengths are monitored separately with two detectors. We can then describe the process by the simultaneous decay of two individual gratings (a,b), one for each species respectively. Consequently, both LOD signals $I_{1,2} = I_{1,2}(a) + I_{1,2}(b)$ are given by the superposition of the diffraction intensities of the individual gratings (a) and (b). Now, if $\Delta R/R(\lambda_{1,2}(a))$ and $\Delta R/R(\lambda_{1,2}(b))$ are known for each species, the fractions $I_{1,2}(a,b)$ can be separated and the individual diffusion rate for each species can be determined.

As already stated above, gratings with shallow modulation depth should preferably be created and observed to obtain accurate values for the diffusion rate. However, a reproducible creation of such gratings was found to be challenging (see section 9.1.1). Additional tools to monitor also the shape of the grating would therefore be useful. Information on the shape could on the one hand be used as a feedback loop for the grating creation process itself. On the other hand determining the grating shape, or in other words, determining the complete spatial coverage evolution $\Theta(x,t)$ would allow to perform most accurate surface diffusion measurements also for gratings with a high coverage modulation, even in case of strong adsorbate-adsorbate interactions. In fact, resolving $\Theta(x,t)$ for gratings with full modulation depth theoretically even allows to calculate $D(\Theta)$ for the complete coverage range $0 \leq \Theta \leq 1$ using only a single measurement [21].
Although detection of higher diffraction orders would in principle provide all information necessary to determine $\Theta(x,t)$, the corresponding measurement is extremely challenging due to the very low signal intensities (see section 4.2). Hence, such measurements have not even been realized for LOD in vacuum. For the devel-

oped experimental setup, the second order diffraction signal would occur under the same angle where the HeNe probe beam is incident. In order to measure this signal, it had to be separated from from the incident beam by an additional beam-splitter. Although this is in principle possible, it remains questionable whether the second order LOD signal could be detected with sufficient signal to noise ratio. Moreover, detection of *only* the second order LOD signal would probably not even provide sufficient information to make justified assumptions about the grating shape. The idea of directly measuring higher order diffraction signals was therefore discarded.

In a complementary approach, the grating and thus $\Theta(x,t)$ could also be observed directly using a high resolution microscopy setup. As the currently used grating periodicity of $\Lambda = 650$ nm is merely within the diffraction limit of light in the optical spectrum, the grating constant had to be increased to about 5 μm in order to obtain a sufficient spatial resolution. Similar to LOD measurements, the grating could be probed with a HeNe laser. However, in contrast to diffraction based methodologies, also the illumination with incoherent light sources would be possible. Thus, adapting the probe wavelength to the adsorption bands of the adsorbate-substrate system in order to increase the grating contrast is much easier than in traditional LOD measurements. Specifically, an ultra bright, highly stable white light source, like the Energetiq EQ-99X-FC would be sufficient for this purpose. Depending on the chosen wavelength, a surface area of about 100 μm could be imaged with a highly sensitive, high resolution 2D-detector, resolving grating structures as small as the diffraction limit. However, due to the low spatial variation in $\Delta R/R$, especially gratings with small modulation depth will be hardly resolved within the acquired images. Increasing the integration time and further integrating the image in direction of the lattice rods (y-direction) would probably still lead to poor results. For further noise reduction, a fourier analysis can be applied to probe the spatial grating periodicity in x-direction. In principle, this can be seen as equivalent to physical diffraction phenomena, so that the resulting fourier coefficients Θ_n equal the coefficients from equation 4.12. Consequently, also the SNR obtained by the microscopy method should in principle be comparable to traditional LOD measurements. Yet, the methods differ at two points, which could make microscopy superior. Firstly, as already mentioned, tuning the probe wavelength in order to enhance the grating contrast is much easier for microscopy. And secondly, electronically separating the grating signal from the background noise (diffuse scattering) by fourier transform may be more effective than directly measuring its physical counterpart (the diffraction signal). This has largely experimental reasons. In theory, the detector could of course be precisely aligned, with a pinhole that is matched exactly to the spatial dimensions of the diffraction order. In practice, however, we will always loose intensity by a certain miss-alignment or increase the detected noise if the pinhole aperture is too large. In other words, the microscopy method would be certainly superior in terms of alignment. Also, instead of measuring separated diffraction orders which requires multiple detectors (LOD), microscopy requires only a single detector. Still, the question remains whether higher order fourier coefficients could be resolved with a sufficient SNR. Certainly, further methods to increase the SNR would be necessary, like the application of an additional polarization-modulation scheme similar to the one described

in section 4.2. In the author's opinion such modifications should be sufficient to resolve also higher order fourier coefficients, at least for adsorbates that induce high reflectance changes $\Delta R/R$. In summary, the proposed method could be valuable in cases where reproducible grating creation is challenging, and especially in cases where grating creation leads to high modulation depths. Information on higher grating harmonics $\Theta_n(t)$ could then allow resolving $D(\Theta)$ for the complete coverage range in only few measurements. However, resolving the higher grating harmonics with sufficient SNR would probably still be limited to gratings of adsorbates that induce strong reflectance changes (as for example the strongly chemisorbing sulfur).

At the end of this section, where we have proposed improvements and alternatives for the *in situ* LOD methodology, we want to note that for many of the proposed improvements, also major changes in the electrochemical cell design are necessary. Especially if the grating periodicity needs to be adapted, also the detection angles of the LOD signal are affected. With the current cell, such adaptions are not possible due to the fixed angles of the probe beam. These restrictions could be avoided by using a thin film cell design with only one front window. This would not only allow greater flexibility in changing the grating constant and the detection angles. A thin film cell would also increase the range of usable wavelengths for grating creation and detection. Specifically wavelengths in the near UV and IR range that have greater absorption cross sections within the electrolyte could be used.

9.2 SUBSEQUENT STUDIES

After we have revisited the experimental pitfalls and possible improvements for the *in situ* LOD methodology at the beginning of this chapter, we want to close the chapter with a brief look on two specific systems that may be interesting for upcoming *in situ* LOD studies.

9.2.1 *CO diffusion on Pt(111)*

Adsorbed CO on platinum electrodes is often used as a model system, but has also practical relevance in electrocatalysis, e.g., for CO hydrogenation. Surface diffusion of CO on platinum has already been investigated in several studies in vacuum environment [94–99]. Investigations using LOD revealed a weak dependence of CO diffusion on the adsorbate coverage (repulsive interaction) and also on the specific surface morphology [14–17]. Accordingly, the CO diffusion rate at room temperature and low coverages (0.1 ML) is about $4.4 \cdot 10^{-10}$ cm^2s^{-1} and slightly elevated at high coverages (0.67 ML) with $2.6 \cdot 10^{-9}$ cm^2s^{-1} (see figure 3.2). In optical reflectance studies performed in electrochemical environment by Fromondi *et al.* [51, 92, 100–102] a weak influence of the adsorbed CO on the optical reflectance of platinum was found. However, to our knowledge, there is no systematic surface diffusion studies of adsorbed CO on platinum electrodes in electrochemical environment so far.
Consequently, first evaluations have been been made in order to prepare *in situ* LOD studies of this system. In a first step, the optical reflectance change $\Delta R/R$

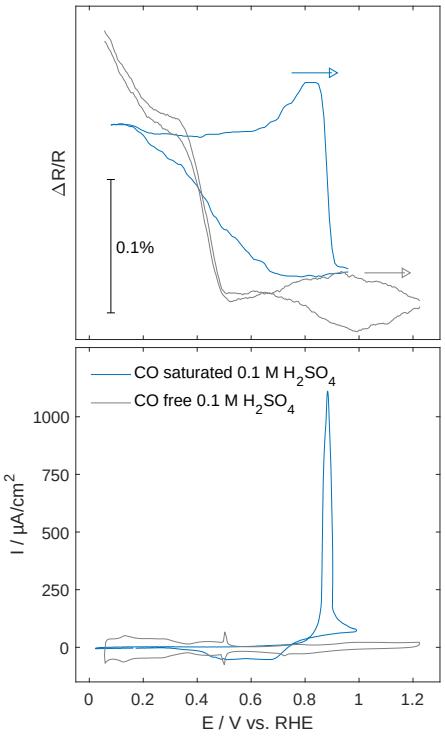

Figure 9.1: Averaged and smoothed differential reflectance data $\Delta R/R$ (top) and CVs (bottom) from a P(111) single crystal sample in CO-free (gray) and CO-saturated (blue) 0.1 M H_2SO_4 electrolyte solution, acquired at $\lambda = 633$ nm with a sweep rate of 50 mVs^{-1}. The sweep direction is indicated by arrows.

induced by adsorbed CO on the Pt(111) electrode in H_2SO_4 was investigated. Specifically, the electrode potential of a Pt(111) single crystal electrode in CO saturated 0.1 M H_2SO_4 electrolyte solution was cycled in a range between 0 V and 0.95 V. The obtained $\Delta R/R$ data (figure 9.1, top panel, blue line) and electrochemical data (figure 9.1, bottom panel, blue line) agree well with observations by Fromondi *et al.* [101]. The $\Delta R/R$ signal remains largely constant up to potentials of about 0.7 V. Then a slight signal increase up to potentials of about 0.9 V can be observed, followed by a sharp drop. The initial plateau can be associated with adsorbed CO covering the complete electrode surface and thus inhibiting the adsorption of other species. The subsequent signal increase is usually explained by an initial surface reorder of adsorbed CO [101]. The sharp drop coincides with the pronounced peak in the electrochemical data (figure 9.1, bottom panel) and can therefore be associated with CO oxidative desorption and simultaneous adsorption of species from the electrolyte [102], in this case SO_4^{2-}. After reversing the potential, the signal starts to increase at potentials ≤ 0.7 V until reaching its original value at about 0.1 V, which is due to the adsorption of CO from the electrolyte.
An additional reflectogram was acquired for the same electrode in CO-free 0.1 M H_2SO_4 electrolyte solution (grey line). This measurement is described in detail in section 7.1. Starting in the double layer region, between 0.35 V and 0.05 V $\Delta R/R$ increases due to hydrogen adsorption. For potentials ≥ 0.35 V up to ≈ 0.55 V, $\Delta R/R$ drastically decreases as result of sulfate adsorption. At higher potentials

$\Delta R/R$ slightly increases and then decreases above 0.95 V. The latter decrease was associated with adsorption of oxygenated species (see section 7.1). Apart from this region, all changes in $\Delta R/R$ are highly reversible.
Driven by the question in which potential range an adequate reflectance contrast for CO gratings can be obtained, both reflectograms were compared. The absolute reflectance of both measurements was assumed equal at a potential of 0.95 V, where a sulfate covered surface can be expected in both cases. In the double layer region of the first measurement (around $\approx$ 0.35 V, positive sweep), the surface can be expected to be covered with adsorbed CO (blue), while for the second measurement the surface should be largely adsorbate-free (grey). Unfortunately, the reflectance difference between both measurements is very small within this region. Hence, CO gratings would develop only weak optical contrast and are therefore difficult to detect in this potential range. It should be noted that for the above comparison, the optical reflectance behaviour of the *fully* CO covered surface was used. However, as we have seen in the reordering process at potentials $\geq$ 0.7 V, the optical reflectance can also be strongly dependent on the CO adsorption site and thus the CO coverage. Consequently, at lower CO coverages, the reflectance difference between CO covered and uncovered electrodes may differ. Still, in the hydrogen adsorption region $\leq$ 0.35 V, and the region $\geq$ 0.55 V where sulfate is adsorbed, the reflectance differences between both measurements are much more pronounced. Consequently, in these regions the optical contrast of CO gratings should be enhanced, which facilitates their detection. Note that co-adsorption of hydrogen or sulfate only occurs for sufficiently small CO coverages, where CO site-blocking is negligible. In either case, the LOD signal intensities can be expected much weaker than the intensities detected for gratings of chemisorbed sulfur. The LOD signal strength can be approximated by using equation 4.13. Assuming $\Delta R/R$ values of about 0.1% for adsorbed CO and values around 1% for adsorbed sulfur, leads to LOD signals of CO gratings that have only 1% of the signal strength of similar sulfur adsorbate gratings. In principle, such gratings should nevertheless be detectable using the developed setup, especially if further methods to enhance the SNR are used (see section 4.2).
It may still be advantageous to further increase the grating contrast, e.g., by changing the electrolyte or tuning the probe wavelength (see section 9.1.2). Using perchloric acid as electrolyte leads to a similar $\Delta R/R$ values as already shown for sulfuric acid [92]. However, for a probe wavelength of $\lambda = 360$ nm, Beden *at al.* found a much larger reflectance change induced by adsorbed CO on polychristalline platinum electrodes, which was on the order of $\Delta R_{CO} \approx 0.25\%$ [103]. Based on these values, we conclude that probing CO adsorbate gratings with UV light could increase the LOD signal strength by about a factor 5, as compared to probing the grating with red light.

Also the creation of CO gratings by laser enhanced oxidative desorption should in principle be possible. Herrero *et al.* already found a strong influence of the CO stripping potential on the interface temperature [58, 59]. Assuming similar diffusion rates as in vacuum environment ($4.4 \cdot 10^{-10}$ cm^{2}s^{-1} - $2.6 \cdot 10^{-9}$ cm^{2}s^{-1}, see above), created CO gratings should dissolve within a half decay time of about 0.08 s $-$ 0.01 s, assuming a grating periodicity of $\Lambda = 650$ nm. For an increased

grating periodicity of $\Lambda = 5$ μm, the half decay time would be on the order of 5.0 s $-$ 0.8 s. Based on these values and referring to section 9.1.2, CO surface diffusion could in principle be measured using a grating periodicity of $\Lambda = 650$ nm, if a single pulse is sufficient to create detectable adsorbate gratings. Still, due to the short detector integration times and the low optical grating contrast, a very low signal to noise ratio would be expected, which might be insufficient for reliable LOD studies. In order to use multiple pulses for the grating creation process, an increased grating periodicity of at least 5 μm would be necessary. This would also allow longer detector integration times, resulting in a much better signal to noise ratio. If such measurements were performed with a thin film cell with small cell volume, CO adsorption could even be realized in *in situ* by using a CO saturated electrolyte. Subsequently, the electrolyte would be exchanged with CO free solution for the actual *in situ* LOD measurements. With the current cell, such measurements are only possible to a limited extent. Here, small traces of CO remain after exchanging the electrolyte due to the big cell volume.

9.2.2 *Au self diffusion*

All presented studies so far were focused on the diffusion of adsorbates on single crystal electrodes. However, also the self diffusion of larger islands or single metal atoms or vacancies on metal electrodes are of great interest. As an example, gold electrodes are often used as a model system to study self diffusion. For the self-diffusion of Au(100) in 50 mM H_2SO_4, Ikemiya *et al.* found a strong dependency on the applied potential and smallest diffusion rates of 10^{-15} cm^2s^{-1} in vicinity to the potential of zero charge by observing collective diffusion with atomic force microscopy [104]. Studying the step and island dynamics of Au, also Giesen *et al.* quantified the potential dependence of Au self diffusion [39] and moreover found a strong influence of coadsorbed species like chlorine on the latter [38, 105].

The developed *in situ* LOD setup can in principle be used for the preparation of Au surfaces with spatially periodic defect densities, and thus also for the corresponding measurement of self diffusion. In previous measurements on Pt(111), permanent (grating) structures could be created within the crystal substrate and detected via LOD by using Nd:YAG pulse energies of about 150 mJ (see section 5.3). Due to the enhanced absorption of Au at $\lambda = 532$ nm as compared to Pt [46], the usage of much smaller pulse energies should be sufficient to create similar structures within the Au surface. Still, the exact nature of these structures needs to be investigated, as LOD does not directly provide these information. For high pulse energies, usually grating structures of several nanometers depth are created within the substrate [43]. For low pulse energies the creation of single vacancies or atomic step edges seems to be likely. Measuring the surface diffusion rate of isolated vacancies could thus be possible, if the optical grating contrast between areas of lower, respectively higher vacancy density is sufficient to be observed via LOD. The corresponding diffusion rate should be well within the measurement range of the developed *in situ* LOD setup, presuming similar diffusion rates as determined by Ikemiya *et al.*.

10

SUMMARY

Within this work, a new all-optical method to measure surface diffusion at electrochemical interfaces was developed and first proof-of-principle measurements on sulfur diffusion on Pt(111) electrodes were performed. Technically, our so-called *in situ* LOD methodology is based on the linear optical diffraction (LOD) method, which has already been extensively used to study surface diffusion of adsorbates under ultrahigh vacuum (UHV) conditions. For LOD measurements, first a periodic spatial modulation of the adsorbate coverage is generated via interfering laser pulses. Subsequently, the diffusion-induced decay of this pattern is monitored using the LOD signal of a second laser. From the exponential decrease of the LOD signal intensity, the surface diffusion rate of adsorbates can then be determined. We showed that LOD measurements can also be applied at electrochemical interfaces between solid electrodes and liquid electrolytes. In contrast to LOD in vacuum environment, at electrochemical interfaces the presence of the electrolyte inhibits the creation of adsorbate coverage modulations via thermal desorption. However, adsorbates can often be removed from electrodes by oxidative desorption, a process which is in many cases temperature dependent. We showed that laser induced temperature modulations at the interface can be used to locally increase the adsorbate oxidation rate in order to create adsorbate coverage modulations. Similar to conventional LOD measurements in vacuum, the equilibration of these gratings can then be observed via LOD to determine adsorbate surface diffusion rates.

After the development and implementation of the above sketched method, which in fact represented the main part of this work, we started by investigating the optical and electrochemical properties of chemisorbed sulfur (S_{ad}) on Pt(111) in 0.1 M H_2SO_4 (section 7.1). In particular, combined electrochemical and optical differential reflectance studies were performed on sulfur-covered and uncovered electrodes in a potential range between 0.05 and 1.22 V vs SHE. These measurements were important for two reasons. Firstly, they allowed us to study the sulfur oxidation mechanism, in which the role of intermediate species is not yet completely understood. By combining electrochemical and optical methods, we could assign two cathodic current peaks in the corresponding cyclic voltammograms to intermediates of the oxidation process. And secondly, the combination of both methods allowed us to determine the relation between the sulfur coverage (change) and the optical reflectance change $\Delta R/R$ of the electrode. In the subsequent surface diffusion studies, we used this relation to determine S_{ad} coverages.
After these preliminary studies, we demonstrated the feasibility of our *in situ* LOD methodology through proof-of-principle measurements of sulfur surface diffusion on the Pt(111) electrode (section 8.1). In these studies, potential and coverage dependent S_{ad} diffusion rates could be observed, which were on the order of $10^{-14} - 10^{-13}$ cm^2s^{-1}. This is at least an order of magnitude faster than diffusion rates under UHV conditions and thus barely within the measurement range of

other methods like electrochemical video-rate STM (VSTM). We emphasize that, with the current setup, our method allows the detection of even faster diffusion rates of up to about 10^{-10} cm^2s^{-1}. Regarding this upper detection limit, two things are noteworthy. Firstly, the limit strongly depends on the grating creation efficiency and on the optical grating contrast of the individual system to be studied (see section 9.1). And secondly, the limit can be further increased by orders of magnitude with minor modifications of the setup.
During our proof-of-principle measurements, we observed that the LOD signal in certain cases differs from a single exponential decrease, usually observed in UHV measurements. There, a single exponential decrease stems from a shallow modulation depth of the adsorbate gratings, and can be used to precisely quantify surface diffusion rates. The interpretation of the observed non-single exponential decrease in order to determine quantitative diffusion rates is more difficult. In section 8.2, we focus on the interpretation of such signals by investigating the temporal LOD signal evolution on basis of (i) S_{ad} diffusion measurements and (ii) additional numerical simulations of the equilibration of adsorbate gratings (section 8.2). Specifically, we investigated the implications of different grating modulation depths and strong adsorbate-adsorbate interaction to the LOD signal. At low and medium S_{ad} coverages and high coverage modulation depths, the decay of the LOD signal exhibits two time scales, which can be explained by coverage dependent diffusion rates. At high S_{ad} coverages, a further, ultra-slow decay process or even a complete termination of the decay are observed, which was attributed to (semi) stable grating structures of ordered adlayer phases with low sulfur mobility. These findings gave not only further insight into the interpretation of LOD signals, but were explicitly used to develop approaches required for extracting quantitative surface diffusion rates.

Although *in situ* LOD measurements on gratings of shallow modulation depth should be preferred, we have seen that the reproducible creation of such gratings can be demanding. To further improve the accuracy of diffusion rates determined from LOD signals of gratings with higher modulation depth, one could probe not only the coverage modulation of the grating's first harmonic (via the first order diffraction signal), but monitor the complete grating in real space. For the realization of such measurements, we proposed a high resolution microscopy instrumentation. A second possible improvement for the methodology addresses the signal to noise ratio: In *in situ* LOD measurements, a main challenge are the low diffraction intensities, which strongly depend on the specific adsorbate-substrate system and on the probe wavelength. The LOD signal to noise ratio for many systems could presumably be strongly enhanced by adapting the probe wavelength to the absorption bands of the system instead of probing the grating at the fixed wavelength of $\lambda = 633$ nm. Although this would require changes in the cell design, these changes would also pave the way for the creation of gratings with variable periodicity. With larger grating periodicity, the measurement of much faster diffusion rates than observed so far would become possible. This could prove particularly useful for the measurement of CO surface diffusion on the Pt(111) electrode, which we already started to investigate in first preliminary studies.

To conclude, a new method for measuring surface diffusion of adsorbates at electrochemical interfaces was developed. Diffusion rates magnitudes faster than accessible so far with established methods like VSTM can be measured, which paves the way for studying surface diffusion also on electrodes of more applied systems, e.g., for energy conversion and storage.

PUBLICATIONS

[LK1] L. Kattwinkel and O. M. Magnussen, "Optical reflectance studies on the oxidation of chemisorbed sulfur at the pt(111) electrode," Electrochimica Acta **434**, 141297 (2022).

[LK2] L. Kattwinkel and O. M. Magnussen, "Measurement of surface diffusion at the electrochemical interface by in situ linear optical diffraction," ACS Measurement Science Au, in press. (2023).

[LK3] L. Kattwinkel and O. M. Magnussen, "Influence of coverage on adsorbate diffusion measurements at electrode surfaces by in situ linear optical diffraction," The Journal of Chemical Physics, submitted manuscript. (2023).

[1]B. S. Vishnugopi, F. Hao, A. Verma, and P. P. Mukherjee, "Surface diffusion manifestation in electrodeposition of metal anodes," Physical Chemistry Chemical Physics **22**, 11286 (2020).

[2]R. Aogaki and T. Makino, "Morphological instability in nonsteady galvanostatic electrodeposition: I . Effect of surface diffusion of adatoms," Journal of The Electrochemical Society **131**, 40 (1984).

[3]R. Aogaki and T. Makino, "Morphological instability in nonsteady galvanostatic electrodeposition: II . Experimental demonstration of the surface diffusion effect of adatoms by means of image analysis," Journal of The Electrochemical Society **131**, 46 (1984).

[4]R. Williford and L. Chick, "Surface diffusion and concentration polarization on oxide-supported metal electrocatalyst particles," Surface Science **547**, 421 (2003).

[5]T. Mattos and F. D. A. Reis, "Effects of diffusion and particle size in a kinetic model of catalyzed reactions," Journal of Catalysis **263**, 67 (2009).

[6]J. Libuda and H.-J. Freund, "Molecular beam experiments on model catalysts," Surface Science Reports **57**, 157 (2005).

[7]J. Li, I. Maresi, Y. Lum, and J. W. Ager, "Effects of surface diffusion in electrocatalytic CO2 reduction on Cu revealed by kinetic monte carlo simulations," The Journal of Chemical Physics **155**, 164701 (2021).

[8]J. Barth, "Transport of adsorbates at metal surfaces: from thermal migration to hot precursors," Surface Science Reports **40**, 75 (2000).

[9]R. Gomer, "Diffusion of adsorbates on metal surfaces," Reports on Progress in Physics **53**, 917 (1990).

[10]Y.-C. Yang and O. M. Magnussen, "Quantitative studies of adsorbate dynamics at noble metal electrodes by in situ Video-STM," Physical Chemistry Chemical Physics **15**, 12480 (2013).

[11]X. D. Zhu, T. Rasing, and Y. R. Shen, "Surface diffusion of CO on Ni(111) studied by diffraction of optical second-harmonic generation off a monolayer grating," Physical Review Letters **61**, 2883 (1988).

[12]G. X. Cao, E. Nabighian, and X. D. Zhu, "Diffusion of hydrogen on Ni(111) over a wide range of temperature: exploring quantum diffusion on metals," Physical Review Letters **79**, 3696 (1997).

[13]C. Z. Zheng, C. K. Yeung, M. M. T. Loy, and X. Xiao, "Quantum diffusion of H on Pt(111): step effects," Physical Review Letters **97**, 166101 (2006).

[14]J. Ma, X. Xiao, N. J. DiNardo, and M. M. T. Loy, "Diffusion of CO on Pt(111) studied by an optical diffraction method," Physical Review B **58**, 4977 (1998).

[15]J. Ma, X. Xiao, and M. Loy, "Experimental study of surface diffusion rate enhancement along steps: CO on Pt(111)," Surface Science **436**, L661 (1999).

[16]J. Ma, L. Cai, X. Xiao, and M. M. Loy, "On the mechanism limiting CO diffusion perpendicular to steps on Pt(111)," Surface Science **425**, 131 (1999).

[17]J. Ma, X. Xiao, and M. Loy, "Observation of two diffusion channels in a single diffusion measurement: CO on P-contaminated Pt(111) surface," Surface Science **423**, 85 (1999).

[18]X. D. Zhu and Y. R. Shen, "Generation and detection of a monolayer grating by laser desorption and second-harmonic generation: CO on Ni(111)," Optics Letters **14**, 503 (1989).

[19]X. D. Zhu, A. Lee, and A. Wong, "Detection of monolayer gratings of adsorbates by linear optical diffractions," Applied Physics A **52**, 317 (1991).

[20]X. D. ZHU, "Optical diffractions as probes to surface diffusion of adsorbates," Modern Physics Letters B **06**, 1217 (1992).

[21]X.-D. Xiao, "Surface diffusion studies by optical diffraction techniques," PhD thesis (University of California, 1992).

[22]X.-D. Xiao, X. D. Zhu, W. Daum, and Y. R. Shen, "Optical second-harmonic diffraction study of anisotropic surface diffusion: CO on Ni(110)," Physical Review B **46**, 9732 (1992).

[23]X.-D. Xiao, Y. Xie, and Y. Shen, "Surface diffusion probed by linear optical diffraction," Surface Science **271**, 295 (1992).

[24]X.-D. Xiao, Y. Xie, and Y. R. Shen, "Coverage dependence of anisotropic surface diffusion: CO/Ni(110)," Physical Review B **48**, 17452 (1993).

[25]A. Lee, X. D. Zhu, L. Deng, and U. Linke, "Observation of a transition from over-barrier hopping to activated tunneling diffusion: H and D on Ni(100)," Physical Review B **46**, 15472 (1992).

[26]W. Schmickler, *Grundlagen der Elektrochemie* (Springer Berlin, 1996).

[27]H. Ibach, *Physics of surfaces and interfaces* (Springer Berlin, 2006).

[28]D. Kolb and R. J. Gale, "Spectroelectrochemistry theory and practice - UV-visible reflectance spectroscopy," Plenum Press, 10.1007/978-1-4613-0985-7 (1988).

[29]Z. Yang, R. Wu, and J. A. Rodriguez, "First-principles study of the adsorption of sulfur on Pt(111): S core-level shifts and the nature of the Pt-S bond," Physical Review B **65**, 155409 (2001).

[30]T. Tansel and O. M. Magnussen, "Video STM studies of adsorbate diffusion at electrochemical interfaces," Physical Review Letters **96**, 026101 (2006).

[31]S. Baier and M. Giesen, "Determination of activation energies of mass transport processes on Ag(111) electrodes in aqueous electrolyte," Physical Chemistry Chemical Physics **2**, 3675 (2000).

[32]T. Tansel, "Video-STM-Untersuchungen der Diffusion von Adsorbaten in elektrochemischer Umgebung," PhD thesis (CAU Kiel, 2006).

[33]M. Giesen, G. Beltramo, S. Dieluweit, J. Müller, H. Ibach, and W. Schmickler, "The thermodynamics of electrochemical annealing," Surface Science **595**, 127 (2005).

[34]G. Kellogg, "Field ion microscope studies of single-atom surface diffusion and cluster nucleation on metal surfaces," Surface Science Reports **21**, 1 (1994).

[35]J. Ellis, A. P. Graham, and J. P. Toennies, "Quasielastic helium atom scattering from a two-dimensional gas of Xe atoms on Pt(111)," Physical Review Letters **82**, 5072 (1998).

[36]J. Trost, H. Brune, J. Wintterlin, R. J. Behm, and G. Ertl, "Interaction of oxygen with Al(111) at elevated temperatures," The Journal of Chemical Physics **108**, 1740 (1998).

[37]S. Renisch, "On the diffusion of adsorbed particles on single crystal surfaces: dynamical investigations with the scanning tunneling microscope," PhD thesis (FU Berlin, 1999).

[38]M. Giesen, R. Randler, S. Baier, H. Ibach, and D. Kolb, "Step dynamics on Cu (100) and Ag (111) electrodes in an aqueous electrolyte," Electrochimica Acta **45**, 527 (1999).

[39]M. Giesen, "Step and island dynamics at solid/vacuum and solid/liquid interfaces," Progress in Surface Science **68**, 1 (2001).

[40]P. Babu, J.-H. Chung, E. Oldfield, and A. Wieckowski, "CO surface diffusion on platinum fuel cell catalysts by electrochemical NMR," Electrochimica Acta **53**, 6672 (2008).

[41]C. Z. Zheng, C. K. Yeung, M. M. T. Loy, and X. Xiao, "Step effects and coverage dependence of hydrogen atom diffusion on Pt(111) surfaces," Physical Review B **70**, 205402 (2004).

[42]H. J. Eichler and A. Hermerschmidt, "Light-induced dynamic gratings and photorefraction," in *Photorefractive materials and their applications 1: basic effects*, edited by P. Günter and J.-P. Huignard (Springer New York, 2006), pp. 7–42.

[43]L. Kattwinkel, "Messung der Oberflächendiffusion an Fest-Flüssig-Grenzflächen durch in situ lineare optische Beugung," CAU Kiel, master thesis, unpublished, 2016.

[44]V. Climent, N. Garcia-Araez, R. G. Compton, and J. M. Feliu, "Effect of deposited bismuth on the potential of maximum entropy of Pt(111) single-crystal electrodes," The Journal of Physical Chemistry B **110**, 21092 (2006).

[45]J. J. Martin, P. H. Sidles, and G. C. Danielson, "Thermal diffusivity of platinum from 300° to 1200°K," Journal of Applied Physics **38**, 3075 (1967).

[46]W. Werner, K. Glantschnig, and C. Ambrosch-Draxl, "Optical constants and inelastic electron-scattering data for 17 elemental metals," Journal of Physical and Chemical Reference Data **38**, 10.1063/1.3243762 (2009).

[47]M. D. Lechner, *Taschenbuch für Chemiker und Physiker*, edited by M. D. Lechner (Springer Berlin, Heidelberg, 2012).

[48]G. M. Hale and M. R. Querry, "Optical constants of water in the 200-nm to 200-μm wavelength region," Appl. Opt. **12**, 555 (1973).

[49]C. S. Feigerle, S. R. Desai, and S. H. Overbury, "The kinetics of CO desorption from Ni(110)," The Journal of Chemical Physics **93**, 787 (1990).

[50]X. D. Zhu, A. Lee, A. Wong, and U. Linke, "Surface diffusion of hydrogen on Ni(100): an experimental observation of quantum tunneling diffusion," Physical Review Letters **68**, 1862 (1992).

[51]I. Fromondi, "In situ optical techniques as applied to the study of surface dynamics," PhD thesis (Case Western Reserve University, 2007).

[52]I. Fromondi and D. Scherson, "(Bi)sulfate adsorption on quasiperfect Pt(111) facets from acidic aqueous electrolytes as monitored by optical techniques," The Journal of Physical Chemistry C **111**, 10154 (2007).

[53]Y. Mo, E. Hwang, and D. A. Scherson, "Simultaneous normalized optical reflectivity and microgravimetric measurements at electrode/electrolyte interfaces: the adsorption of bromide on gold in aqueous media," Analytical Chemistry **67**, 2415 (1995).

[54]G. B. Blanchet, P. J. Estrup, and P. J. Stiles, "Surface-reflectance-spectroscopy studies of h on w(110): surface band structure and adsorbate geometry," Physical Review Letters **44**, 171 (1979).

[55]R. Verhoef and M. Asscher, "Diffusion on surfaces using laser diffraction: effect of adsorbate lateral interactions," Surface Science **376**, 395 (1997).

[56]Y.-E. Sung, W. Chrzanowski, A. Wieckowski, A. Zolfaghari, S. Blais, and G. Jerkiewicz, "Coverage evolution of sulfur on Pt(111) electrodes: from compressed overlayers to well-defined islands," Electrochimica Acta **44**, 1019 (1998).

[57]A. Zolfaghari, G. Jerkiewicz, W. Chrzanowski, and A. Wieckowski, "Energetics of the underpotential deposition of hydrogen on platinum electrodes: II. Presence of coadsorbed sulfur," Journal of The Electrochemical Society **146**, 4158 (1999).

[58]E. Herrero, J. M. Feliu, S. Blais, Z. Radovic-Hrapovic, and G. Jerkiewicz, "Temperature dependence of CO chemisorption and its oxidative desorption on the Pt(111) electrode," Langmuir **16**, 4779 (2000).

[59]E. Herrero, B. Álvarez, J. M. Feliu, S. Blais, Z. Radovic-Hrapovic, and G. Jerkiewicz, "Temperature dependence of the CO_{ads} oxidation process on Pt(111), Pt(100), and Pt(110) electrodes," Journal of Electroanalytical Chemistry **567**, 139 (2004).

[60]G. New, *Introduction to nonlinear optics* (Cambridge University Press, 2011).

[61]F. Reikowski, "In situ x-ray scattering studies of ultrathin epitaxial metal oxide films," PhD thesis (CAU Kiel, 2019).

[62]I. Thormählen, J. Straub, and U. Grigull, "Refractive index of water and its dependence on wavelength, temperature, and density," Journal of Physical and Chemical Reference Data **14**, 933 (1985).

[63]V. Climent and J. M. Feliu, "Thirty years of platinum single crystal electrochemistry," Journal of Solid State Electrochemistry **15**, 1297 (2011).

[64]V. Climent and J. M. Feliu, "Surface electrochemistry with Pt single-crystal electrodes," in *Advances in electrochemical science and engineering* (John Wiley & Sons, Ltd, 2017) Chap. 1, pp. 1–57.

[65]M. Ruge, J. Drnec, B. Rahn, F. Reikowski, D. A. Harrington, F. Carlà, R. Felici, J. Stettner, and O. M. Magnussen, "Structural reorganization of Pt(111) electrodes by electrochemical oxidation and reduction," Journal of the American Chemical Society **139**, 4532 (2017).

[66]L. Jacobse, Y.-F. Huang, M. T. M. Koper, and M. J. Rost, "Correlation of surface site formation to nanoisland growth in the electrochemical roughening of Pt(111)," Nature Materials **17**, 277 (2018).

[67]T. Fuchs, J. Drnec, F. Calle-Vallejo, N. Stubb, D. J. S. Sandbeck, M. Ruge, S. Cherevko, D. A. Harrington, and O. M. Magnussen, "Structure dependency of the atomic-scale mechanisms of platinum electro-oxidation and dissolution," Nature Catalysis **3**, 754 (2020).

[68]E. Seebauer and L. Schmidt, "Surface diffusion of hydrogen on Pt(111): laser-induced thermal desorption studies," Chemical Physics Letters **123**, 129 (1986).

[69]D. Meixner and S. M. George, "Coverage dependent surface diffusion of noble gases and methane on Pt(111)," Surface Science **297**, 27 (1993).

[70]J. Clavilier, R. Faure, G. Guinet, and R. Durand, "Preparation of monocrystalline Pt microelectrodes and electrochemical study of the plane surfaces cut in the direction of the {111} and {110} planes," Journal of Electroanalytical Chemistry and Interfacial Electrochemistry **107**, 205 (1979).

[71]T. Loučka, "The adsorption of sulphur and of simple organic substances on platinum electrodes," Journal of Electroanalytical Chemistry and Interfacial Electrochemistry **36**, 369 (1972).

[72]E. Lamy-Pitara, L. Bencharif, and J. Barbier, "Adsorption du soufre sur le platine," Electrochimica Acta **30**, 971 (1985).

[73]Y. .-. Sung, W. Chrzanowski, A. Zolfaghari, G. Jerkiewicz, and A. Wieckowski, "Structure of chemisorbed sulfur on a Pt(111) electrode," Journal of the American Chemical Society **119**, 194 (1997).

[74]E. Protopopoff and P. Marcus, "Effects of chemisorbed sulphur on the hydrogen adsorption and evolution on metal single crystal surfaces," Journal de Chimie Physique **88**, 1423 (1991).

[75]T. Loučka, "Adsorption and oxidation of sulphur and of sulphur dioxide at the platinum electrode," Journal of Electroanalytical Chemistry and Interfacial Electrochemistry **31**, 319 (1971).

[76]A. Björling and J. M. Feliu, "Electrochemical surface reordering of Pt(111): a quantification of the place-exchange process," Journal of Electroanalytical Chemistry **662**, 17 (2011).

[77]Y. Nagahara, S. Sugawara, and K. Shinohara, "The impact of air contaminants on PEMFC performance and durability," Journal of Power Sources **182**, 422 (2008).

[78]E. Lamy-Pitara, Y. Tainon, B. Beden, and J. Barbier, "Nature and effects of sulphur adsorbed on platinum in acid medium. An investigation using UV-visible reflectance spectroscopy," Journal of Electroanalytical Chemistry and Interfacial Electrochemistry **279**, 291 (1990).

[79]C. Quijada, A. Rodes, J. Vázquez, J. Pérez, and A. Aldaz, "Electrochemical behaviour of aqueous sulphur dioxide at polycrystalline Pt electrodes in acidic medium. A voltammetric and in-situ FT-IR study Part II. Promoted oxidation of sulphur dioxide. Reduction of sulphur dioxide," Journal of Electroanalytical Chemistry **398**, 105 (1995).

[80]R. Bucur, "State of the pre-adsorbed sulfur on a rough platinum electrode in voltammetric conditions: microgravimetric measurements with electrochemical quartz crystal microbalance," Electrochimica Acta **87**, 186 (2013).

[81]C.-H. Chen, C. Brennan, S. C. S. Lai, D. J. Fermin, P. R. Unwin, and P. Rodriguez, "Adsorption and electrochemical oxidation of small sulfur containing anions on Pt electrodes in organic media," ChemElectroChem **5**, 2228 (2018).

[82]V. A. Sethuraman and J. W. Weidner, "Analysis of sulfur poisoning on a PEM fuel cell electrode," Electrochimica Acta **55**, 5683 (2010).

[83]D. E. Ramaker, D. Gatewood, A. Korovina, Y. Garsany, and K. E. Swider-Lyons, "Resolving sulfur oxidation and removal from Pt and Pt3Co electrocatalysts using in situ x-ray absorption spectroscopy," The Journal of Physical Chemistry C **114**, 11886 (2010).

[84]P. Jayaraj, P. Karthika, N. Rajalakshmi, and K. Dhathathreyan, "Mitigation studies of sulfur contaminated electrodes for PEMFC," International Journal of Hydrogen Energy **39**, 12045 (2014).

[85]C.-H. Chen, A. Halford, M. Walker, C. Brennan, S. C. Lai, D. J. Fermin, P. R. Unwin, and P. Rodriguez, "Electrochemical characterization and regeneration of sulfur poisoned Pt catalysts in aqueous media," Journal of Electroanalytical Chemistry **816**, 138 (2018).

[86]A. Contractor and H. Lal, "Two forms of chemisorbed sulfur on platinum and related studies," Journal of Electroanalytical Chemistry and Interfacial Electrochemistry **96**, 175 (1979).

[87]A. U. Nilekar, J. Greeley, and M. Mavrikakis, "A simple rule of thumb for diffusion on transition-metal surfaces," Angewandte Chemie **118**, 7204 (2006).

[88]C. R. B. Rodríguez and J. A. Santana, "Adsorption and diffusion of sulfur on the (111), (100), (110), and (211) surfaces of FCC metals: density functional theory calculations," The Journal of Chemical Physics **149**, 204701 (2018).

[89]R. Walder, N. Nelson, and D. K. Schwartz, "Single molecule observations of desorption-mediated diffusion at the solid-liquid interface," Phys. Rev. Lett. **107**, 156102/1 (2011).

[90]M. J. Skaug, J. Mabry, and D. K. Schwartz, "Intermittent molecular hopping at the solid-liquid interface," Phys. Rev. Lett. **110**, 256101/1 (2013).

[91]H. Yoon, N. Materer, M. Salmeron, M. V. Hove, and G. Somorjai, "Coverage-dependent structures of sulfur on Pt(111) studied by low-energy electron diffraction (LEED) and scanning tunneling microscopy (STM)," Surface Science **376**, 254 (1997).

[92]I. Fromondi and D. A. Scherson, "Oxidation of adsorbed CO on Pt(111) in CO-saturated perchloric acid aqueous solutions: simultaneous in situ time-resolved reflectance spectroscopy and second harmonic generation studies," The Journal of Physical Chemistry B **110**, 20749 (2006).

[93]F. Molina and R. Parsons, "Electroreflectance of well-defined Pt surfaces," Journal de Chimie Physique **88**, 1339 (1991).

[94]A. von Oertzen, H. Rotermund, and S. Nettesheim, "Diffusion of carbon monoxide and oxygen on Pt(110): experiments performed with the PEEM," Surface Science **311**, 322 (1994).

[95]B. Poelsema, L. K. Verheij, and G. Comsa, "He-scattering investigation of CO migration on Pt(111)," Phys. Rev. Lett. **49**, 1731 (1982).

[96]J. E. Reutt-Robey, D. J. Doren, Y. J. Chabal, and S. B. Christman, "CO diffusion on Pt(111) with time-resolved infrared-pulsed molecular beam methods: critical tests and analysis," The Journal of Chemical Physics **93**, 9113 (1990).

[97]V. Kwasniewski and L. Schmidt, "Surface diffusion of CO on Pt(111)," Surface Science **274**, 329 (1992).

[98]J. V. Nekrylova and I. Harrison, "Single hop diffusion of CO from bridge to top sites on Pt(111)," The Journal of Chemical Physics **101**, 1730 (1994).

[99]H. Froitzheim and M. Schulze, "Surface diffusion of CO on Pt(111): a HREELS study at high temperatures," Surface Science **320**, 85 (1994).

[100]I. Fromondi and D. Scherson, "Surface dynamics at well-defined single crystal microfacetted Pt(111) electrodes: in situ optical studies," Farday Discussions, https://doi.org/10.1039/B805040F (2008).

[101]I. Fromondi, H. Zhu, and D. A. Scherson, "In situ spectroscopy at the quasi-perfect Pt(111) single-crystal facet | aqueous electrolyte interface," The Journal of Physical Chemistry C **116**, 19613 (2012).

[102]I. Fromondi, H. Zhu, Z. Feng, and D. Scherson, "Dynamics of oxidation of well-defined adsorbed CO phases on Pt(111) in aqueous acidic electrolytes: simultaneous in situ second harmonic generation and differential reflectance spectroscopy," The Journal of Physical Chemistry C **118**, 27901 (2014).

[103]B. Beden, N. Collas, C. Lamy, J. Léger, and V. Solis, "Electrosorption of carbon monoxide at the platinum-electrolyte interface," Surface Science **162**, 789 (1985).

[104]N. Ikemiya, M. Nishide, and S. Hara, "Potential dependence of the surface self-diffusion coefficient on Au(100) in sulfuric acid solution measured by atomic force microscopy," Surface Science **340**, L965 (1995).

[105]E. Pichardo-Pedrero, G. Beltramo, and M. Giesen, "Electrochemical annealing and its relevance in metal electroplating: an atomistic view," Applied Physics A **87**, 461 (2007).

ACRONYMS

AR	Anti-reflective (coated).
CV	Cyclic Voltammetry / Cyclic Voltamogram.
FEM	Field Emission Microscopy.
FFPM	Perfluoroelastomer.
FIM	Field Ion Microscopy.
HeNe	Helium-Neon (laser).
LITD	Laser-induced Thermal Desorption.
LOD	Linear Optical Diffraction.
ML	Monolayer.
Nd:YAG	Neodymium-doped Yttrium Aluminum Garnet (laser).
NMR	Nuclear Magnetic Resonance Spectroscopy.
OR	Optical Reflectance.
PEEK	Polyether Ether Ketone.
PEEM	Photoemission Electron Microscopy.
PEM	Photoelastic Modulator.
PMT	Photomultiplier Tube (detector).
QHAS	Quasielastic Helium Atom Scattering.
SHD	Second Harmonic Diffraction.
SHE	Standard Hydrogen Electrode.
SHG	Second Harmonic Generation.
SNR	Signal to Noise Ratio.
STM	Scanning Tunneling Microscopy.
UHV	Ultrahigh Vacuum.
VSTM	Video-rate Scanning Tunneling Microscopy.
XPS	X-ray Photoelectron Spectroscopy.

SWORN DECLARATION / EIDESSTATTLICHE VERSICHERUNG

I hereby declare that – apart from the guidance of my supervisors Prof. Dr. Olaf M. Magnussen – the content and design of this thesis is my own work. No other sources than those stated have been used.
This work or parts of it have not been submitted as part of a doctoral examination procedure to another examining body. The thesis was prepared adhering to the Rules of Good Scientific Practice of the German Research Foundation. None of my academic degrees have ever been withdrawn. Part of this work is already published, my own contributions to these publications are summarized in the following chapter.

Ich erkläre, dass diese Arbeit nach Inhalt und Form die eigene Arbeit ist, abgesehen von der Beratung durch meinen Betreuer Prof. Dr. Olaf M. Magnussen, und ich keine weiteren Quellen bzw. Hilfestellungen erhalten habe, abgesehen von den angegebenen.
Die Arbeit ist unter Einhaltung der Regeln guter wissenschaftlicher Praxis der Deutschen Forschungsgemeinschaft entstanden. Es wurde mir kein akademischer Grad entzogen. Die eingereichte Arbeit hat weder ganz noch zum Teil schon bei einer anderen Stelle im Rahmen eines Prüfungsverfahrens vorgelegen. Teile der Arbeit wurden jedoch in wissenschaftlichen Journalen veröffentlicht. Eine Übersicht aller im Rahmen dieser Arbeit entstandenen Veröffentlichungen, inklusive einer Einschätzung des erbrachten Eigenanteils, ist dem folgendem Kapitel zu entnehmen.

Kiel, den

Lasse Kattwinkel

SCIENTIFIC CONTRIBUTIONS

PUBLICATIONS

- **Optical reflectance studies on the oxidation of chemisorbed sulfur at the Pt(111) electrode**
  Lasse Kattwinkel and Olaf M. Magnussen
  Electrochimica Acta 434, 141297 (2022)

  Contribution statement:
  Lasse Kattwinkel: conceptualization (equal), methodology (lead), software (lead), validation (lead), formal analysis (lead), investigation (lead), data curation (lead), visualization (lead), writing – original draft (lead).
  Olaf M. Magnussen: conceptualization (equal), writing – review & editing (lead), supervision (lead), funding acquisition (lead).

- **Measurement of surface diffusion at the electrochemical interface by in situ linear optical diffraction**
  Lasse Kattwinkel and Olaf M. Magnussen
  ACS Measurement Science Au, in press. (2023)

  Contribution statement:
  Lasse Kattwinkel: conceptualization (equal), formal analysis (lead), investigation (lead), methodology (lead), software (lead), visualization (lead), writing-original draft (lead).
  Olaf M. Magnussen: conceptualization (equal), funding acquisition (lead), supervision (lead), writing-review & editing (lead).

- **Influence of coverage on adsorbate diffusion measurements at electrode surfaces by in situ linear optical diffraction**
  Lasse Kattwinkel and Olaf M. Magnussen
  The Journal of Chemical Physics, submitted manuscript. (2023)

  Contribution statement:
  Lasse Kattwinkel: conceptualization (equal), formal analysis (lead), investigation (lead), methodology (lead), software (lead), visualization (lead), writing-original draft (lead).
  Olaf M. Magnussen: conceptualization (equal), funding acquisition (lead), supervision (lead), writing-review & editing (lead).

ACKNOWLEDGMENTS

First of all, I would like to express my sincere gratitude to my supervisor Prof. Dr. Olaf M. Magnussen, who came up with the idea of developing this new methodology and gave me the opportunity to work upon its realisation. Thank you for the inspiration and for having the opportunity to spend a lot of time on various ideas, which not always worked out from the beginning on, but made this a really exciting project. In particular, I appreciated the continuous guidance and support, and the extensive background knowledge he was always happy to share. No matter the question, no matter the issue, there was always time for a helpful explanation or a short (and also a longer) discussion. I really enjoyed working in this group over the last few years.

Reflecting on how I got here, I still have fond memories of my bachelor thesis under the supervision of Dr. Jochim Stettner. Although I have to mention that your coffee is really indigestible, I want to thank you for giving me the first impetus to work in this group on electrochemical interfaces. Now I really appreciate you as a colleague.

In particular, I want to thank my fellow colleagues for the good time. Timo, for all the good brainstorming and discussions. Andrea, for the garden time after work. Ole, for the positive mood and the introduction into green tea drinking. Reihanneh for all the good chats in between. Actually, I would like to thank the whole group once again for the good atmosphere and team spirit we developed. I will always remember our excursions, Mett-Mittwoch and the good old office-ham.

Another special thanks goes to Karsten and Matthias for their technical support in all the smaller and bigger projects. It is a pleasure to have you as colleagues. The same applies to the central IEAP workshop where, among other things, the electrochemical cell was built.

And of course, I want to thank Monika Seeger and Claudia Läufer for taking care of us.

Finally, I want to thank my family and friends for all the support especially in hard times. I will always remember the working holidays in Denmark with my little brother. In such a "holiday" one year ago, the basis of this work was laid with the first draft of the first publication. At the time writing, almost one year later, it remains to finish the acknowledgements and give a final thank to Malte and Finn for taking so much time lecturing this work and just being good friends.

APPENDICES

A.1 CELL CLEANING AND SAMPLE TRANSFER

For cleaning the cell, all single parts are firstly immersed to cold caro acid (95% H_2SO_4 and 30% H_2O_2 with a ratio of 2:1) for about 24 hours. While concentrated acid can be used for the teflon parts, FFPM o-rings, and fused silica windows, the acid has to be diluted (water and caro acid with a ratio of 4:1) for the PEEK parts. To remove any residues, glassware and FFPM o-rings are then repeatedly rinsed and boiled in ultrapure water. PEEK and Teflon parts are cleaned with the same procedure, but using lukewarm ultrapure water to prevent deformation. After reassembling the cell with a teflon sample dummy inserted, it is once again flushed with several liters of ultrapure water. The electrolyte inlet is therefore connected directly to the ultrapure water dispenser (see figure A.1a). After finishing this process, the cell can be used for electrochemical measurements. In between single measurements, it is sufficient to repeat the flushing procedure with ultrapure water to keep the cell clean. Storage is possible over several weeks when keeping the cell filled with ultrapure water. In this case, repeated purging with caro acid is only necessary every few months.
Prior to each experiment, the single crystal electrode has to be freshly prepared (see section 6) and transferred into the cell. The transfer process is depicted in figure A.1b. After preparation, the crystal surface is first covered with a protective droplet of electrolyte to reduce contamination. In this condition, the crystal is placed onto the sample holder (a) and covered with a teflon sealing hut (b). The cell body then is mounted on top and tightened using wingnuts (c). Subsequently, the crystal is pressed into the cell body from behind using the micrometer screw. Completely sealed, the cell can be filled with electrolyte. During this process, bubble formation can be avoided by turning the cell on the holder. The whole process is usually completed in less than 90 seconds.

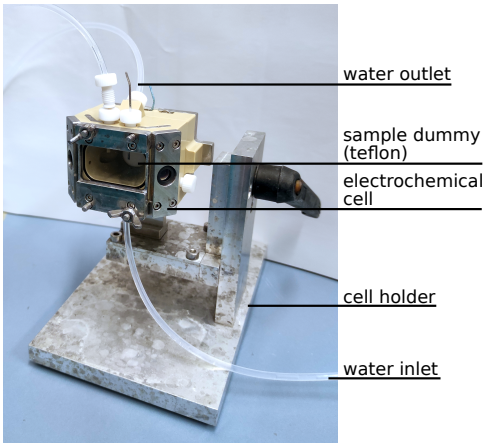

(a)

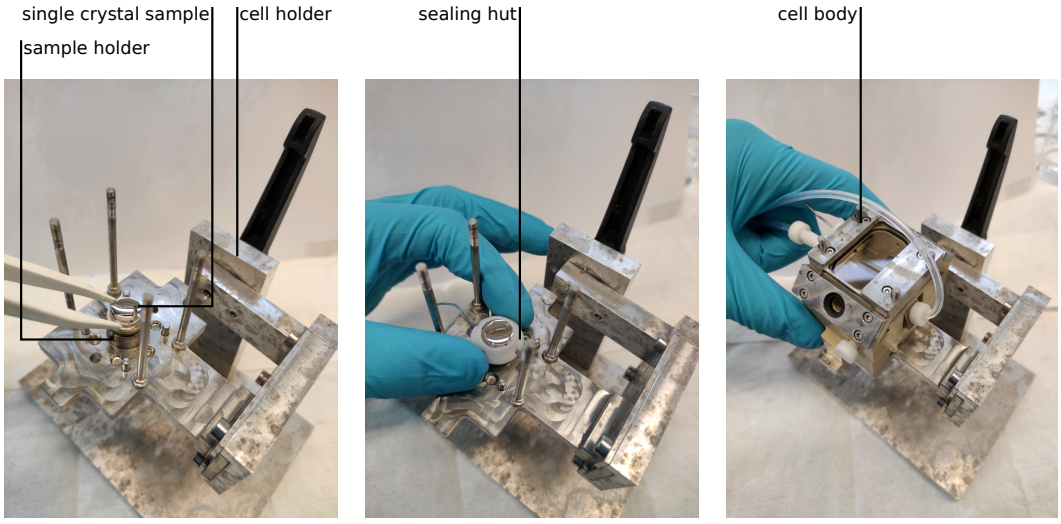

(b)

Figure A.1: (a) Cell cleaning using a steady ultrapure water flow. (b) Crystal transfer into the electrochemical cell.

A.2 MEASUREMENT DATA

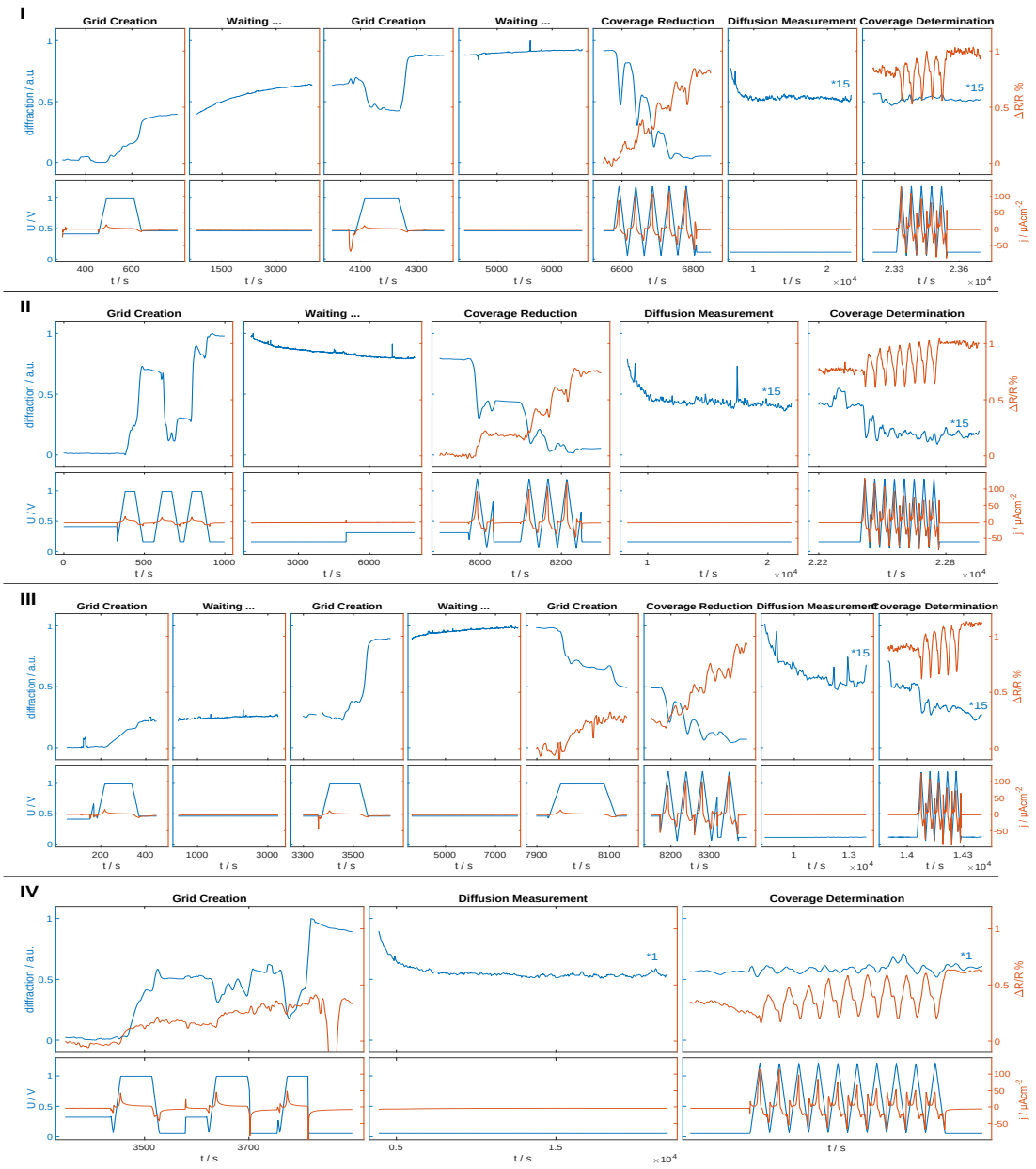

Figure A.2: Measurement data for diffusion in the hydrogen region.

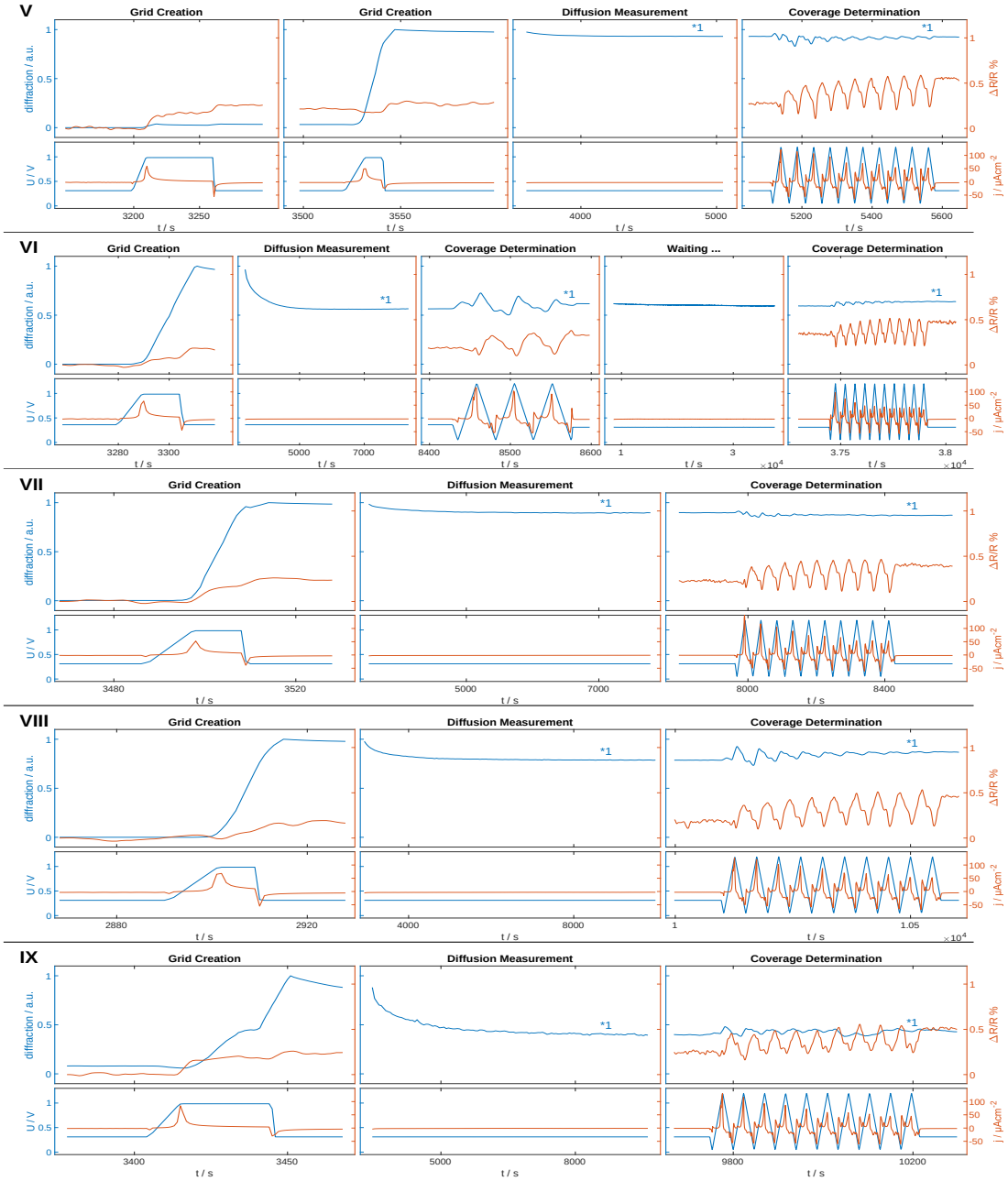

Figure A.3: Measurement data for diffusion in the double layer region.

A.3 PERMISSIONS FOR REPRINT - OWN PUBLICATIONS

Elsevier: Electrochimica Acta

> "Can I include/use my article in my thesis/dissertation?
> Yes. Authors can include their articles in full or in part in a thesis or dissertation for non-commercial purposes."
>
> `https://www.elsevier.com/about/policies/copyright/permissions`
> `https://www.elsevier.com/about/policies/copyright`

American Chemical Society: ACS Measurement Science Au

> License: CC BY-NC-ND:
>
> You are free to:
> **Share** — copy and redistribute the material in any medium or format.
> **Attribution** — You must give appropriate credit, provide a link to the license, and indicate if changes were made. You may do so in any reasonable manner, but not in any way that suggests the licensor endorses you or your use.
> **NonCommercial** — You may not use the material for commercial purposes.
> **NoDerivatives** — If you remix, transform, or build upon the material, you may not distribute the modified material.
> **No additional restrictions** — You may not apply legal terms or technological measures that legally restrict others from doing anything the license permits.
>
> `https://creativecommons.org/licenses/by-nc-nd/3.0/`

A.4 PERMISSIONS FOR REPRINT - ADDITIONAL MATERIAL

- Figure 3.1:

  > License Agreement between Lasse Kattwinkel ("User") and Copyright Clearance Center, Inc. ("CCC") on behalf of the Rightsholder identified in the order details below:
  > Order Date: 18-Jan-2023, Order License ID: 1312524-1, ISSN: 0167-5729, Type of Use: Republish in a thesis/dissertation, Publisher: ELSEVIER BV, Portion: Chart/graph/table/figure

- Figure 3.2:

  This license agreement between the American Physical Society ("APS") and Lasse Kattwinkel ("You") consists of your license details and the terms and conditions provided by the American Physical Society and SciPris:
  License Number: RNP/23/JAN/062258, License date: 18-Jan-2023, DOI: 10.1103/PhysRevB.58.4977, Reuse Category: Reuse in a thesis/dissertation, Publisher: American Physical Society, Items for Reuse : Figures/Tables

- Figure 3.3:

  License Agreement between Lasse Kattwinkel ("User") and Copyright Clearance Center, Inc. ("CCC") on behalf of the Rightsholder identified in the order details below:
  Order Date: 18-Jan-2023, Order License ID: 1312734-1, ISSN: 1463-9084, Type of Use: Republish in a thesis/dissertation, Publisher: ROYAL SOCIETY OF CHEMISTRY, Portion: Chart/graph/table/figure

- Figure 3.4:

  License Agreement between Lasse Kattwinkel ("User") and Copyright Clearance Center, Inc. ("CCC") on behalf of the Rightsholder identified in the order details below:
  Order Date: 20-Jan-2023, Order License ID: 1313875-1, ISSN: 0167-5729, Type of Use: Republish in a thesis/dissertation, Publisher: ELSEVIER BV, Portion: Chart/graph/table/figure

- Table 3.1:

  License Agreement between Lasse Kattwinkel ("User") and Copyright Clearance Center, Inc. ("CCC") on behalf of the Rightsholder identified in the order details below:
  Order Date: 18-Jan-2023, Order License ID: 1312524-1, ISSN: 0167-5729, Type of Use: Republish in a thesis/dissertation, Publisher: ELSEVIER BV, Portion: Chart/graph/table/figure

- Figure 4.2:

  License Agreement between Lasse Kattwinkel ("User") and Copyright Clearance Center, Inc. ("CCC") on behalf of the Rightsholder identified in the order details below:
  Order Date: 22-Feb-2023, Order License ID: 1326583-1, ISBN-13: 9780387251912, Type of Use: Republish in a thesis/dissertation, Publisher: SPRINGER, Portion: Chart/graph/table/figure